

Electronic Thesis and Dissertation Repository

4-20-2021 1:45 PM

Using Ionic Liquids in Fabrication of VO₂ for Thermo-chromic Coatings

Shidokht Nazari, *The University of Western Ontario*

Supervisor: Charpentier, Paul, *The University of Western Ontario*

A thesis submitted in partial fulfillment of the requirements for the Doctor of Philosophy degree in Chemical and Biochemical Engineering

© Shidokht Nazari 2021

Follow this and additional works at: <https://ir.lib.uwo.ca/etd>

 Part of the [Other Chemical Engineering Commons](#)

Recommended Citation

Nazari, Shidokht, "Using Ionic Liquids in Fabrication of VO₂ for Thermo-chromic Coatings" (2021). *Electronic Thesis and Dissertation Repository*. 7755.
<https://ir.lib.uwo.ca/etd/7755>

This Dissertation/Thesis is brought to you for free and open access by Scholarship@Western. It has been accepted for inclusion in Electronic Thesis and Dissertation Repository by an authorized administrator of Scholarship@Western. For more information, please contact wlsadmin@uwo.ca.

Abstract

Energy-efficient or smart windows are an important part of net-zero energy housing as excellent candidates for energy conservation. They can control the amount of light and heat passing through them in response to an external stimulus such as heat (thermochromic) or electricity (electrochromic). Vanadium Oxide (VO_2) is a potential thermochromic material to provide an automatic reversible semiconductor-metal phase transition from the monoclinic structure to tetragonal at 68 °C. However, there remain major challenges in fabricating desirable VO_2 -based films to meet the requirements for large-scale implementation. Mainly, the phase transition temperature (T_c) should be close to the ambient temperature (25 °C), while the integrated luminous transparency (T_{lum}), and solar modulation ability should be high. Another obstacle is the preparation of pure and highly crystalline VO_2 (M) with a small hysteresis width for fast switching ability while using green solvents and milder conditions for large-scale production. The selection of a suitable polymeric matrix for long-term stabilization of VO_2 nanostructure is another crucial concern for industrial goals. This doctoral research project aimed to develop new approaches to the synthesis and fabrication of VO_2 thermochromic films using imidazolium ionic liquids (ILs) or imidazolium poly-ionic liquids (PIL). In “Chapter 2”, Vanadium oxide VO_2 (M) synthesis is studied using supercritical CO_2 (scCO_2), imidazolium ionic liquids (ILs), and their biphasic combination as environmentally benign solvents under mild condition. The role of ILs and scCO_2 on the gelation yield as well as the crystallinity, morphology, and optical properties of final VO_2 (M) is investigated. In “Chapter 3”, the role of different imidazolium ILs on stabilization of $\text{VO}(\text{acac})_2$ precursor is studied, and a new fabrication method is suggested to prepare pure and high crystalline VO_2 (M) using a fast processing time. In Chapter 4, two complementary methods for the fabrication of VO_2 and VO_2/SO_2 nanostructures are suggested using PIL as a dielectric host. In this doctoral thesis, we have tried to respond to the main challenges regarding the synthesis and fabrication of VO_2 (M) thermochromic films with improved optical properties by using simple synthetic methods and green solvents.

Lay of Audience

Energy consumption is continuously increasing worldwide, and energy conversion has been a great challenge to sustainable development. A substantial component of primary energy (~40%) is used in form of air conditioning and it is estimated that energy exchange through the windows is responsible for more than 50% of a building's energy loss. Other than high energy costs, this energy loss can also lead to a higher carbon footprint through increased CO₂ emissions. Applying self-controlled coatings to glass windows or using so-called "energy-efficient windows" can be one effective method to reduce energy loss. The energy-efficient windows or smart windows typically function by an external stimulus such as electricity (electrochromic windows) or heat (thermochromic windows). Vanadium oxide (VO₂) as a typical thermochromic material has been receiving extensive attention as it undergoes a reversible semiconductor-to-metal phase transition which is accompanied by remarkable changes in electrical and optical properties. However, there are remaining challenges in the synthesis and fabrication of VO₂. It is important to prepare pure and highly crystalline VO₂ with fast switching ability using green solvents and milder conditions. The selection of a suitable polymeric matrix for long-term stabilization of VO₂ nanostructure is also another crucial concern for industrial goals. This doctoral research project is aimed to use ionic liquids (ILs) or poly-ionic liquids (PIL) to develop new approaches in the synthesis and fabrication of VO₂ thermochromic films.

Keywords

VO₂ Nanostructure, Thermochromic Coatings, Poly-Ionic Liquids, Imidazolium Ionic Liquids, Supercritical CO₂, Green Solvent, Sol-Gel, UV-Curing, In-situ Polymerization,

Dedication

Dedicated to the memory of passengers of the flight PS752 who have lost their lives in a tragic plane downing in Iran on January 8, 2020.

Acknowledgments

I would like to express my deepest gratitude to my advisor, Dr. Paul A. Charpentier, his relentless guidance, caring, and patience. He has constantly challenged me to push my intellectual limits and think on different fundamental limits.

I would also like to appreciate several people that made possible the successful completion of the adventure that was my dissertation:

I would like to thank Dr. Tim Goldhawk (Nanofabrication, Western University) for providing a Scanning Electron Microscope (SEM) facility.

I would like to express my sincere gratitude to Dr. Zakir Hossain, Dr. Mohammed Abdolhameed, and my other fellow members in Dr. Charpentier's lab for their valuable advice, constructive comments, and discussions regarding my research projects.

Last, but certainly not least, I owe my sincere thanks to my parents and my brother for their support and belief in me. Finally, I would like to thank my husband, Ehsan, for his unwavering love and support.

Table of Contents

Abstract	ii
Keywords	iv
Dedication	v
Acknowledgments.....	vi
Table of Contents	vii
List of Tables	xii
List of Figures	xiv
List of Scheme	xix
List of Appendices	xx
List of Abbreviations	xxi
Chapter 1	1
1 Introduction and Literature Review	1
1.1 Vanadium Oxide (VO ₂)	4
1.2 Effect of Doping in Vanadium Dioxide (VO ₂).....	6
1.3 Synthetic Techniques to Synthesize VO ₂ (M)	8
1.4 Using supercritical CO ₂ in the sol-gel synthesis of metal oxides	10
1.5 Stability of Vanadium (IV) Oxide	11
1.5.1 Chemical Stability of VO ₂	11
1.5.2 Agglomeration of VO ₂ Nanostructures.....	11

1.5.3	Polymer-Based Coatings.....	11
1.6	Optical Properties Measurement.....	12
1.7	Using Ionic Liquids (ILs) in Fabrication of VO ₂ Nanostructures.....	17
1.8	ILs' Heat Capacity and Optical Properties	17
1.9	ILs' Dielectric Constant.....	18
1.10	ILs as Stabilizer of Nanoparticles	19
1.11	Poly Ionic Liquids (PILs).....	20
1.12	Research Objective	22
Chapter 2	24
2	Sol-gel processing of VO ₂ (M) in supercritical CO ₂ and supercritical CO ₂ / ionic liquid biphasic system*	24
2.1	Introduction.....	25
2.2	Experimental	26
2.2.1	Materials	26
2.2.2	Preparation of Vanadium Oxide Aerogel in scCO ₂	27
2.2.3	Preparation of Vanadium Oxide Ionogel in ILs.....	28
2.2.4	Preparation of Vanadium Oxide Ionogel in scCO ₂ / IL biphasic system ..	28
2.2.5	Characterization	29
2.3	VO ₂ Film Preparation	29
2.4	Results and Discussion	30
2.4.1	Influence of Temperature and Pressure on Gelation Yield.....	30

2.4.2	Influence of Solvent and Poly Condensation Reagent Ratio on Gelation Process	33
2.4.3	Characterization of the Aerogel/ Ionogel.....	34
2.4.4	Final Products of Calcination.....	40
2.4.5	Morphology Studies by SEM	47
2.4.6	Optical Properties of the films	49
2.5	Conclusions.....	51
Chapter 3	52
3	Stabilizing vanadyl acetylacetonate using Imidazolium Ionic liquids for VO ₂ thermochromic thin films.....	52
3.1	Introduction.....	53
3.2	Experimental	54
3.2.1	Materials	54
3.2.2	Synthesis of 1-ethyl-3-vinyl imidazolium bis (trifluoromethanesulfonylimide)) ionic liquid	55
3.2.3	Preparation of Poly (1-Ethyl-3-Vinylimidazolium bis (trifluoromethanesulfonylimide))	56
3.2.4	Stability of vanadium acetylacetonate in different ionic liquids	57
3.2.5	Preparation of VO ₂ thin film in IL/ MeOH solution.....	57
3.3	Results and Discussion	58
3.3.1	Stability of vanadium acetylacetonate in MeOH solution	58
3.3.2	Preparation of VO ₂ thin film.....	65

3.4 Conclusion	69
Chapter 4.....	70
4 Novel Fabrication Methods Vanadium Dioxide Using Polymerized Ionic Liquid	70
4.1 Introduction.....	71
4.2 Experimental.....	72
4.2.1 Synthesis of nanorod VO ₂ (M)	72
4.2.2 Synthesis of Mo-nanorod VO ₂ (M).....	73
4.2.3 Synthesis of VO ₂ /SiO ₂ Nanorods.....	73
4.2.4 Preparation of EVA Thermochromic Films Using Solution Casting	74
4.2.5 Preparation of 1-Ethyl-3-Vinylimidazolium bis(trifluoromethanesulfonylimide)	74
4.2.6 Preparation of Poly (1-Ethyl-3-Vinylimidazolium bis (trifluoromethanesulfonylimide)):	75
4.2.7 Preparation of PIL Thermochromic Composite Films Using Solution Casting	76
4.2.8 Preparation of PIL Thermochromic Films Using UV-Curing	77
4.3 Results and Discussion	77
4.3.1 Effect of Calcination Condition on Synthesis of VO ₂ (M)	77
4.3.2 Effect of Mo-doping on VO ₂ (M).....	84
4.3.3 Effect of SiO ₂ coating on optical properties of VO ₂	86
4.3.4 PIL Solution Casting method for fabrication of VO ₂	88
4.3.5 UV-curing method for fabrication of VO ₂	90

4.3.6 Comparison of optical properties of the films prepared by solution casting and UV-curing	91
4.4 Conclusion	95
Chapter 5	96
5 Conclusion and future work	96
References	100
Appendices	122
Copyright Permissions	124
Curriculum Vitae	129

List of Tables

Table 1-1. Specific Heat Capacity	18
Table 1-2. Dielectric Constants.....	18
Table 2-1 .Yield of gel product (wt %) prepared a-g) in scCO ₂ h-n) in [EMIM][TF ₂ N] + scCO ₂ biphasic system o-u) [EMIM][TFO] + scCO ₂ biphasic system at different temperatures and pressures.....	30
Table 2-2. The yield of gel product (wt %) prepared, a) in scCO ₂ at 60 °C and 27.6 MPa in the presence of HOAc as a polycondensation reagent, b-e) in scCO ₂ / IL biphasic at 60 °C and 27.6 MPa and f) IL at 60 °C and atmospheric pressure. (+) is in the presence of scCO ₂ , (-) is in the absence of scCO ₂	34
Table 2-3. Summary of XPS analysis for gel samples prepared in scCO ₂ , scCO ₂ / [EMIM][TF ₂ N], scCO ₂ / [EMIM][TFO] at 27.6 MPa at 60 °C.	39
Table 2-4. BET results of gel samples prepared in a) scCO ₂ only b) scCO ₂ / [EMIM][TF ₂ N] c) [EMIM][TF ₂ N] only d) scCO ₂ / [EMIM][TFO]	40
Table 2-5. Sol-gel conditions to obtain crystalline and pure VO ₂ (M).....	47
Table 2-6. Solar transmittance and luminescence transmittance differences of VO ₂ films at 25 °C and 90 °C.....	49
Table 3-1. Decomposition percentage of PIL at different temperatures.....	67
Table 4-1 DSC results for the heating and cooling cycles of samples obtained at different calcination conditions	81
Table 4-2. Nanostructures size and shape by changing the calcination temperature and duration	82
Table 4-3. Optical properties of EVA films with different loadings of VO ₂	83
Table 4-4. Optical properties of EVA films with the different TEOS volume ratio	87

Table 4-5. Viscosity (η) and molecular weight (M_w) of PIL by changing volume ratio of the monomer to the solvent (M/S) and the molar ratio of the monomer to the initiator (M/I).....	88
Table 4-6. The thickness and optical properties of the VO ₂ -PIL films using PIL with different molecular weight and using various spin-coating speed.....	89
Table 4-7. Comparison of optical properties of various VO ₂ films.....	92

List of Figures

Figure 1-1. Total Secondary energy use by sector in Canada.....	1
Figure 1-2. Commercial/ Institutional secondary energy use in Canada	1
Figure 1-3. Diagrammatic sketch of ideal windows. The ideal windows for (a) summer and (b) winter are shown. The orange arrows represent solar radiation, the yellow arrows represent long-wave thermal radiation emitted by the outdoor environment, and the blue arrows represent the long-wave thermal radiation emitted by indoor surfaces[3] Reprinted with the permission of Scientific Report Journal	3
Figure 1-4. Left: The rutile structure of VO ₂ , when T > T _c . The large red circles represent V ⁴⁺ ions, and the small blue circles are O ₂ ⁻ ions, Right: The M1 monoclinic structure of semiconducting VO ₂ when T < T _c . Two types of oxygen ions can be distinguished Reprinted with the permission of the Royal Society of Chemistry.	5
Figure 1-5. Schematic band structure diagram of VO ₂ . The hybridization of the V 3d and O 2p levels reflects the symmetries of the atomic arrangement in the crystal lattice[5,13]. Reprinted with permission of the Royal Society of Chemistry	6
Figure 1-6. Carbon dioxide temperature- pressure phase diagram	10
Figure 1-7. Spectral reflectance (a) and transmittance (b) for a 0.05- μ m-thick VO ₂ film in semiconducting and metallic states. Panel (c) illustrates typical spectra for the luminous efficiency of the human eye and solar irradiance[7,50,51]. Reprinted with the permission of Elsevier.	13
Figure 1-8. Thickness dependence of (a) transmittance and (b) reflectance spectra for typical samples with different thicknesses (43 nm, 102 nm, 215 nm, and 428 nm corresponding to the black squares, the red triangles, the blue pentagrams, and the green circles, respectively). The transmittance was measured at both 20 °C (lines with solid symbols) and 90 °C (lines with open symbols) and the reflectance was measured at only 20 °C[56]. Reprinted with permission of the American Chemical Society.	15

Figure 1-9. a) Schematic of inclusion of metal nanoparticles (M-NPs) in the supramolecular IL network with electrostatic and steric stabilization is indicated through the formation of a suggested primary anion layer around the M-NPs[83]. Reprinted with permission of the Royal Society of Chemistry.....	20
Figure 2-1. a) effect of temperature on the wt % yield b) effect of pressure on the wt % yield. Symbol (Δ) represents the reactions carried out in $scCO_2$, the reactions symbol (\circ) represents the reactions carried out in $scCO_2 + [EMIM][TF_2N]$ and symbol (\square) represents the reactions carried out in $scCO_2 + [EMIM][TFO]$	32
Figure 2-2. a) TGA thermogram and b) differential thermal gravimetric (DTG) curves of gel samples prepared in $scCO_2/[EMIM][TF_2N]$ (black line), $scCO_2/[EMIM][TFO]$ (red line), and $scCO_2$ (blue line). The heating rate is $10\text{ }^\circ\text{C}\cdot\text{min}^{-1}$	35
Figure 2-3. a) XRD pattern of gel product prepared in $scCO_2$ (blue line), in $scCO_2 + [EMIM][TFO]$ (red line), and in $scCO_2 + [EMIM][TF_2N]$. symbol of (*) represents the vanadyl diacetate peaks b) one-dimensional chain of VO_6 octahedra in vanadyl diacetate.[46]	36
Figure 2-4. XPS survey analysis of sample which is prepared in a) $scCO_2$ only 27.6 MPa at $60\text{ }^\circ\text{C}$, b) $scCO_2/[EMIM][TF_2N]$ 27.6 MPa at $60\text{ }^\circ\text{C}$ and c) $scCO_2/[EMIM][TFO]$ 27.6 MPa at $60\text{ }^\circ\text{C}$	37
Figure 2-5. XPS spectra of the products prepared in a) $scCO_2$ b) $scCO_2/[EMIM][TF_2N]$ c) $scCO_2/[EMIM][TFO]$ at 27.6 MPa and $60\text{ }^\circ\text{C}$. Black line represents $V_{2p\ 3/2}\ V(V)$, red line represents $V_{2p\ 3/2}\ V(IV)$, blue line represents $V_{2p\ 1/2}\ V(V)$ and green line represents $V_{2p\ 1/2}\ V(IV)$	38
Figure 2-6. XRD pattern of the product prepared in $scCO_2/[EMIM][TF_2N]$ prepared at a) $40\text{ }^\circ\text{C}$, b) $60\text{ }^\circ\text{C}$ and c) $80\text{ }^\circ\text{C}$ at a constant pressure of 27.6 MPa and after one hour annealing. XRD pattern of the product prepared in $scCO_2/[EMIM][TF_2N]$ at d) $40\text{ }^\circ\text{C}$, e) $60\text{ }^\circ\text{C}$ and f) $80\text{ }^\circ\text{C}$ at a constant pressure of 27.6 MPa and after two hours. Symbol (α) represents peaks of V_2O_3 , symbol (*) represents peaks of $VO_2(M)$, and symbol (Δ) represents peaks of V_4O_7	41

Figure 2-7. DSC curves of product prepared in $scCO_2$ / [EMIM][TF₂N] prepared a) 40 °C, b) 60 °C and c) 80 °C at constant pressure of 27.6 MPa and after one hour annealing. DSC curves of product prepared in $scCO_2$ / [EMIM][TF₂N] prepared at d) 40 °C, e) 60 °C and f) 80 °C at constant pressure of 27.6 MPa and after two hours. Curve b) shows peaks of 60 °C on cooling cycle and 73 °C on heating cycle and curve d) shows peaks at 50 °C on cooling cycle and 66 °C on heating cycle..... 42

Figure 2-8. XRD pattern of the product prepared in $scCO_2$ / [EMIM][TF₂N] prepared at a) 27.6 MPa, b) 34.5 MPa and c) 41.4 MPa at a constant temperature of 40 °C and after one-hour annealing. XRD pattern of the product prepared in $scCO_2$ / [EMIM][TF₂N] prepared at d) 27.6 MPa, e) 34.5 MPa and f) 41.4 MPa at a constant temperature of 40 °C and after two hours. Symbol (⌘) represents peaks of V₂O₃ symbol (*) represents peaks of VO₂ (M)..... 43

Figure 2-9. DSC curves of product prepared in $scCO_2$ / [EMIM][TF₂N] prepared at a) 27.6 MPa, b) 34.5 MPa and c) 41.4 MPa at a constant temperature of 40 °C and after one-hour annealing. DSC curves of [EMIM][TF₂N] ionogel prepared at d) 27.6 MPa, e) 34.5 MPa and f) 41.4 MPa at a constant temperature of 40 °C and after two hours. Curve d) shows peaks of 50 °C on the cooling cycle and 66 °C on the heating cycle and curve f) shows peaks at 48 °C on the cooling cycle and 66 °C on the heating cycle. 44

Figure 2-10. XRD pattern of the product prepared in $scCO_2$ at a) 40 °C, b) 60 °C and c) 80 °C at a constant pressure of 27.6 MPa and after one-hour annealing. XRD pattern of the product prepared in $scCO_2$ at d) 40 °C, e) 60 °C and f) 80 °C at a constant pressure of 27.6 MPa and after two hours. Symbol (⌘) represents peaks of V₂O₃, symbol (*) represents peaks of VO₂ (M). 45

Figure 2-11. XRD pattern of the product prepared in $scCO_2$ at a) 27.6 MPa, b) 34.5 MPa and c) 41.4 MPa at a constant temperature of 40 °C and after one-hour annealing. XRD patterns of the product prepared in $scCO_2$ at d) 27.6 MPa, e) 34.5 MPa and f) 41.4 MPa at a constant temperature of 40 °C and after two hours. Symbol (⌘) represents peaks of V₂O₃, symbol (*) represents peaks of VO₂ (M)..... 46

Figure 2-12. SEM images of vanadium oxide prepared in: a) in biphasic [EMIM][TF₂N]/ $scCO_2$ at 60 °C and 27.6 MPa and after 1 h calcination (sample 1) b) in [EMIM][TF₂N] at 60

°C and ambient pressure and after 2h calcination (sample 2) c) in scCO₂ at 80 °C and 27.6 MPa and 1 h calcination (sample 3) d) in biphasic [EMIM][TFO]/ scCO₂ at 60 °C and 27.6 MPa and after 2 h calcination (sample 4)..... 48

Figure 2-13. UV-Vis-NIR transmittance spectra of (a) Sample 1 (b) Sample 2 (c) Sample 3 (d) Sample 4, at the measurement temperature of 25 °C (black line), and at 90 °C (red line) 50

Figure 3-1. a) Chemical structure of vanadium acetylacetonate, VO(acac)₂, b) Electronic energy level of vanadium acetylacetonate, VO (acac)₂. 58

Figure 3-2. UV-Vis spectrum of VO(acac)₂ in methanol solution after different aging times. 59

Figure 3-3. UV-Vis spectrums of VO(acac)₂ methanol solution with a) volume ratio of MeOH: [EVIM][TFSI]= 20, b) volume ratio of MeOH: [EVIM][TFSI]= 1, c) volume ratio of MeOH: [EVIM][TFSI]= 0.2. 61

Figure 3-4. UV-Vis spectrums of VO(acac)₂ methanol solution with a) volume ratio of MeOH: [EMIM][TFO] = 20, b) volume ratio of MeOH: [EMIM][TFO] = 1, c) volume ratio of MeOH: [EMIM][TFO] = 0.2. 62

Figure 3-5. UV-Vis spectrums of VO(acac)₂ methanol solution with a) volume ratio of MeOH: [EMIM][AcO] = 20, b) volume ratio of MeOH: [EMIM][AcO] = 1, c) volume ratio of MeOH: [EMIM][AcO] = 0.2 64

Figure 3-6. a) XRD patterns of samples before and after annealing at different temperatures and duration, b) DSC Curve of the sample after annealing at 400°C for 10 minutes..... 66

Figure 3-7. a) Transmission spectra of VO₂ film at 30°C and 85°C b) Hysteresis loop characteristic analysis of VO₂ film c) Optical calculations of VO₂ film 68

Figure 4-1. XRD patterns of hydrothermal samples prepared at 200 °C -250 °C for different reaction times. (*) symbol represents V₃O₅ and symbol (□) represents VO₂ (B)..... 78

Figure 4-2. XRD patterns of samples at different annealing conditions; the annealing temperature varies from 400 °C to 500 °C and the annealing time varies from 30 minutes to 4 hours. Symbol (↓) represents VO ₂ (M).....	79
Figure 4-3. DSC curves of samples after various annealing conditions.	80
Figure 4-4. SEM images of samples after annealing a) at 500 °C for 60 minutes b) at 500 °C for 30 minutes c) at 400 °C after 120 minutes d) at 400 °C after 240 minutes	82
Figure 4-5. DSC curves of VO ₂ nanorods samples with 0.3, 1.2, and 2.1 atm% Mo.....	84
Figure 4-6. EDX of Mo-doped VO ₂ (M)	85
Figure 4-7. SEM images of a) VO ₂ (M) with 0.6 atm% Mo before annealing treatment b) VO ₂ (M) with 0.6 atm% Mo after annealing treatment c) VO ₂ (M) with 0.3 atm% before annealing treatment d) VO ₂ (M) with 2.13 atm% after annealing treatment.	86
Figure 4-8. XRD patterns of VO ₂ -SiO ₂ nanostructures upon increasing the different volume of the TEOS.....	87
Figure 4-9. FTIR spectra of monomer IL, monomer and crosslinker (CL) and PIL samples as a function of the crosslinker molar percentage.	91
Figure 4-10. UV-Vis-NIR transmittance spectra of a) VO ₂ -PIL and VO ₂ /SiO ₂ - PIL prepared by solution casting b) VO ₂ -PIL and VO ₂ /SiO ₂ - PIL prepared by UV-curing.	93
Figure 4-11. FTIR of UV-Cured film in range of a) 600 cm ⁻¹ - 4000 cm ⁻¹ b) 1400 cm ⁻¹ - 3500 cm ⁻¹ (Zoomed in).	94

List of Scheme

Scheme 2-1. Chemical structure of ILs examined in this work: a) 1-ethyl 3 methylimidazolium bis (trifluoromethansulfonylimide) ([EMIM][TF2N]), b) 1-ethyl 3-methyl imidazolium trifluoromethanesulfonate ([EMIM][TFO]), c) 1-ethyl 3-methyl imidazolium hydrogen sulfate ([EMIM][HSO ₄]), d) 1-ethyl 3-methyl imidazolium acetate ([EMIM][AcO]).	27
Scheme 3-1. Chemical structure of ILs examined in this work: a) 1-ethyl 3 vinyl imidazolium bis (trifluoromethansulfonylimide) ([EVIM][TFSI]), b) 1-ethyl 3-methyl imidazolium trifluoromethanesulfonate ([EMIM][TFO]), c) 1-ethyl 3-methyl imidazolium acetate ([EMIM][AcO]).	55
Scheme 3-2. a) procedure to prepare 1-ethyl-3-vinyl imidazolium bromide b) to prepare 1-ethyl-3-vinyl imidazolium bis(trifluoromethanesulfonylimide)	56
Scheme 3-3. Polymerization procedure to prepare poly (1-ethyl-3-vinyl imidazolium bis(trifluoromethanesulfonylimide))	57
Scheme 4-1. Reaction scheme to prepare 1-ethyl-3-vinyl imidazolium bromide.	75
Scheme 4-2. Reaction scheme to prepare 1-ethyl-3-vinyl imidazolium bis(trifluoromethanesulfonylimide).	75
Scheme 4-3. Reaction scheme to prepare poly (1-ethyl-3-vinyl imidazolium bis(trifluoromethanesulfonylimide))	76

List of Appendices

Appendix A: ^1H NMR spectrum of 1-ethyl-3-vinyl imidazolium bis(trifluoromethanesulfonylimide) in DMSO- d_6	122
Appendix B: $^1\text{HNMR}$ spectrum of poly (1-ethyl-3-vinylimidazolium bis(trifluoromethanesulfonylimide)) in acetone- d_6	122

List of Abbreviations

IL	Ionic Liquid
PIL	Poly Ionic Liquid
TGA	Thermogravimetric analysis
XRD	X-ray powder diffraction
XPS	X-ray photoelectron spectroscopy
SEM	Scanning electron microscope
DSC	Differential scanning calorimetry
NMR	Nuclear magnetic resonance
FTIR	Fourier-transform infrared spectroscopy
PVD	Physical vapor deposition
CVD	Chemical vapor deposition
VTIP	Vanadium oxytriisopropoxide
VO ₂ (M)	Monoclinic vanadium oxide
PVP	Polyvinylpyrrolidone
EVA	Ethylene-vinyl acetate
ΔT_{sol}	Solar modulation efficiency
T_{lum}	Luminous transmittance
T_c	Transition temperature
<i>scCO</i> ₂	Supercritical CO ₂

Chapter 1

1 Introduction and Literature Review

One of the current mega challenges is on finding new and efficient ways to reduce energy usage while transitioning to clean energy sources. In Canada, the building sector is a significant consumer of energy in the form of electricity and natural gas. The building sectors, which combines Residential and Commercial/Institutional sectors, consume approximately 30% of Canada's Secondary Energy (Figure 1-1) (Office of Energy Efficiency 2013 report on Energy Efficiency Trends in Canada 1990-2010). Secondary energy includes resources that have been converted to other types of energy such as electricity while primary energy is unconverted or original fuels such as natural gas or coal.

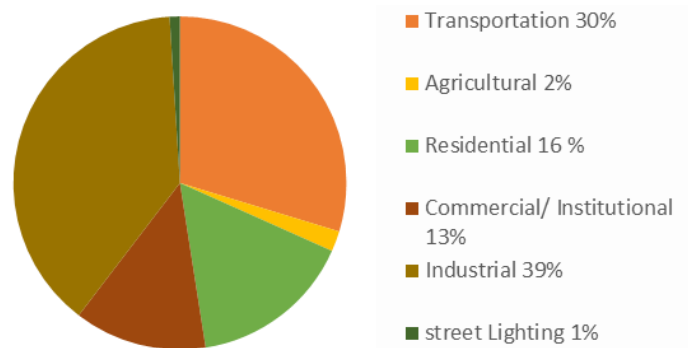


Figure 1-1. Total Secondary energy use by sector in Canada

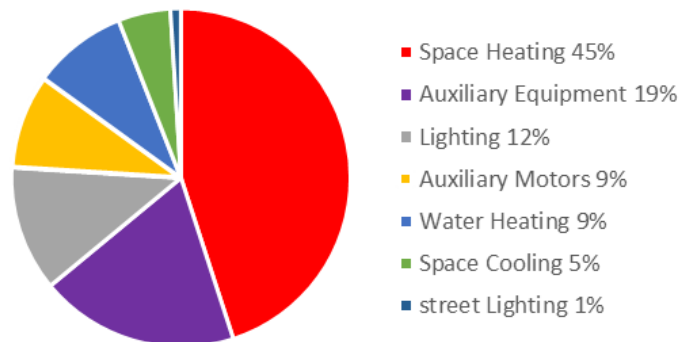


Figure 1-2. Commercial/ Institutional secondary energy use in Canada

Furthermore, space conditioning (space heating + space cooling) accounts for nearly half of the energy used in commercial and institutional operations (Figure 1-2). It is estimated that energy exchange through the windows is responsible for more than 50% of a building's energy loss[1]. For reducing energy consumption, energy-efficient walls or windows, especially smart windows, have attracted considerable interest. Studies have shown that smart windows can reduce energy consumption in buildings by up to 20 % during winter and more than 40 % during warmer seasons. Researchers at Lawrence Berkeley National Laboratory (LBNL) estimate that smart window technologies could save as much as 1 quadrillion BTUs of energy each year – more than 1 percent of the United States annual energy consumption, or more than \$10 billion in annual energy costs. Consequently, the tremendous growth of energy needs and high energy costs, are promoting demand for innovative products to develop energy efficiency in buildings. This contribution to the energy efficiency of the building sector offers a proven pathway to generate positive effects on Canada's economy and environment.

Various intelligent coatings have been investigated to be used as energy-efficient materials in buildings. In terms of energy efficiency, two types of radiation flux should be regulated by windows: the longwave thermal radiation emitted at normal temperature and the solar radiation by the sun. “Low Emittance (low- E) Windows” and “Chromogenic Windows” are two typical energy-efficient windows for passive control of longwave thermal radiation and solar energy throughput. Low- E windows contain a coating film with low emissivity aimed to transmit visible light while blocking infrared (IR) and ultra-violet (UV) wavelengths which generally create heat[2,3]. Therefore, the long-wave thermal radiation from the outdoor environment cannot enter the room in the summer, and the thermal radiation from indoor surfaces cannot escape the room in the winter resulting in lower energy consumption during both seasons (Figure 1-3).

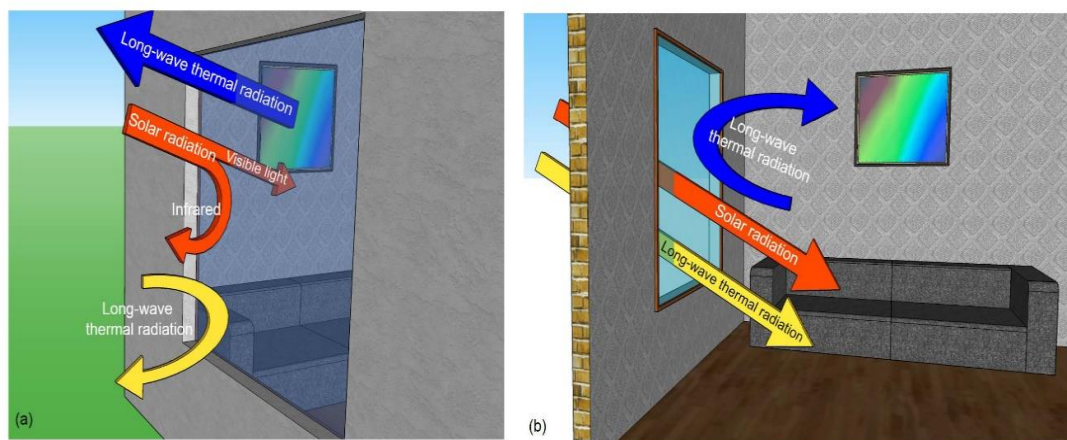


Figure 1-3. Diagrammatic sketch of ideal windows. The ideal windows for (a) summer and (b) winter are shown. The orange arrows represent solar radiation, the yellow arrows represent long-wave thermal radiation emitted by the outdoor environment, and the blue arrows represent the long-wave thermal radiation emitted by indoor surfaces[3] Reprinted with the permission of Scientific Report Journal

There are two types of Low-E coatings, i.e. tin oxide-based hard coatings and silver-based soft coatings, both of which are high reflectance materials that can attenuate the propagation of IR radiation[2,4]. On the other hand, chromogenic windows are those that can change their optical properties due to some external stimulus. Thermochromic, photochromic and electrochromic materials are the most common types of chromogenic materials in which the stimuli are a change in temperature, irradiation by light, and an applied field respectively[5]. Thermochromic windows are those that exhibit temperature-dependent changes in the optical properties of a material. Continuous thermochromism involves a gradual color change over a range of temperatures while discontinuous thermochromism refers to a structural phase change at a specific temperature which is called the transition temperature[6]. The phase change can be first-order or second-order, reversible, or irreversible depending on their thermodynamics.

The thermochromic coatings which are widely used as intelligent window coatings have a transparent state with a higher solar transmittance when the temperature of the window is below the transition temperature (T_c); consequently, the solar radiation and associated heat will reach the interior of the building. On the other hand, thermochromic coatings have an opaque state with a lower solar transmittance when the temperature of the window is above T_c , where part of the energy from the sun will be reflected due to the higher material's IR reflectance[5,7,8]. Therefore, thermochromic windows have the potential to have excellent energy performance as the heat gain from solar radiation will be high in winter and much lower in summer, resulting in a reduction of energy consumption in space conditioning. Vanadium dioxide (VO_2) is one of the most promising thermochromic materials with a transition temperature of about 68 °C for its pure single crystalline form. The optical properties of vanadium oxide change suddenly and reversibly at its transition temperature (T_c) due to a first-order metal-insulator transition [9].

1.1 Vanadium Oxide (VO_2)

Vanadium oxides (VO_2) is representative of a binary compound with a variety of crystal structures including monoclinic VO_2 (B), monoclinic VO_2 (M), rutile VO_2 (R), tetragonal VO_2 (A), orthorhombic VO_2 (C)[10], and recently added VO_2 (D). Among all VO_2 polymorphs, monoclinic VO_2 (M) is the most important structure as it shows a reversible first-order metallic-insulator transition (MIT) at a specific transition temperature of 68 °C. VO_2 (M) is an insulator and IR transparent while at the temperatures above T_c , VO_2 (M) is changed to VO_2 (R) which is metallic and highly IR reflective (Figure 1-4). It should be noted that the pure monoclinic VO_2 phase is referred to as M1 since doping of vanadium (IV) oxide results in another monoclinic arrangement which is called M2. The nature of the metallic to insulator transition of vanadium oxide has been investigated via computational, experimental, and theoretical studies by many researchers[5]. However, the detailed mechanism of this transition is not exactly clear. Three VO_2 phases exhibit different crystal structures while they have the same electronic properties, such as the existence of the semiconductor-to-metal transition, similar activation energies, and conductivities based on the Mott–Hubbard model of correlating electrons[11].

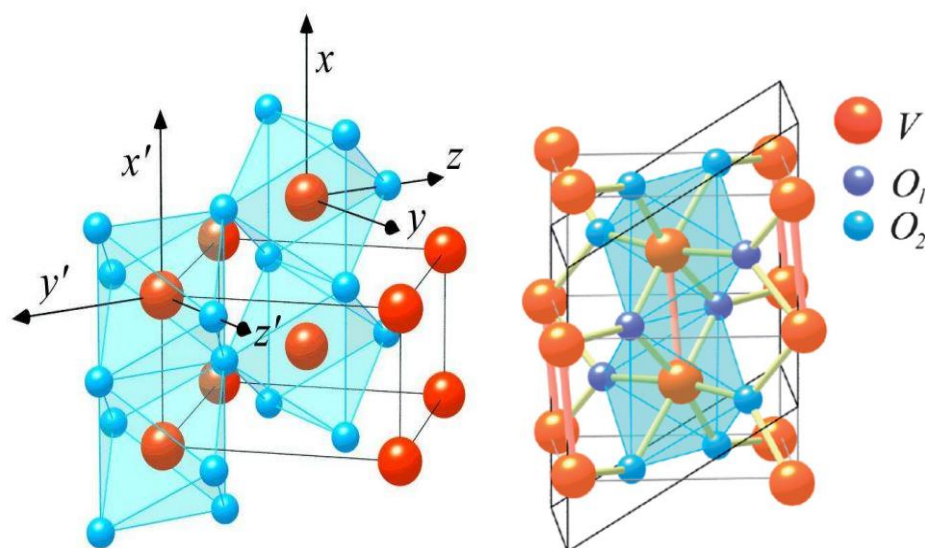


Figure 1-4. Left: The rutile structure of VO₂, when $T > T_c$. The large red circles represent V⁴⁺ ions, and the small blue circles are O₂⁻ ions, Right: The M1 monoclinic structure of semiconducting VO₂ when $T < T_c$. Two types of oxygen ions can be distinguished Reprinted with the permission of the Royal Society of Chemistry.

Goodenough[12] performed theoretical studies using molecular orbitals and band structure diagrams as is shown in Figure 1-5. He proposed the possibility of an anti-ferroelectric transition which causes the metallic-semiconductor transition in vanadium dioxide. It was argued that V⁴⁺-V⁴⁺ pairing in the tetragonal phase becomes energetically stable on cooling after the rearrangement of the band structure in making the monoclinic phase. Subsequently, there are two transition temperatures, T_c as the result of anti-ferroelectric distortion and T_c' due to the crystallographic distortion which happens to be synchronized for VO₂. It was concluded that the anti-ferroelectric component of the monoclinic low-temperature phase of VO₂ is the driving force for the distortion. T_c was found to be not controlled by thermal excitation of electrons into the antibonding bands but by the entropy of the lattice electrons into the antibonding bands of vibrational modes.

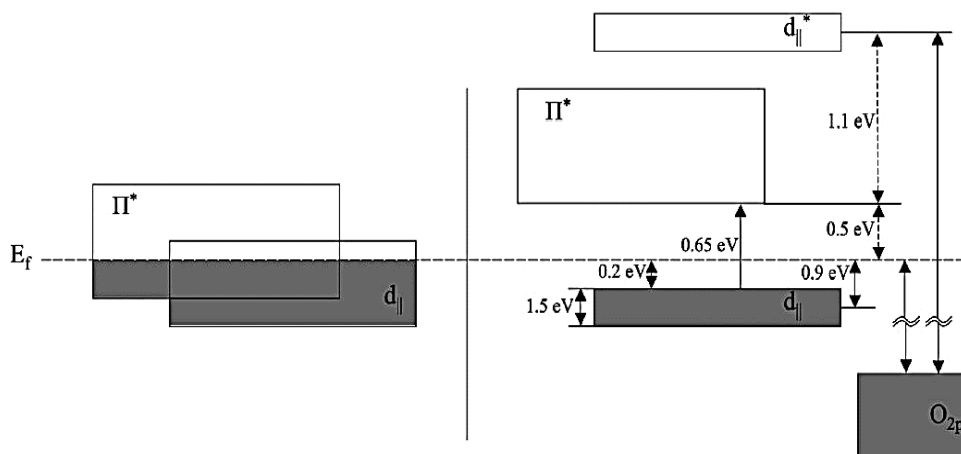


Figure 1-5. Schematic band structure diagram of VO₂. The hybridization of the V 3d and O 2p levels reflects the symmetries of the atomic arrangement in the crystal lattice[5,13]. Reprinted with permission of the Royal Society of Chemistry

The metallic-insulator transition is followed by a dramatic change in electrical conductivity and IR reflectivity in the NIR and with no change in the visible region [5]. The material reflects IR above T_c , but is transparent below T_c , which is crucial in applications such as thin-film coatings of “smart windows”. However, the critical temperature of VO₂, 68 °C, is considered too high (in comparison to room temperature) for smart thermochromic windows applications. Therefore, many efforts have been made to reduce the transition temperature of VO₂ by using different dopants[3].

1.2 Effect of Doping in Vanadium Dioxide (VO₂)

The ideal transition temperature for intelligent glazing is between 20 °C - 25 °C[3]. On the other hand, when the transition temperature is between 68 °C – 90 °C, VO₂ can be used in solar thermal applications[14]. Introducing impurities at sufficient levels into the VO₂ lattice can tune the thermochromic switching temperature, making the VO₂ more commercially viable.

There are various theories about the action of doping in VO₂ based on empirical observations and theoretical calculations. Goodenough[12] discussed in detail the doping effect based on x-ray diffraction observations proposing the existence of a second

semiconducting phase in doped samples between the low-temperature monoclinic phase and the high-temperature tetragonal phase. The semiconducting phase has an orthorhombic structure for low-valent dopant ions, and it has a rutile structure for high-valent ions. He then investigated different possible scenarios of doped VO₂ based on his theory of metal-insulator transition. Dopants that can participate through p-bonding, not the d bonds (e.g. Al³⁺, Ti⁴⁺, d0), decrease the crystallographic transition temperature. However, dopants that introduce electrons to the vanadium d bands (e.g. Mo⁶⁺, W⁶⁺, Nb⁵⁺) reduce the antiferroelectric stabilization of the low-temperature phase by introducing P* electrons into the antiferroelectric state. Subsequently, the antiferroelectric transition temperature T_c can be reduced. Furthermore, McChesney and Guggenheim reported that dopants with an ionic radius smaller than V⁴⁺ can increase the transition temperature while dopants with a larger ionic radius than V⁴⁺ decrease the transition temperature[15].

Various metal ions have been doped into the VO₂ lattice using different methods including physical vapor deposition (PVD)[16], chemical vapor deposition (CVD)[17], sol-gel[18], and hydrothermal methods[19]. Extensive studies have been conducted using tungsten as a dopant to reduce the thermochromic switching temperature of VO₂. Substitutional doping with tungsten on average depresses both the metal to insulator and insulator to metal phase transition temperature by 23-26 °C/ at. % W[20]. For all methods of preparation, approximately 2 atom % W doped into vanadium dioxide films have shown a thermochromic temperature of 25 °C, which is ideal for intelligent window coatings[5].

Even though tungsten can reduce the thermochromic switching temperature of VO₂ by the greatest extent per atom%, several other dopants can be incorporated into vanadium dioxide including molybdenum, niobium, and gold or co-doping of molybdenum and tungsten[21]. Molybdenum (Mo) dopants cause a relatively smaller depression of phase transition temperature compared to tungsten dopants. However, the local symmetry around Mo atoms is closely related to the high-temperature rutile phase compared to the low-temperature monoclinic phase. This suggests a structural contribution of Mo atom to the depression of the transition temperature[22]. Indeed, the Mo atom not only adds electrons to the vanadium dioxide band structure but also serves as a seed for nucleation of the high-temperature metallic phase[19].

Furthermore, it has been reported that the effects of doping are substantially amplified upon scaling to nanoscale dimensions as tungsten doping within nanowires induces an 80 °C/ at. % W depression in the phase transition temperature within a linear regime ranging up to 0.90 at. % doping.[23] As was also noted, the influence of Mo doping is not as much as W doping, although a remarkable depression in transition temperature was noted from 20 - 29 °C/at. % Mo using vanadium oxide nanowires.

1.3 Synthetic Techniques to Synthesize VO₂ (M)

There are various synthetic methods to synthesize monoclinic vanadium oxide. However, to have an economical and environmentally friendly process, it is necessary to synthesize VO₂ at low temperatures and durations using inexpensive and nontoxic precursors and environmentally friendly solvents.

Thin-film formation by the sol-gel technique has been widely used[21,24,25] for depositing thermochromic VO₂ thin films due to the simplistic nature of this method. The sol-gel method involves the formation of thin films by dip or spin coating substrates using metal alkoxide solutions[8]. To synthesize crystalline VO₂, the initial coating is partially hydrolyzed and then annealed in a reducing atmosphere. The most common precursors for sol-gel method preparation of VO₂ are vanadyl tri(isopropoxide) and vanadyl tri(tertamyloxiide)[5]. Furthermore, Yin et al.[26] also indicated that V₂O₅ can be used as a precursor instead of vanadium alkoxide in a sol-gel process as it is cheap and easy to obtain, and the sol made by the quenching method is stable. Dopants such as tungsten[27] and molybdenum[21] can also be introduced in the precursor solution in the necessary proportion.

Physical Vapor Deposition (PVD) has gathered great interest in depositing thermochromic VO₂ film[5,8]. The technique involves the four steps of evaporation, transportation, reactions, and deposition. The material to be deposited is known as a target which is usually a solid-state metal precursor that is bombarded by a high energy source under reduced pressure conditions. Under these conditions, the atoms or molecules are displaced or vaporized from the surface of the metal target. The quantity of material removed from the target and the quantity of gas present in the deposition chamber can be used to control the

composition of the thin film on the glass. There are various systems employed to remove atoms from the target to prepare VO₂ films including laser ablation[28], magnetic sputtering[29], or ion beam sputtering[30]. Doping can also be done by ion implantation on the substrate in the deposition chamber. However, the PVD method is an expensive process due to the reduced pressure and vacuum conditions and expensive evaporation/sputtering/ablation equipment[8].

The Chemical Vapor Deposition (CVD) method and especially the Atmospheric Pressure Chemical Vapor Deposition (APCVD) is a common industrial process for the production of VO₂ thin films by using organometallic precursors[5,8]. In the CVD process, the substrate is exposed to a volatile precursor that reacts on the substrate surface to produce the desired deposit. Vanadyl tri(isopropoxide) or vanadyl tri(isobutoxide) are common precursors for CVD of VO₂ films[31]. Vanadyl acetylacetonate, VO(acac)₂ has also been used as a precursor to prepare VO₂ (B), which can then be converted to VO₂ (M) by annealing under a controlled atmosphere[32].

Recently, the hydrothermal method for the synthesis of VO₂ has garnered significant attention due to its relatively simple route, low cost, and large scale production compared to other synthetic methods[10,33,34]. Hydrothermal synthesis is generally defined as crystal synthesis or crystal growth under high temperature and high-pressure water conditions[5,8]. Vanadium pentoxide (V₂O₅) is commonly used as the precursor for the hydrothermal process. Hydrogen peroxide (H₂O₂), ethanol, and oxalic acid have also been used as reducing agents during the process to produce VO₂ with different morphologies. Different dopants can be introduced into the solution at the beginning of the process with appropriate compositions to reduce the transition temperature[21,35].

Although all the mentioned synthetic strategies including sol-gel, PVD, and hydrothermal methods can be used to prepare VO₂ nanostructures, the variation of synthetic parameters can have a considerable effect on morphology and crystallinity of nanostructures, strengths of the metal-insulator phase transition, and extents of hysteresis.

1.4 Using supercritical CO₂ in the sol-gel synthesis of metal oxides

supercritical carbon dioxide (scCO₂) has been used as an environmentally friendly solvent in a sol-gel process instead of common conventional solvents for the synthesis of metal oxide nanostructures[36–39]. The phase diagram of the carbon dioxide has been shown in the Figure 1-6. The sol-gel precursors such as alkoxides are often chosen in this technique due to their ability to dissolve in scCO₂. The sol-gel precursors under a high-pressure reactor are converted into sol via polycondensation reactions. The sol can either form aerogel particles by depressurization or can be used for the formation of gel solid networks [38]. The aerogel particles normally have larger dimensions than the sol as a result of aggregation steps whereas the aerogel monolith maintains the size and shape of the original gel. ScCO₂ is considered an environmentally benign solvent and a substitute for conventional organic solvents as it is nontoxic, nonflammable, inexpensive, and naturally abundant[40]. Another advantage of using scCO₂ is that by ‘tuning’ the temperature and pressure during the process, the solvent physical properties such as density and solubility ability can be altered to produce various product structures. Additionally, isolating the product by venting the CO₂ after the reaction leads to maintaining the microstructure of the aerogel.

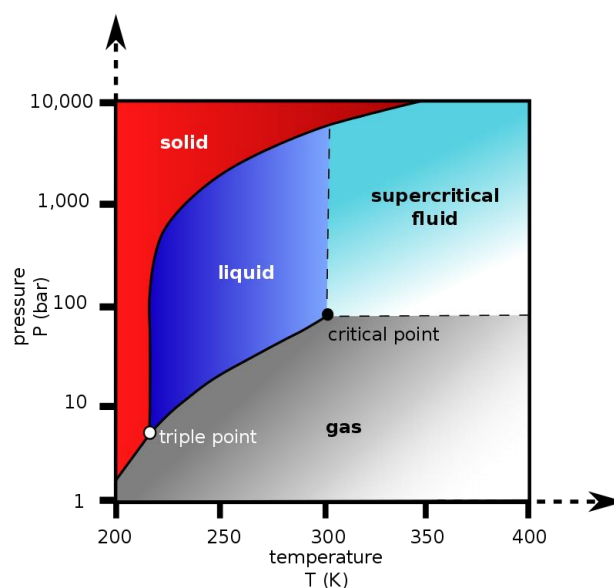


Figure 1-6. Carbon dioxide temperature- pressure phase diagram

1.5 Stability of Vanadium (IV) Oxide

1.5.1 Chemical Stability of VO₂

VO₂ films have poor long-term oxidation resistance in a wet ambient atmosphere due to the thermodynamical instability of VO₂. It has been reported that VO₂ can gradually be oxidized into V₂O₅ when exposed to the air for a long time, which leads to considerable deterioration of its thermochromic properties[41]. Therefore, enhancing the chemical stability of VO₂ against oxidation is urgently required. In one successful method, the VO₂ nanostructure can be coated with an inert barrier shell to form a core-shell structure. The core-shell VO₂@TiO₂ nano-rods[41] and VO₂@SiO₂ nanoparticles[42] have been fabricated showing enhanced chemical stability. More recently, L. Zhao et al.[43] indicated that VO₂-SiO₂ composite film showed higher chemical stability against oxidation compared to VO₂ film.

1.5.2 Agglomeration of VO₂ Nanostructures

Agglomeration of VO₂ nanostructures is another obstacle for the preparation of uniform VO₂ nanostructures. Agglomeration can happen during the gel formation stage in a sol-gel method or during a post-heating process in the hydrothermal method due to the sintering effect[44,45]. Modification of VO₂ nanostructures surface with a layer of inert capping layers such as SiO₂ or TiO₂ can eliminate the agglomeration issue[44,45]. X. Cao et al.[46] also reported that using freeze-drying in the fabrication of VO₂ nanoparticles largely hinders agglomeration.

1.5.3 Polymer-Based Coatings

Another effective method to prevent VO₂ nanostructures from agglomeration is the dispersion of particles in a polymer solution. Various transparent polymers such as polyvinyl pyrrolidone (PVP)[47] and polyvinyl alcohol (PVA)[48] have been used for the modification of VO₂ films. It also has been shown that vanadium precursors can be stabilized in PVP polymer solution via interactions among polymers and V⁴⁺ aqua ions. L. Kang et al.[47] used different polymers such as PVP, polyacrylamide (PAM), and poly(N-vinyl acetamide) (PNVA) for the synthesis of thermochromic VO₂ thin films. It was

indicated that the polymer additive can be used as a film forming promoter due to the formation of a cross-linked gel film via the interactions of oppositely charged functional groups of polymer molecules with VO_2^+ . Furthermore, PVP additives could help induce the formation of M/R-phase VO_2 , which was attributed to an overlap of the crystallization temperature of VO_2 with the degradation temperature of PVP. The prepared films showed excellent optical properties by T_{lum} of 54.5 % and ΔT_{sol} of 41.5 % due to the dielectric matrix provided as a result of addition of PVP.

1.6 Optical Properties Measurement

Incident light can interact with matter in three modes: it can transmit, reflect, or absorb. These processes must obey the energy conservation law (Equation 1) at each wavelength:

$$T(\lambda) + R(\lambda) + A(\lambda) = 1 \quad (1)$$

where λ is the wavelength and $T(\lambda)$, $R(\lambda)$ and $A(\lambda)$ refer to the wavelength-dependent transmittance, reflectance, and absorbance, respectively. However, the part of absorbed energy that will heat the material is known as the thermal emittance, which is defined based on Kirchhoff's law (Equation 2):

$$A(\lambda) = \varepsilon_{therm}(\lambda) \quad (2)$$

where $\varepsilon_{therm}(\lambda)$ is the wavelength-dependent thermal emittance, which is defined as the fraction of blackbody radiation released at a certain temperature and wavelength.

As described above, VO_2 based coatings are a semiconductor and fairly IR transparent at $T < T_c$, whereas they are metallic and IR reflecting at $T > T_c$. Hence, they can offer smartness and energy efficiency features to the window by controlled lighting and heat control. The wavelength-dependent luminous transmittance (T_{lum}), reflectance (R_{lum}), solar transmittance (T_{sol}) and reflectance (R_{sol}) are the characteristic features of thermochromism which can be defined as [7,49]:

$$T_{lum,sol}(\lambda, \tau) = \frac{\int \varphi_{lum,sol}(\lambda) T(\lambda, \tau) d\lambda}{\int \varphi_{lum,sol}(\lambda) d\lambda} \quad (3)$$

$$R_{lum,sol}(\lambda, \tau) = \frac{\int \varphi_{lum,sol}(\lambda) R(\lambda, \tau) d\lambda}{\int \varphi_{lum,sol}(\lambda) d\lambda} \quad (4)$$

where τ is the temperature, φ_{lum} is the luminous efficiency of the human eye, and φ_{sol} is the solar irradiance spectrum corresponding to the sun standing 37° above the horizon.

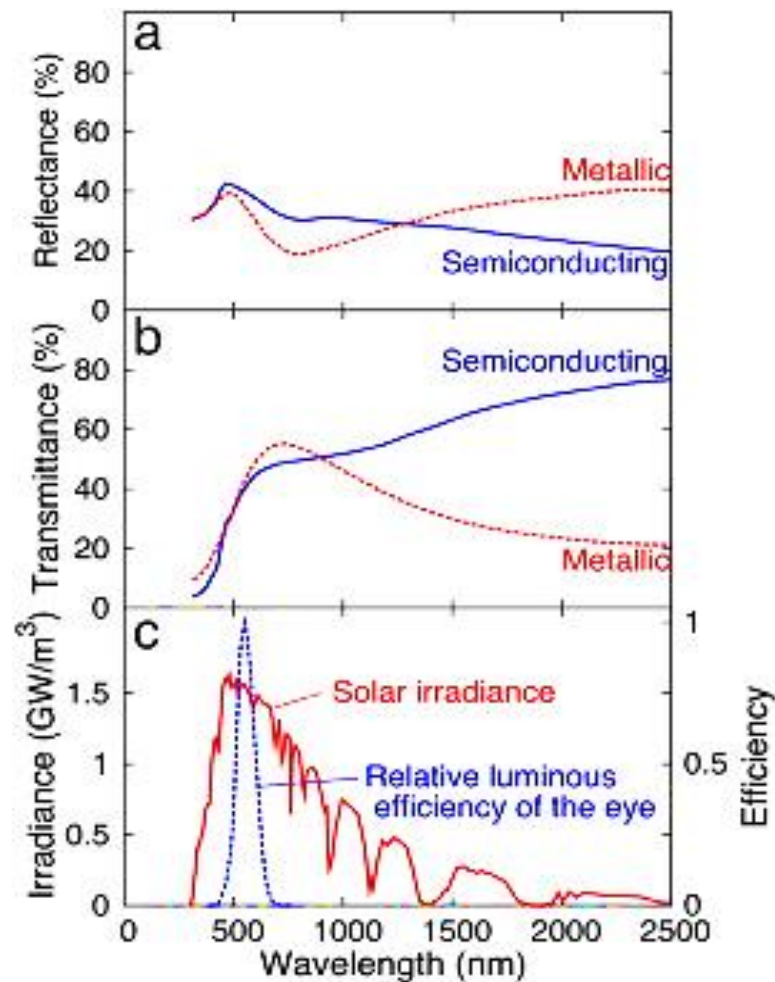


Figure 1-7. Spectral reflectance (a) and transmittance (b) for a 0.05- μm -thick VO_2 film in semiconducting and metallic states. Panel (c) illustrates typical spectra for the luminous efficiency of the human eye and solar irradiance[7,50,51]. Reprinted with the permission of Elsevier.

Figure 1-7 (a) and (b) indicate the typical spectral reflectance (R_{sol}) and transmittance (T_{sol}) expected from a 50 nm thick VO_2 film on a glass substrate at 22°C (blue line) and 100°C

(red line)[7]. As shown, the optical properties at short wavelength are similar at both temperatures, while the IR reflectance is higher at $\lambda > 1 \mu\text{m}$ for $\tau > \tau_c$ than for $\tau < \tau_c$, indicating the metal insulator transition. As shown in Figure 1-7 (c), the spectral sensitivity of the human eye, ϕ_{lum} , is extended in the $0.4 < \lambda < 0.7 \mu\text{m}$ wavelength range and the solar irradiance spectrum is in the range of $0.3 < \lambda < 3 \mu\text{m}$ for an air mass of 1.5 (corresponding to the sun standing 37° above the horizon)[7].

There are two properties of thermochromic VO₂ films that can limit their application as energy-efficient glazing[3]:

- (i) The solar transmittance modulation (ΔT_{sol}) is used to evaluate the thermochromic switching performance of VO₂ films which is not usually larger than 10 %.

$$\Delta T_{sol} = T_{sol}(\tau < \tau_c) - T_{sol}(\tau > \tau_c) \quad (5)$$

- (ii) The luminous transmittance (T_{lum}) is usually less than 40 % for the films with high ΔT_{sol} .

There is a current challenge to improve both T_{lum} and ΔT_{sol} by an economical method. Studies have shown that some dopants such as Mg²⁺ and F⁻ can increase the visible transmittance by widening the bandgap of VO₂ and lowering the visible absorption and inducing a blue-shift of the absorption edge[52,53]. Furthermore, VO₂ nanocomposites offer much higher luminous transmittance combined with significantly enhanced solar energy transmittance modulation compared to a VO₂ continuous film[54]. Optical calculations show that increasing amounts of pores with air in VO₂ films is the other component that can improve ΔT_{sol} without decreasing T_{lum} resulting in a better optical performance of the film[55,56]. The optical properties of the VO₂ film can be improved by increasing the film thickness as the result of enhancement in ΔT_{sol} ; however, the optimized film thickness is required to avoid the depression of T_{lum} (Figure 1-8)[56].

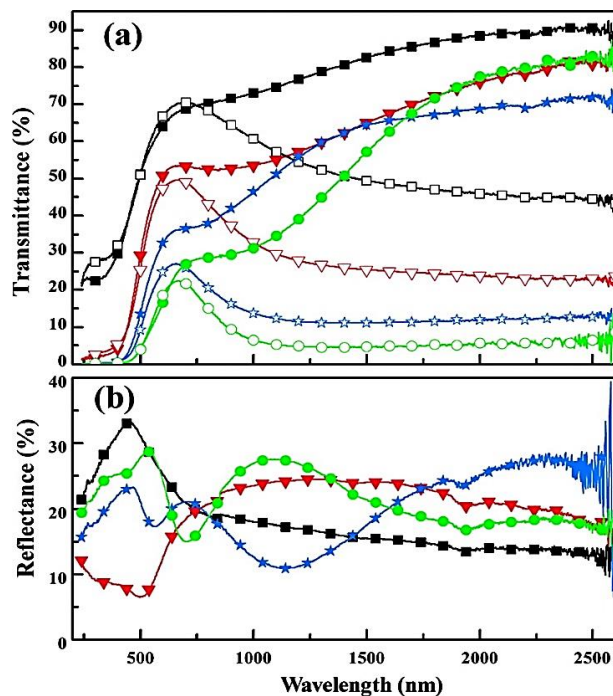


Figure 1-8. Thickness dependence of (a) transmittance and (b) reflectance spectra for typical samples with different thicknesses (43 nm, 102 nm, 215 nm, and 428 nm corresponding to the black squares, the red triangles, the blue pentagrams, and the green circles, respectively). The transmittance was measured at both 20 °C (lines with solid symbols) and 90 °C (lines with open symbols) and the reflectance was measured at only 20 °C[56]. Reprinted with permission of the American Chemical Society.

Another method to enhance T_{lum} is the deposition of a single or multi-layered anti-reflection (AR) layer with high reflective index dielectric materials (such as TiO_2 , SiO_2 , and ZrO_2)[57,58]. However, this method requires an additional heating process that affects the crystallinity of VO_2 and the presence of the AR layer usually decreases the switching efficiency (ΔT_{sol})[43]. Mlyuka et al.[59] prepared a five-layer $TiO_2/VO_2/TiO_2/VO_2/TiO_2$ film which showed relatively high luminous transmittance ($T_{lum} = 45\%$) but moderate solar modulation ($\Delta T_{sol} = 12\%$) which is the best results compared to single-layer VO_2 film ($T_{lum} = 41.0\%$, $\Delta T_{sol} = 6.7\%$)[59] and double-layered TiO_2/VO_2 film ($T_{lum} = 46.0\%$, $\Delta T_{sol} = 7\%$)[60].

Furthermore, it was reported that VO₂ nanoparticles embedded in a dielectric medium can be considered as an “effective medium”[61] and the optical properties are intermediate between those of nanoparticles and their matrix. The effective dielectric function (ϵ^{MG}) can be shown as the following[7]:

$$\epsilon^{MG} = \epsilon_m \frac{1 + \frac{2}{3}f\alpha}{1 - \frac{1}{3}f\alpha} \quad (6)$$

where ϵ_m is the dielectric permeability of the matrix and f is the filling factor i.e. the volume fraction which is occupied by particles. The filling factor for VO₂ film with a thickness of 5 μ m is 0.01 and ϵ_m is usually set to 2.25, presuming that there are no strong near IR absorption bands in the embedding medium such as glass or polymer. There are many effective medium formulations applicable to different nano-topologies. Specifically, equation 6 is appropriate for a topology with nanoparticles dispersed in a continuous matrix based on the Maxwell-Garnett (MG) theory[62]. It should be noted that nanoparticle clustering is disregarded in this equation. The parameter α is expressed as:

$$\alpha = \frac{\epsilon_p - \epsilon_m}{\epsilon_m - L(\epsilon_p - \epsilon_m)} \quad (7)$$

where ϵ_p is the dielectric function of the particles and L is the appropriate depolarization factor which is L= 1/3 for sphere particles.

Calculations have indicated that VO₂ nanostructures embedded in a transparent dielectric medium show much higher luminous transmittance combined with significantly enhanced solar energy transmittance modulation. This offers a new perspective to achieve desirable optical properties[54]. Li et al.[41] fabricated a core-shell VO₂@TiO₂ composite that exhibited thermochromic and photocatalytic properties with a solar efficiency of 10.3 % and luminous transmittance of 27 %. Gao et al.[42] prepared flexible VO₂ nanocomposite foils based on SiO₂/ VO₂ core-shell with an improved T_{lum} from 29.2% to 55.3 %, while ΔT_{sol} exhibited a decrease from 13.6 % to 7.5 %. There are also various reports about using SiO₂ either as a coating matrix or as a shell for VO₂ nanostructure. R. Li et al.[42] prepared thermochromic foils that were fabricated using VO₂@ SiO₂ core-shell nanoparticles,

showing a visible transmittance of 35.9 % and modulation ability of 8.4 %. More recently, VO₂-SiO₂ composite films were fabricated by L. Zhao[43], showing enhanced luminous transmittance ($T_{lum} = 48.5 \%$) as well as an increase in solar modulation ($\Delta T_{sol} = 15.7 \%$).

1.7 Using Ionic Liquids (ILs) in Fabrication of VO₂ Nanostructures

Ionic liquids (ILs) are molten salts with melting points typically below 100 °C. ILs possess a combination of outstanding properties such as non-volatility, thermo-oxidative stability, relatively high thermal stability, and high ion conductivity which can be tuned by changing the cation or anion counterpart[63]. F. Zhou first reported the excellent antioxidation properties of a series of imidazolium-based ILs as an additive for poly (ethylene glycol) for steel/steel contacts[64]. IL is an alternative candidate as a solvent for a sol-gel process[65,66]. It was shown that the anion counterpart of the IL has a significant role in catalyzing the reaction, hence reducing the gelation duration time [65,67]. Due to the wide range of properties of ILs, they have been investigated for several technologies including batteries[63,68], fuel cells[69], and dye-sensitized solar cells[70]. Some other desirable features of ILs such as high heat capacity make them excellent candidates for a new generation of heat storage materials[71]. Therefore, some specific properties of ILs such as transparency, high heat capacity, antioxidation properties, and their moderate-high dielectric constants draw our attention to their potential application as a modifier for VO₂ thermochromic coatings.

1.8 ILs' Heat Capacity and Optical Properties

For the fabrication of thermochromic VO₂ coatings, it is important to have a matrix to absorb the heat and light obtained from sunlight to help accelerate the optical switching process. Consequently, different polymers have previously been investigated as solar absorbing materials. However, it is important to have a transparent material as a coating to prevent any decrease in light transmission of the desired coating. Specific heat capacity is one of the factors indicating the quantity of heat which can be absorbed by one mole of a substance to raise its temperature by one degree. As shown in Table 1-1, imidazolium-based ILs have a much larger specific heat capacity compared to the polymers which have

been used in the existing coatings[72–74]. Furthermore, studies on optical properties of imidazolium-based ILs have shown that they are transparent in most of the UV region and are fully transparent in the visible and near IR region[75,76]. Therefore, the high heat capacity of ILs along with their transparency makes them a potential candidate to be used as a coating's modifier for thermochromic windows application.

Table 1-1. Specific Heat Capacity

Compound	Specific Heat Capacity (J/Mol. K)
Poly Vinyl Alcohol (PVA)	54.7[77]
1-methyl-3-tetradecylimidazolium bis(trifluoromethanesulfonyl)imide	680[74]
1-butyl-3-methylimidazolium bis(trifluoromethylsulfonyl)imide	567.33[74]

1.9 ILs' Dielectric Constant

As mentioned in section 1.4, VO₂ nanoparticles in dielectric hosts show enhanced luminous transmittance and solar energy transmittance based on effective medium theory. IL is an ionic compound with a relatively high dielectric constant, which has dipolar as well as an ionic contribution[78,79].

Table 1-2. Dielectric Constants

Compound	Dielectric Constant (ϵ)
Silicon Dioxide (SiO ₂)	3.9[80]
Titanium Dioxide (TiO ₂)	80[80]
1-ethyl-3-methylimidazolium bis(trifluoromethylsulfonyl)imide	12[78]
1-butyl-3-methylimidazolium bis(trifluoromethylsulfonyl)imide	14[78]
(2-hydroxyethyl) ammonium formate	61[78]
(2-hydroxyethyl) ammonium lactate	85.6[78]

Like other properties of ILs, their dielectric constants can be tuned over a wide range by varying the cation or anion. Replacement of highly symmetric anions with some dipolar anions can enhance the dielectric constant. Additionally, protic ILs show a higher value of dielectric constant than aprotic ILs. According to the dielectric constant data provided in Table 1-2, ILs can be great dielectric hosts for a new generation of thermochromic coatings.

1.10 ILs as Stabilizer of Nanoparticles

The synthesis of nanoparticles in ionic liquids has received considerable attention recently. There are several reports showing nanoparticles prepared in ionic liquids are mono-dispersed and non-agglomerated because of ionic liquid stabilization. The physiochemical properties of ionic liquids can directly affect the size and size distribution of the nanoparticles[81,82].

The most common mechanism for the stabilization of nanoparticles in ILs is the formation of an electrical double layer. For this layer, a solvation shell of anion surrounds the nanoparticle surface, followed by a less ordered layer of cations and so on (Figure 1-9)[81,83]. There is also some evidence regarding the stabilization of nanoparticles via interactions of nanoparticles with the imidazolium cation ring[84]. Furthermore, DFT calculations have been used to study the stabilization of nanoparticles in ILs showing the interaction of nanoparticles with different anion counterparts[85].

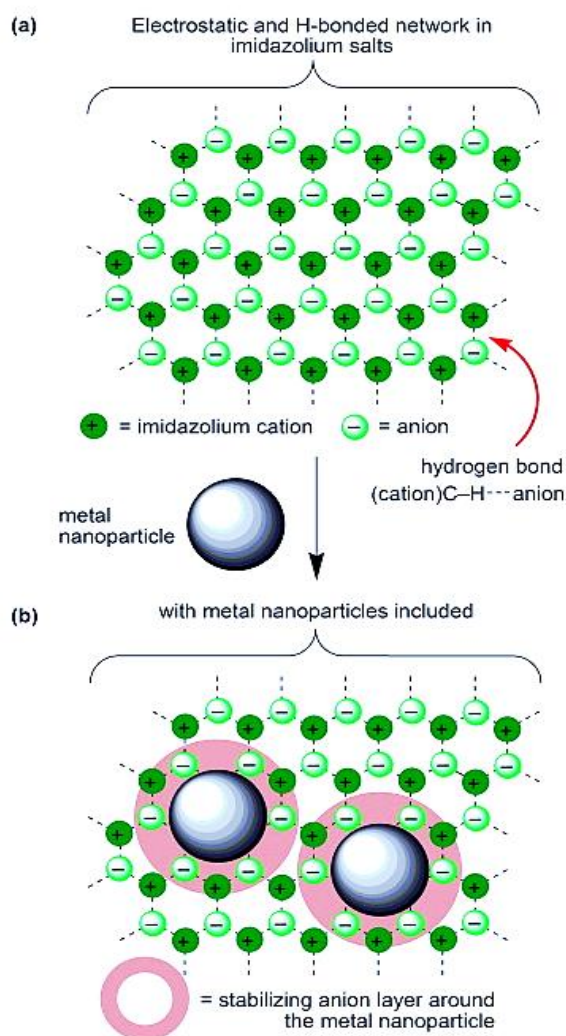


Figure 1-9. a) Schematic of inclusion of metal nanoparticles (M-NPs) in the supramolecular IL network with electrostatic and steric stabilization is indicated through the formation of a suggested primary anion layer around the M-NPs[83].

Reprinted with permission of the Royal Society of Chemistry

1.11 Poly Ionic Liquids (PILs)

Despite the ILs' properties as a potential coating for thermochromic materials, their liquid nature limits their application as a coating. Poly Ionic Liquids (PILs), which also are called polymerized ILs, are a new class of polymeric materials that feature IL species in each monomer repeating unit. PILs are attracting great interest, not only because of the

combination of the unique properties of ILs with the macromolecular architecture, but also a matter of amplifying the properties of ILs[86,87]. The main advantages of using a PIL instead of an IL are enhanced mechanical stability, improved processability, durability, and spatial controllability over the IL species[88]. Shen et al.[89] examined the dielectric properties of several PILs containing either imidazolium or ammonium cations. It was shown that PILs have a higher dielectric constant and dielectric loss compared to most common polymers, due to the high density of strong dipoles[90].

PILs have also been used as dispersants to help stabilize single and multi-wall carbon nanotubes[88,91]. Furthermore, several imidazolium-based polymers have been reported as excellent stabilizers for metal nanoparticles. K. Vijayakrishna et al.[92] reported an imidazolium-based PIL stabilized Ni nanoparticles which are employed as a catalyst in transfer hydrogenation reactions of carbonyl compounds to their alcohol derivatives. Rhodium nanoparticles were also stabilized by ionic copolymers in IL which was used as a catalyst for benzene hydrogenation[93]. PILs have been used as vehicles for phase transfer of different nanoparticles and nanorods. This was achieved by the anion exchange-induced precipitation of a cationic PIL in an aqueous dispersion of the corresponding nanomaterial[94]. It was also reported that PILs can trap the nanomaterials during their precipitation forming PIL nanocomposites[95]. A. Pourjavadi et al.[96] reported a functionalized PIL coated magnetic nanoparticle ($\text{Fe}_3\text{O}_4@\text{PIL}$) catalyst that was synthesized by polymerization of a functionalized vinyl imidazolium in the presence of surface modified magnetic nanoparticles. The synthesized nano-catalyst showed high thermal stability and recyclability as a result of the PIL coating.

It has been indicated that further processing of PIL nanomaterials by spin coating can provide a simple method for preparing a new generation of nanocomposite material[87]. For instance, irreversible thermochromic behavior was observed for Au and Ag nanorods/PIL nanocomposite films[97]. Using a similar methodology, PIL graphene oxide composite films were prepared and used as an electrode in high-performance supercapacitors[98]. PILs have also been used as a polymer matrix for QDs for practical applications such as optoelectronic devices[99]. In this regard, Shen et al. reported cadmium/tellurium/ fluorescent imidazolium functionalized ionic polyurethane[100].

Synthesis of PILs can be achieved by polymerization of IL monomers in which one or more polymerizable units are incorporated into the polymer structure. Polymerizable units can be either on the cation (cationic PILs) or anion part (anionic PILs) depending on the desired polymer architecture[87]. Furthermore, copolymerization of two IL monomers has been applied to tune the distribution of the IL species along the polymer chain and modify the physicochemical properties of the PILs.

1.12 Research Objective

Based on the literature review, there are still major challenges in the fabrication of thermochromic VO₂ smart windows with desirable optical properties:

- 1) Using environmentally friendly solvents along with mild temperature conditions for the synthesis of VO₂(M) nanoparticles showing thermochromic properties.
- 2) Synthesizing pure phase VO₂ (M/R) with a shape-controlled nanostructure with sharp and narrow hysteresis loops for practical application in smart thermochromic devices
- 3) Improving the solar modulation efficiency, ΔT_{sol} and luminescence transmittance (T_{lum}) simultaneously, which is the key factor for the evaluation of smartness of a window.
- 4) Finding a suitable polymeric matrix and a dielectric host for long term stabilization of VO₂ nanostructures
- 5) Synthesis of pure and high crystalline VO₂ with small hysteresis width for fast responding switching

To address these issues, we proposed that complementary features of ILs can be used for the synthesis and fabrication of VO₂ thermochromic coatings. In Chapter 2, we hypothesize that ILs as knowing green solvents can be used alone or in combination with supercritical CO₂ in the sol-gel process for the preparation of pure and high crystalline monoclinic VO₂ with good optical properties. In Chapter 3, we hypothesized that ILs can stabilize the precursor solution and would facilitate the formation of pure and high crystalline VO₂ (M). In Chapter 4, we hypothesized that a polymerized ionic liquid with the advantage of

excellent optical properties, high dielectric constant, and high heat capacity can be used as a great alternative for thermochromic coatings with enhancing luminous transmittance and solar modulation ability. This work will also investigate the role of Mo doping in decreasing the transition temperature of VO₂. Specifically, we hypothesized that post-treatment of synthesized VO₂ by annealing at high temperatures might induce the formation of pure nanostructure VO₂ monoclinic with small hysteresis width for fast switching properties.

Chapter 2

2 Sol-gel processing of VO₂ (M) in supercritical CO₂ and supercritical CO₂/ ionic liquid biphasic system*

*S. Nazari, P. Charpentier, *Journal of Supercritical Fluids* (165), 104989

Abstract: Vanadium oxide VO₂ (M) synthesis was investigated using supercritical CO₂ (scCO₂), imidazolium ionic liquids (ILs), and their biphasic combination. VTIP was used as the vanadium precursor while examining [EMIM] ionic liquids based on anions of [TF₂N]/ [TFO]/ [AcO]/ [HSO₄]. Gelation yields up to 80 % were formed using scCO₂/HOAC or simply with [EMIM][TF₂N] IL, indicating the role of scCO₂ in the gelation process. The sol-gel temperature was found to have a large effect on the gelation yield compared to the pressure. TGA, XRD, and XPS results confirmed that the ILs were incorporated into the ionogel structure, having an effect on the surface area, porosity, and morphology of the VO₂ (M). The optical properties of the VO₂ films were analyzed using UV-Vis-NIR, showing good thermochromism for integration into smart windows.

2.1 Introduction

Vanadium oxide (VO_2) coatings have garnered a large amount of attention since they enable automatic solar/ heat control in response to environmental temperature, without the use of any external switching devices [101–103]. VO_2 (M) is one of the polymorphic crystal structures of VO_2 , which undergoes a reversible metal-semiconductor transition at 68 °C, known as the critical temperature (T_C). This metal-semiconductor transition is followed by drastic changes in the optical properties of VO_2 , which makes it a potential candidate for thermochromic smart windows [104,105]. VO_2 coatings should have reasonable luminescence transmittance (T_{lum}) and solar modulating ability (ΔT_{sol}) simultaneously in order to make them applicable for thermochromic smart applications [105,106]. There are various synthetic methods to synthesize monoclinic vanadium oxides (VO_2 (M)) including sol-gel, [107,108], hydrothermal [109,110], physical vapor deposition (PVD) [16,111] and chemical vapor deposition (CVD) [17,112]. However, the sol-gel approach has been widely used for the preparation of VO_2 considering that it can be tuned by parameters such as solvent, temperature, and aging time for desirable scalable synthesis [108,113]. In order to have an economical and environmentally friendly process, it is essential to synthesize VO_2 at low temperatures using inexpensive and nontoxic reactants and solvents [113,114]. Supercritical carbon dioxide (scCO_2) as a versatile and environmentally benign solvent has been used in many sol-gel processes [36–38]. The products which are prepared using a sol-gel method in scCO_2 have specific advantages such as maintaining nano-features and well-defined morphologies after CO_2 drying and venting [36,37]. Studies have also shown that scCO_2 as a functional solvent is able to shorten the synthesis time considerably, simultaneously affecting the pore characteristics of the obtained materials [36]. On the other hand, the volatile and non-polar characteristic of scCO_2 makes an interesting biphasic system with non-volatile highly polar ionic liquids (ILs) as the result of their different miscibility [65,67,115,116]. These systems are based on the principle that scCO_2 is partially soluble in ILs but ILs are not soluble in scCO_2 . Imidazolium ILs have previously been investigated during the sol-gel process instead of classical organic solvents, resulting in shorter synthesis times and materials with tunable properties [65,66,117,118]. Another advantage of potentially using ILs is that they can be adsorbed or incorporated into the crystal structure of the final product, resulting in a porous material called ionogel. Ivanova

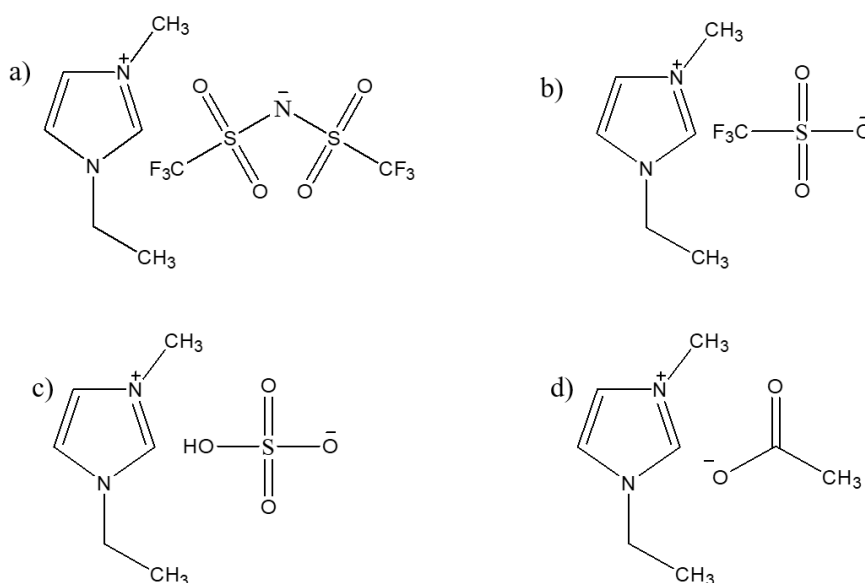
et al. [65] reported using the scCO_2 / IL biphasic system during the sol-gel process for the preparation of silica ionogel. They proposed that the anion component of the IL plays a significant role in catalyzing the reaction, resulting in a shorter gelation time for tetramethyl orthosilicate (TMOS) [39,65]. There are also studies showing ILs having a role in gel growth due to their ionicity, anisotropy and multiple bonding capacity [39,119,120].

This study focused on investigating the importance of scCO_2 and imidazolium ILs on the polycondensation of vanadium oxide precursor for the formation of vanadium gels during sol-gel processing. The gelation yield and porous characteristics of the obtained gels are investigated. We have also studied the effect of temperature and pressure variation during the sol-gel process on the purity, crystallinity, and morphology of final VO_2 products. The sol-gel reaction was studied under different conditions: a) in scCO_2 in the presence of acidic polycondensation reagent, b) in ILs under ambient pressure and c) in biphasic scCO_2 / IL. In the reactions with ILs involved, no polycondensation reagent is used. The second step of the process involves the calcination of the gel to prepare crystalline and pure VO_2 (M).

2.2 Experimental

2.2.1 Materials

The ionic liquids 1-ethyl 3-methyl imidazolium acetate ([EMIM][AcO]) (97 %, Alfa Aesar), 1-ethyl 3-methyl imidazolium hydrogen sulfate ([EMIM][HSO₄]) (98 %, Alfa Aesar), 1-ethyl 3-methyl imidazolium trifluoromethanesulfonate ([EMIM][TFO]) (98 %, Alfa Aesar) and 1-ethyl 3 methylimidazolium bis (tri-fluoromethansulfonylimide) [EMIM][TF₂N] (97 %, Sigma Aldrich) were used without any further purification. The structures of the investigated ILs are presented in Scheme 2-1.



Scheme 2-1. Chemical structure of ILs examined in this work: a) 1-ethyl 3-methylimidazolium bis (trifluoromethanesulfonylimide) ([EMIM][TF₂N]), b) 1-ethyl 3-methyl imidazolium trifluoromethanesulfonate ([EMIM][TFO]), c) 1-ethyl 3-methyl imidazolium hydrogen sulfate ([EMIM][HSO₄]), d) 1-ethyl 3-methyl imidazolium acetate ([EMIM][AcO]).

Vanadium (V) oxy-tri-isopropoxide (VTIP) (98 %, Sigma-Aldrich) was used as the vanadium precursor. Acetic acid (HOAc) (99.7 %, ACS reagent) was used as a polycondensation reagent. Carbon dioxide (CO₂) with a purity of 99 % was supplied by BOC Canada.

2.2.2 Preparation of Vanadium Oxide Aerogel in scCO₂

A 25 mL stainless-steel high-pressure reactor equipped with two sapphire windows was used to synthesize vanadium oxide aerogel [38]. CO₂ was passed through a chiller to cool down before being pumped into the reactor by a syringe pump (ISCO, Model 260D). In a typical experiment, a view cell reactor was preheated to the desired temperature between 40 °C ± 2 °C and 100 °C ± 2 °C (controlled with a T-type thermocouple). Then, the view cell was pressurized to the desired pressure between 27.6 MPa ± 1.4 MPa and 51.7 MPa ± 1.4 MPa (measured with an Omega pressure transducer). A constant volume of 0.5 mL of VTIP (2.2 mmol) was used for all reactions. The reaction mixture was stirred constantly

(300 rpm) for 3h and then aged without agitation at the specified temperature and pressure for five days. After aging, CO₂ was continuously pumped to the view cell to wash the formed gel at a rate of 0.2 mL. min⁻¹ for 48 h at the reaction temperature and pressure to avoid the collapse of a solid network. The dried aerogel product was then collected from the reactor for gravimetric yield measurement and subsequent physicochemical analysis. The deviation in yield is calculated by repeating random reactions three times.

2.2.3 Preparation of Vanadium Oxide Ionogel in ILs

A reaction mixture of 2.2 mmol of VTIP and 2 mL of the IL in a flask was heated to reaction temperature and stirred for 3h. After the reaction, 10 mL of acetone or ethanol depending on the ionic liquid type, was added to the top of the reaction mixture. The solution was aged for five days on the lab bench, then the excess solution was decanted. The remaining solid product was transferred to the reactor to be washed with scCO₂ (27.6 MPa ± 1.4 MPa, 60 °C) at a rate of 0.2 mL. min⁻¹ for 48 h.

2.2.4 Preparation of Vanadium Oxide Ionogel in scCO₂/ IL Biphasic system

To prepare the reaction mixture, 2.2 mmol of VTIP was mixed with 2 mL of ILs. In a typical experiment, the reactor was heated to the desired temperature between 40 °C ± 2 °C to 100 °C ± 2 °C (controlled with a T-type thermocouple). The reactor was pressurized to the chosen pressure between 27.6 MPa ± 1.4 MPa and 51.7 MPa ± 1.4 MPa (controlled with Omega pressure transducer). The reaction mixture was stirred constantly for 3h of reaction time. After five days of gelation, the view cell was depressurized until ambient pressure was reached. Then, the reaction mixture was transferred to a beaker, and 10 mL of acetone or ethanol was added to it at room temperature. The mixture was left for two days. The extra solvent was decanted from the top of the mixture and the remaining gel transferred to a view cell. The mixture was washed with CO₂ at reaction supercritical pressure and temperature for 48 hours under 0.2 mL. min⁻¹ flow rate to obtain a dry ionogel product. The collected aerogel/ ionogel products were calcined in a tubular furnace at 500 °C for (1 to 2) hours under N₂ atmosphere with a heating rate of 20 °C. min⁻¹.

2.2.5 Characterization

Vanadium gel products were characterized using Thermogravimetric Analysis (TGA) at $10\text{ }^{\circ}\text{C}\cdot\text{min}^{-1}$ heating rate, using SDT Q600-TA instruments. The surface area, pore size, and pore volume of the materials were determined by Brunauer-Emmett-Teller (BET). A minimum of 80 mg of sample was degassed at $100\text{ }^{\circ}\text{C}$ for 12 h before measurements to remove any moisture and other adsorbed gases. Photoelectron Spectroscopy (XPS, AXIS Ultra Kratos Analytical Ltd.) with a monochromatic Al K (α) source (15 mA, 15 kV) was used to analyze the surface elemental composition and chemical state of the prepared vanadium oxide samples. The instrument work function was calibrated to give binding energy (BE) of 83.96 eV for the Au 4f_{7/2} line for metallic gold and the spectrometer dispersion was adjusted to give a BE of 932.62 eV for the Cu 2p_{3/2} line of metallic copper. The Kratos charge neutralizer system was used on all specimens. Survey scan analyses were carried out with an analysis area of (300 × 700) microns and a pass energy of 160 eV. High-resolution analyses were carried out with an analysis area of (300 × 700) microns and a pass energy of 20 eV. Spectra were charge corrected to the mainline of the carbon 1s spectrum (adventitious carbon) set to 284.8 eV. Spectra are analyzed using Casa XPS software and curve-fitting of the V2p peak was based on A. Gerson et al. data [121].

The calcined products were analyzed by an X-Ray Powder Diffractometer (XRD, D2 Phaser) using Cu K α ($\lambda = 1.54056\text{ \AA}$) radiation from $2\theta = 10^{\circ}$ to 80° at a scanning rate of $0.1^{\circ}\cdot\text{min}^{-1}$. The phase transition temperature (T_c) was tested by differential scanning calorimetry (SDT Q600, TA Instruments, USA) over the temperature of $10\text{ }^{\circ}\text{C}$ to $90\text{ }^{\circ}\text{C}$ and analyzed using Universal Analysis 2000 (TA Instruments, Inc.). The heating rate and cooling rate were set at $10\text{ }^{\circ}\text{C}/\text{min}$ and $5\text{ }^{\circ}\text{C}/\text{min}$ respectively. The morphologies and size of the samples were characterized by Scanning Electron Microscopy (SEM, Hitachi FlexSEM1000). The samples were coated with a thin layer of about 5 nm of gold/ palladium before SEM imaging.

2.3 VO₂ Film Preparation

The synthesized VO₂ (M) formed from different sol-gel conditions were dissolved in 10 wt % PVP/ acetonitrile solution and sonicated for 10 minutes in a sonication bath. Each

film solution was loaded with 4 mg of synthesized VO₂ (M). The solutions were cast onto 2.5 cm × 7.5 cm × 1.2 mm borosilicate glass microscope slides that were cleaned with ethanol before casting. Films were deposited on the glass by a spin coating instrument (Laurel Spin Coater- Model WS400BZ) with a speed of 2000 rpm for 30 s.

2.4 Results and Discussion

2.4.1 Influence of Temperature and Pressure on Gelation Yield

In a supercritical fluids system, both reaction equilibrium and the reaction rate can be adjusted by tuning temperature and/ or pressure [122,123]. Table 2-1 shows the influence of temperature and pressure on the yield of the sol-gel reactions in scCO₂, in scCO₂/ [EMIM][TF₂N], and scCO₂/ [EMIM][TFO].

Table 2-1 .Yield of gel product (wt %) prepared a-g) in scCO₂ h-n) in [EMIM][TF₂N] + scCO₂ biphasic system o-u) [EMIM][TFO] + scCO₂ biphasic system at different temperatures and pressures.

	Ionic Liquid	T (°C)	P (MPa)	Yield (%)
a	-	40	27.6	76
b	-	60	27.6	80
c	-	80	27.6	82
d	-	100	27.6	82
e	-	40	34.5	78
f	-	40	41.4	78
g	-	40	51.7	80
h	[EMIM][TF ₂ N]	40	27.6	60
i	[EMIM][TF ₂ N]	60	27.6	78
j	[EMIM][TF ₂ N]	80	27.6	80
k	[EMIM][TF ₂ N]	100	27.6	80

	Ionic Liquid	T (°C)	P (MPa)	Yield (%)
l	[EMIM][TF ₂ N]	40	34.5	65
m	[EMIM][TF ₂ N]	40	41.4	67
n	[EMIM][TF ₂ N]	40	51.7	65
o	[EMIM][TFO]	40	27.6	32
p	[EMIM][TFO]	60	27.6	47
q	[EMIM][TFO]	80	27.6	60
r	[EMIM][TFO]	100	27.6	61
s	[EMIM][TFO]	40	34.5	40
t	[EMIM][TFO]	40	41.4	42
u	[EMIM][TFO]	40	51.7	45

As shown in Table 2-1, increasing the temperature of the reaction from 40 °C to 60 °C improves the isolated yield of gels in all media. However, it seems a further increase of the temperature from 80 °C and 100 °C does not help the conversion significantly (Figure 2-1-a). On the other hand, the temperature has a larger effect on the reactions in ILs/ scCO₂ system compared to those synthesized in the scCO₂ system. When using scCO₂ without IL, when the temperature was increased from 40 °C to 80 °C, the yield increased from 76 % to 82 %. However, the yield increased from 60 % to 78 % when scCO₂/[EMIM][TF₂N] was used and from 32 % to 47 % when scCO₂/ [EMIM][TFO] was used as a sol-gel media. Figure 2-1 shows the trend of gelation yield with temperature. This increase in yield with temperature is attributed to an acceleration in the hydrolysis and condensation sol-gel reactions [124,125].

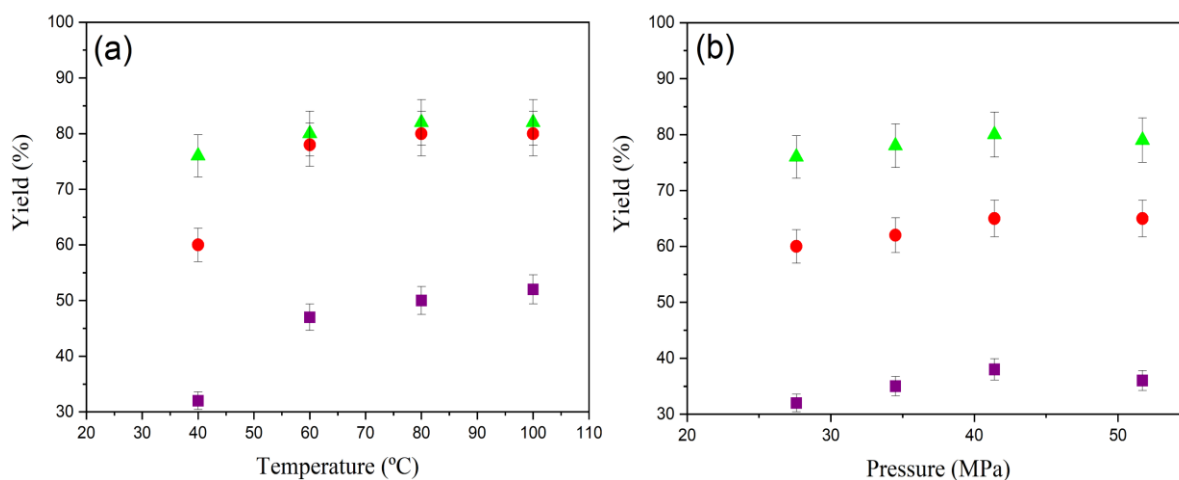


Figure 2-1. a) effect of temperature on the wt % yield b) effect of pressure on the wt % yield. Symbol (Δ) represents the reactions carried out in scCO₂, the reactions symbol (○) represents the reactions carried out in scCO₂ + [EMIM][TF₂N] and symbol (□) represents the reactions carried out in scCO₂ + [EMIM][TFO]

As shown in Figure 2-1 for the 3 investigated systems, increasing pressure enhances gelation yield, although does not have a significant effect. The reaction's pressure in all systems increased from 27.6 MPa to 34.5 MPa, 41.4 MPa, and 51.7 MPa at a constant temperature of 40 °C, but the gelation yield did not increase more than 5 % (Figure 2-1). Increasing CO₂ pressure will increase the density of the system. Generally, in a direct sol-gel reaction in a supercritical fluid, higher pressure increases the solubility of the solute, particularly near the critical pressure. However, acetic acid and CO₂ are miscible in all proportion above 14 MPa. VTIP as a precursor is also shown to be miscible in CO₂ in the range of 27.6 MPa to 51.7 MPa [126]. As a general rule, increasing the pressure in scCO₂/IL systems will increase the solubility of the CO₂ in the IL [116]. As the pressure increases, the rate will slow down as the solubility stabilizes due to CO₂ saturation [127].

2.4.2 Influence of Solvent and Poly Condensation Reagent Ratio on Gelation Process

In order to investigate the effect of different sol-gel media, the reaction's temperature and pressure were maintained constant at 60 °C and 27.6 MPa. Reaction (a) which was performed in scCO₂ and in the absence of any IL, resulted in 80 % ± 5 % conversion. For reactions (b) to (e) in Table 2-2, different ILs were used to make a scCO₂/ IL biphasic system in the absence of HOAc as the polycondensation reagent. As shown in Table 2-2 the anion counterpart of the IL plays a key role in catalyzing the gelation process in the absence of HOAc. The yield of the reaction is 78 % when [EMIM][TF₂N] was used, while the yield dropped to 47 % when [EMIM][TFO] was used. On the other hand, the [EMIM][AcO] and [EMIM][HSO₄] IL systems gave very low gel yields. These results show that either the [EMIM][TF₂N] or [EMIM][TFO] ILs can be substituted for the acidic polycondensation agent in the gelation of VTIP. Although [TF₂N] is the largest anion amongst all ILs investigated in this study, the number of fluorine atoms has an important effect on the catalytic properties of ILs in a sol-gel process. The catalytic properties of the ILs can either be due to their cation or anion component. It has been proposed previously that the imidazolium cation can act as Bronsted acid to catalyze the hydrolysis of silica precursors [128]. However, as the cation counterpart of ILs in this work is the same, the role of the cation in catalyzing the sol-gel process is similar in all reactions. It has also been reported that fluorinated ILs can promote the hydrolytic step during the sol-gel reaction of alkoxy silane leading to faster gelation times [129]. When undergoing hydrolysis, the fluorinated ILs have been shown to release HF, which is a powerful hydrolytic condensation catalyst [129].

Table 2-2. The yield of gel product (wt %) prepared, a) in scCO₂ at 60 °C and 27.6 MPa in the presence of HOAc as a polycondensation reagent, b-e) in scCO₂/ IL biphasic at 60 °C and 27.6 MPa and f) IL at 60 °C and atmospheric pressure. (+) is in the presence of scCO₂, (-) is in the absence of scCO₂

	Ionic Liquid	CO₂ (+/-)	Yield (%)
A	-	+	80 ± 5
B	[EMIM][TF ₂ N]	+	78 ± 5
C	[EMIM][TFO]	+	47 ± 5
D	[EMIM][AcO]	+	2 ± 5
E	[EMIM][HSO ₄]	+	Negligible
F	[EMIM][TF ₂ N]	-	39 ± 5

Improving the gelation time in the scCO₂/ IL system can also be explained by the difference in solubility of CO₂ in the ILs [116,130]. It has been reported that CO₂ solubility in ILs changes based on the anion counterpart of the IL, in the order [TF₂N]> [TFO]> [AcO]> [HSO₄] [130–133]. The dissolved CO₂ reduces the viscosity of the IL, leading to higher molecular mobility and higher condensation rate [129]. On the other hand, CO₂ is well known to form acid in the presence of any moisture in the system, which can catalyze the gelation process. Poor solubility of CO₂ in [EMIM][AcO] and [EMIM][HSO₄] ILs and lack of fluorine atoms in their anion counterparts hinders the gelation process, leading to the small (2 %) and negligible ionogel (~ 0) yield respectively. There is a great decrease in yield (Table 2-2 reactions (e)) when the reaction was carried out in [EMIM][TF₂N] IL at ambient pressure without CO₂ involvement, confirming the role of scCO₂ in the improvement of the sol-gel process by lowering the viscosity and mass transfer enhancement.

2.4.3 Characterization of the Aerogel/ Ionogel

Thermal behavior of [EMIM][TF₂N] and [EMIM][TFO] ionogel samples and scCO₂ aerogel samples were investigated using thermogravimetric analysis (TGA), as shown in Figure 2-2 a.

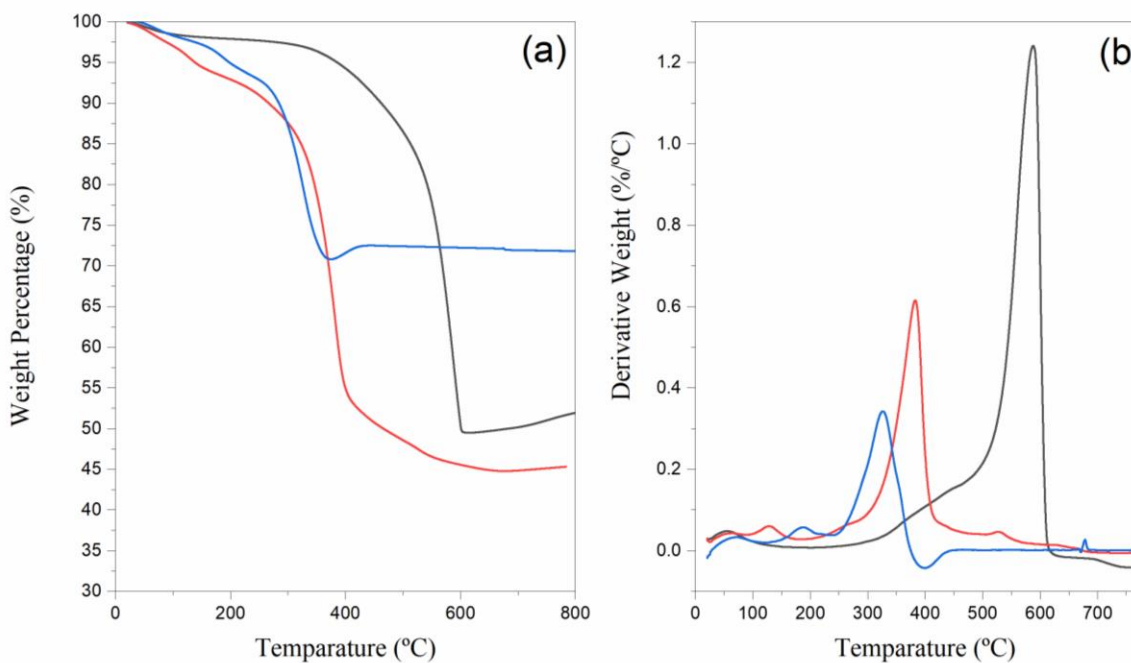


Figure 2-2. a) TGA thermogram and b) differential thermal gravimetric (DTG) curves of gel samples prepared in scCO₂/ [EMIM][TF₂N] (black line), scCO₂/ [EMIM][TFO] (red line), and scCO₂ (blue line). The heating rate is 10 °C. min⁻¹.

The first step in all three curves (up to 180 °C) corresponds to water release from the aerogel structure. The second step shows the main decomposition process for all three samples. The decomposition temperature at 50 % weight loss (T_{g50}) for [EMIM][TF₂N], [EMIM][TFO] ionogel and scCO₂ aerogel samples are 270 °C, 284 °C and 243 °C, respectively. Not only is a difference in the T_{g50} of the samples noticeable, but also the slope and shape of the T_g curves, indicating differences in the decomposition mechanism. The aerogel sample which was prepared in the absence of the IL shows the lowest decomposition temperature, with the highest decomposition rate (highest slope). The ionogel samples show higher decomposition temperatures compared to the aerogel sample, which can be attributed to the existence of entrapped ILs in the solid network of the ionogel [134,135].

The decomposition process of the samples was further investigated using differential thermal gravimetric (DTG) analysis, with the curves shown in Figure 2-2-b. The main peaks which can be assigned to vanadium aerogel are at $308\text{ }^{\circ}\text{C} \pm 2\text{ }^{\circ}\text{C}$, $330\text{ }^{\circ}\text{C} \pm 2\text{ }^{\circ}\text{C}$ and $390\text{ }^{\circ}\text{C} \pm 2\text{ }^{\circ}\text{C}$ for scCO_2 , [EMIM][TFO] and [EMIM][TF₂N] samples, respectively. However, the ionogel samples show a small peak at $530\text{ }^{\circ}\text{C} \pm 2\text{ }^{\circ}\text{C}$ and $680\text{ }^{\circ}\text{C} \pm 2\text{ }^{\circ}\text{C}$ which can be attributed to the degradation of the anion counterpart of ILs in ionogels [136]. Therefore, the TGA results confirm the incorporation of ILs into the structure of the dried gel, even after the washing and drying procedures.

The x-ray diffraction of aerogel and ionogel samples is provided in Figure 2-3- a. The gel sample obtained from the sol-gel process in scCO_2 shows vanadyl diacetate $\text{VO}(\text{CH}_3\text{COO})_2$ peaks as a crystalline product of the reaction.

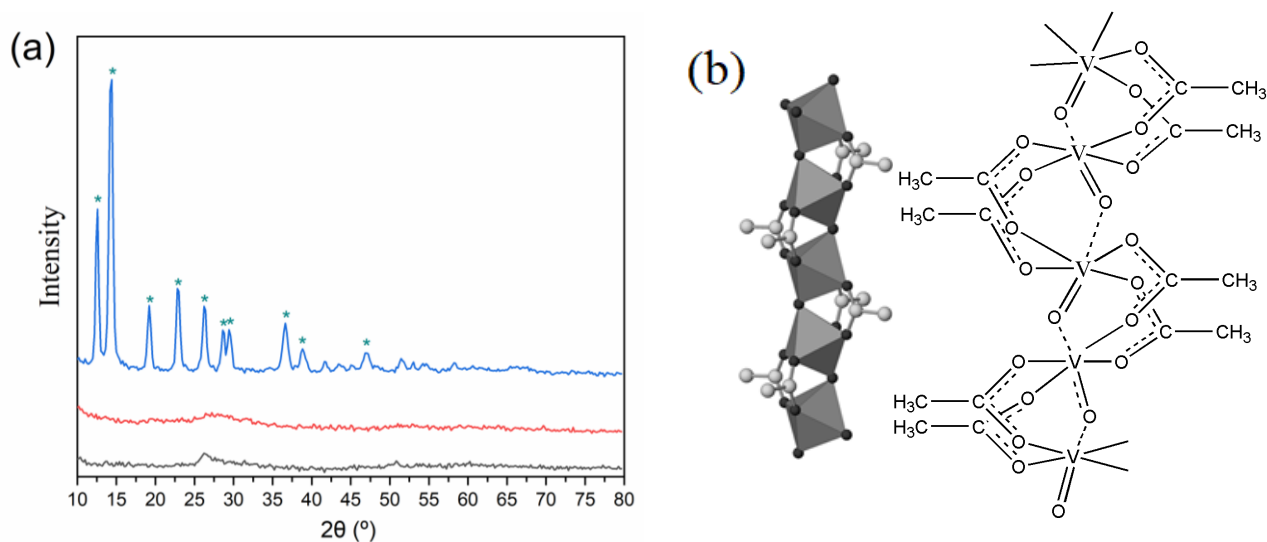


Figure 2-3. a) XRD pattern of gel product prepared in scCO_2 (blue line), in scCO_2 + [EMIM][TFO] (red line), and in scCO_2 + [EMIM][TF₂N]. symbol of (*) represents the vanadyl diacetate peaks b) one-dimensional chain of VO₆ octahedra in vanadyl diacetate.[46]

The result is matched and confirmed with the experimental results reported by M. Stanley Whittingham [137]. For ionogel samples prepared in scCO_2/ILs , there was no obvious peak that can be assigned to any crystalline vanadium complexes as the result of entrapped ILs in the structure, which would lower the crystallinity of vanadyl diacetate. Figure 2-3-b shows the crystal structure of $\text{VO}(\text{CH}_3\text{COO})_2$ which consists of VO_6 octahedra with double bond oxygen [137,138].

XPS analysis was performed on the aerogel and ionogel samples to examine the elemental analysis and to monitor any changes of chemical state for the prepared gels.

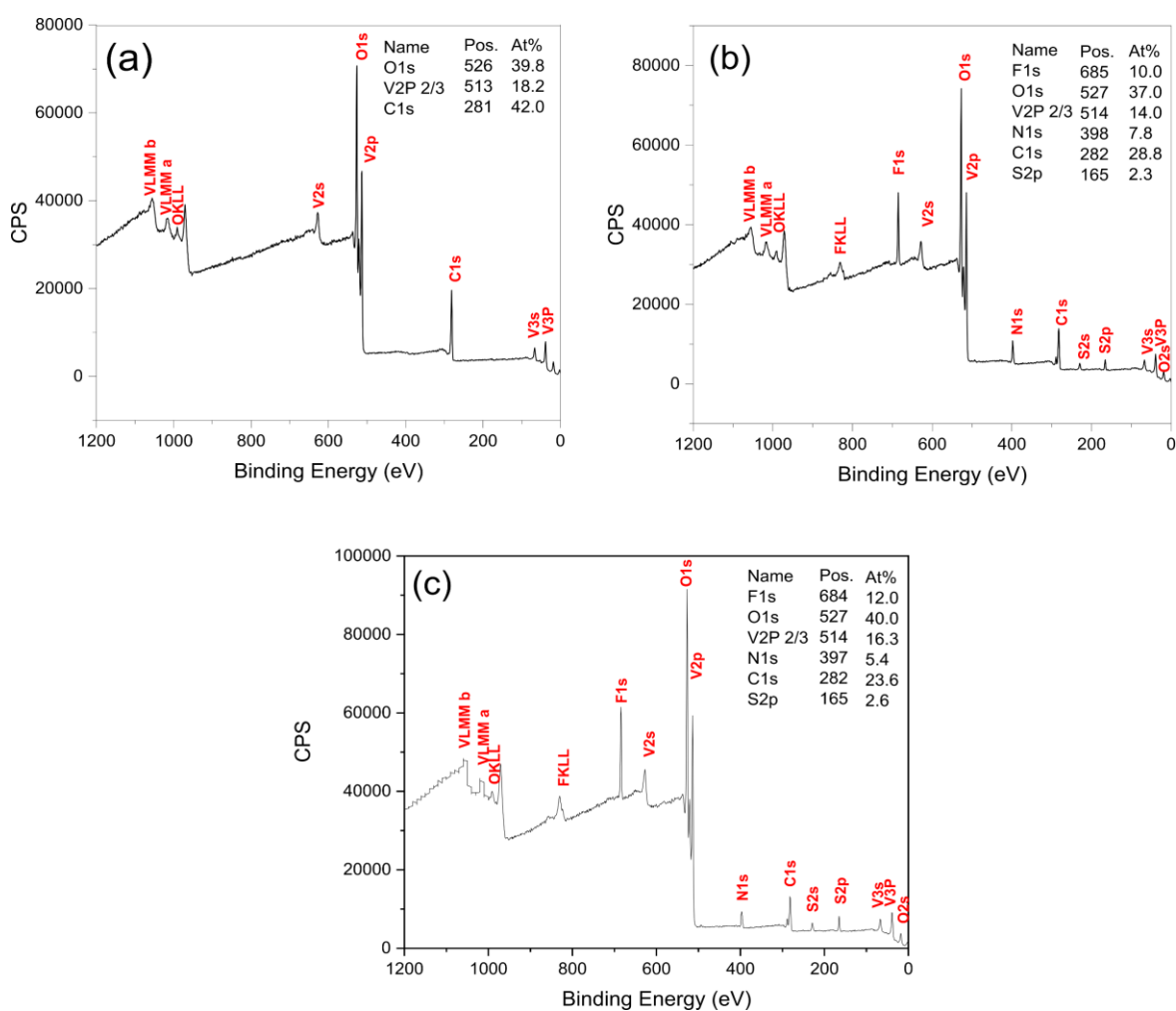


Figure 2-4. XPS survey analysis of sample which is prepared in a) scCO_2 only 27.6 MPa at 60 °C, b) $\text{scCO}_2/[\text{EMIM}][\text{TF}_2\text{N}]$ 27.6 MPa at 60 °C and c) $\text{scCO}_2/[\text{EMIM}][\text{TFO}]$ 27.6 MPa at 60 °C.

The survey spectrum of samples prepared in $scCO_2$ shows only the three elements of carbon, vanadium, and oxygen (Figure 2-4). However, the samples which were prepared in $scCO_2/[EMIM][TF_2N]$ and $scCO_2/[EMIM][TFO]$, show N, S, and F atoms as well, which are related to the presence of $[EMIM][TF_2N]$ and $[EMIM][TFO]$ in the gel samples (Figure 2-4). The XPS results confirm that the ionic liquid was incorporated into the structure of vanadium gel during the sol-gel reaction.

Figure 2-5 shows the XPS patterns of vanadium gels prepared using $scCO_2$, $scCO_2/[EMIM][TF_2N]$, and $scCO_2/[EMIM][TFO]$.

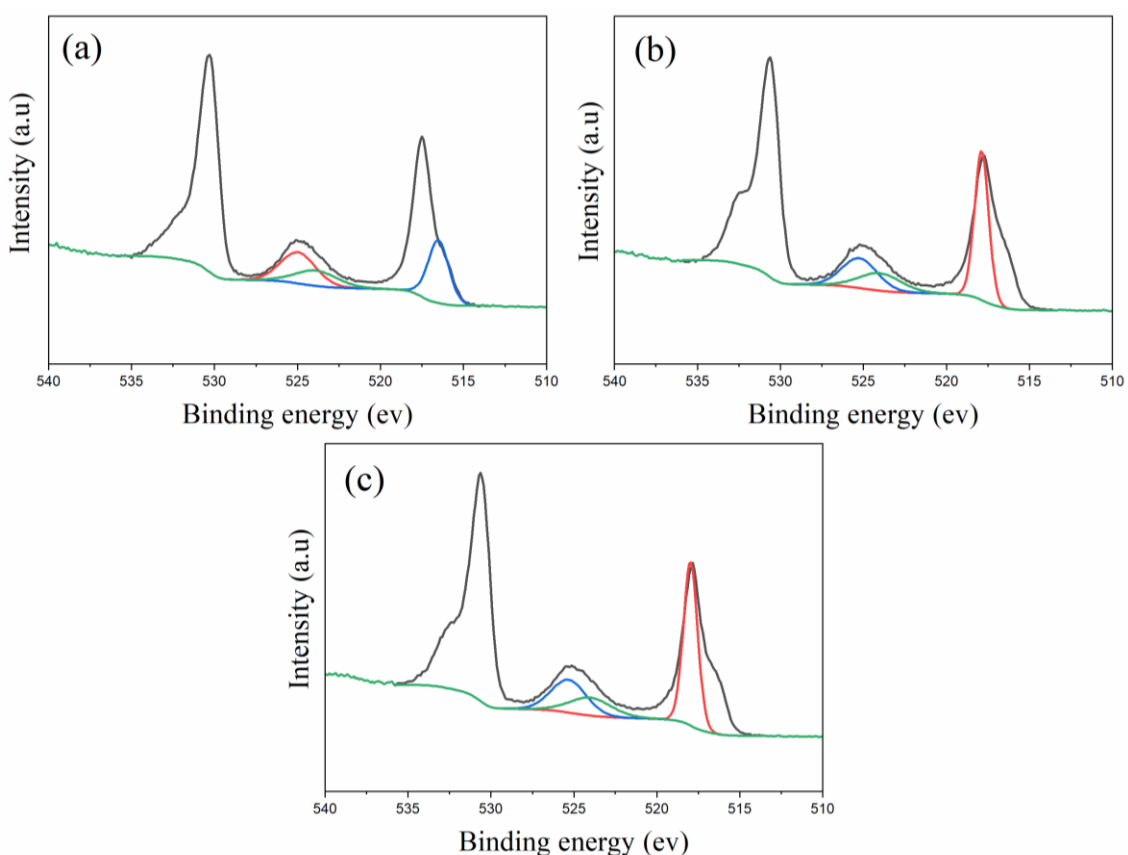


Figure 2-5. XPS spectra of the products prepared in a) $scCO_2$ b) $scCO_2/[EMIM][TF_2N]$ c) $scCO_2/[EMIM][TFO]$ at 27.6 MPa and 60 °C. Black line represents $V2p\ 3/2\ V(V)$, red line represents $V2p\ 3/2\ V(IV)$, blue line represents $V2p\ 1/2\ V(V)$ and green line represents $V2p\ 1/2\ V(IV)$.

The vanadium alkoxide precursor was reduced to a mixture of vanadium oxides with different oxidation states including V^{5+} and V^{4+} ions. Vanadium (V) species in the reaction were hydrolyzed to vanadium (V) gel. The vanadium (V) gel was then reduced to vanadium (IV) by the polycondensation reagent. V^{4+} ions are larger than V^{5+} , favoring condensation and coordination leading to the formation of condensed species from the alkoxide precursors. The results reveal that the choice of ionic liquid does not have a significant effect on the oxidation state of the obtained gel. All three of the reaction media tend to form a mixture of pentavalent and tetravalent vanadium gels.

As shown in Table 2-3 for the summary XPS analysis, the gel product which is obtained in $scCO_2$ / IL biphasic condition has a higher percentage of V^{4+} compared to the one prepared in $scCO_2$ condition.

Table 2-3. Summary of XPS analysis for gel samples prepared in $scCO_2$, $scCO_2$ / [EMIM][TF₂N], $scCO_2$ / [EMIM][TFO] at 27.6 MPa at 60 °C.

	scCO ₂		scCO ₂ / [EMIM][TF ₂ N]		scCO ₂ / [EMIM][TFO]	
	Position	% Area	Position	% Area	Position	% Area
V2p ½ (V)	525.0	0	525.2	0	525.3	0
V2p ½ (IV)	523.9	0	524.0	0	524.0	0
V2p 3/2 (V)	517.6	62.7	517.9	58.5	518.0	60.4
V2p 3/2 (IV)	516.5	37.3	516.6	45.1	516.6	39.6

Table 2-4 provides the BET results for the prepared aerogel and ionogel samples. The sample which was prepared in $scCO_2$ shows the largest specific surface area and the smallest average pore diameter compared to ones synthesized in the presence of ILs. The ionogel samples prepared in a $scCO_2$ / IL biphasic condition show lower surface area and higher average pore size.

Table 2-4. BET results of gel samples prepared in a) scCO₂ only b) scCO₂/ [EMIM][TF₂N] c) [EMIM][TF₂N] only d) scCO₂/ [EMIM][TFO]

	Ionic Liquids	CO ₂ (+/-)	Surface area (m ² /g)	Average pore volume (cm ³ /g)
a	-	+	483	0.07
b	[EMIM][TF ₂ N]	+	120	0.1
c	[EMIM][TF ₂ N]	-	68	0.2
d	[EMIM][TFO]	+	320	0.1

Using ILs during the gelation and extracting it after the reaction normally leads to a porous structure. The sample of [EMIM][TFO] shows a higher surface area and smaller average pore diameter compared to [EMIM][TF₂N] in presence of scCO₂. Although scCO₂ has a higher solubility in [EMIM][TF₂N] than in [EMIM][TFO], it seems the large size of [TF₂N] anion has an effect on the average pore diameter and consequently the surface area of the final ionogel. Furthermore, the sample of [EMIM][TF₂N] prepared in the absence of scCO₂ shows the smallest surface area and largest average pore diameter, helping confirm the role of scCO₂ during the sol-gel process for achieving higher surface area ionogels.

2.4.4 Final Products of Calcination

A more detailed XRD investigation was carried out on the calcined VO₂ products, as changing the temperature and pressure of the sol-gel reaction would change the coordinate bond energy related to vanadyl diacetate,[126] leading to the formation of different vanadium crystal structures under annealing. The gels collected after different supercritical temperatures were calcined and analyzed by XRD. The results are compared with VO₂ (M) peaks (JCPDS Card, no. 72-0514). The XRD results indicate the formation of V₂O₃ from ionogel prepared at 40 °C after 1-hour calcination (Figure 2-6).

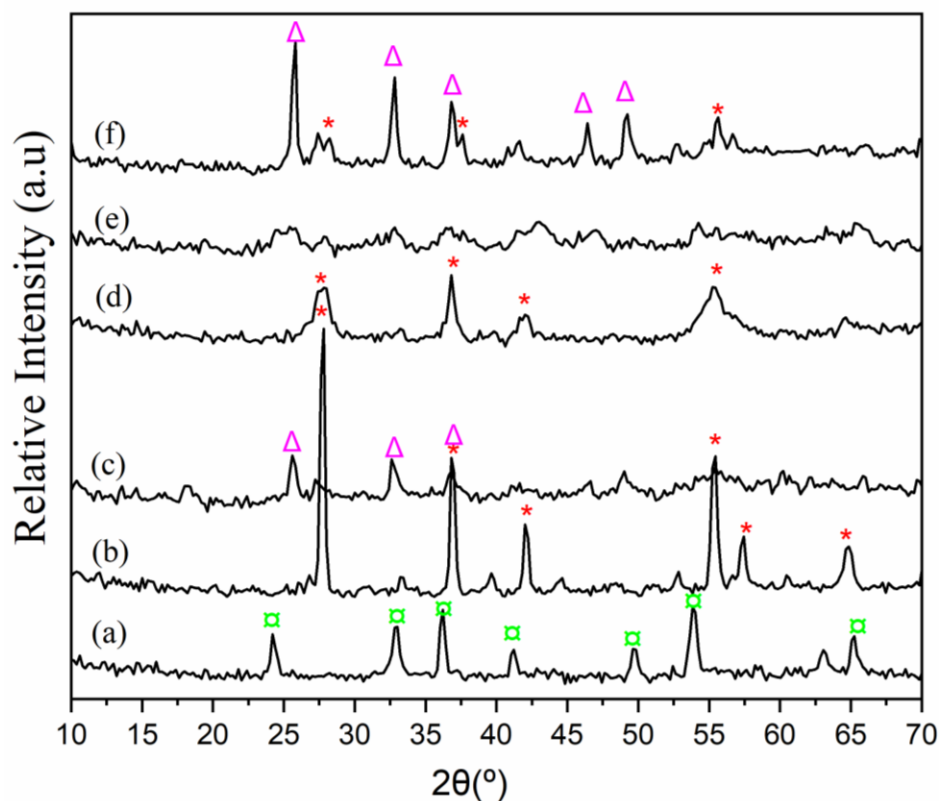


Figure 2-6. XRD pattern of the product prepared in $scCO_2$ / [EMIM][TF₂N] prepared at a) 40 °C, b) 60 °C and c) 80 °C at a constant pressure of 27.6 MPa and after one hour annealing. XRD pattern of the product prepared in $scCO_2$ / [EMIM][TF₂N] at d) 40 °C, e) 60 °C and f) 80 °C at a constant pressure of 27.6 MPa and after two hours. Symbol (\boxtimes) represents peaks of V_2O_3 , symbol (*) represents peaks of VO_2 (M), and symbol (Δ) represents peaks of V_4O_7 .

There are four strong peaks at $2\theta = 24^\circ, 33^\circ, 36^\circ,$ and 54° which are described to (012), (104), (110) and (116) crystal planes of V_2O_3 (JCPDS Card no.34-0187). Furthermore, there is no peak observed in the DSC curve of the product, confirming no VO_2 (M) is formed after calcination (Figure 2-6). When the ionogel was prepared at 60 °C, pure VO_2 (M) was formed after one-hour calcination (JCPDS72-0514, P21/c, $a = 0.5743$ nm, $b = 0.4517$ nm, $c = 0.5375$ nm, and $\beta = 122.61^\circ$). This observation is confirmed by the DSC data, which shows the transition temperature in the range of 60 °C -73 °C, which is typical of a transition temperature of VO_2 (M). Further increase in the sol-gel temperature to 80 °C

leads to the formation of V_4O_7 , which is indexed to JCPDS: 65-6448. By increasing the calcination duration to two hours, the ionogel which was prepared at 40 °C, formed VO_2 (M) (Figure 2-6). However, the purity and intensity of the XRD peaks are similar compared to that prepared at 60 °C after one-hour annealing, although not as sharp. The DSC curve of the product also shows a very broad peak, indicating poor crystalline structure for VO_2 (M) (Figure 2-7).

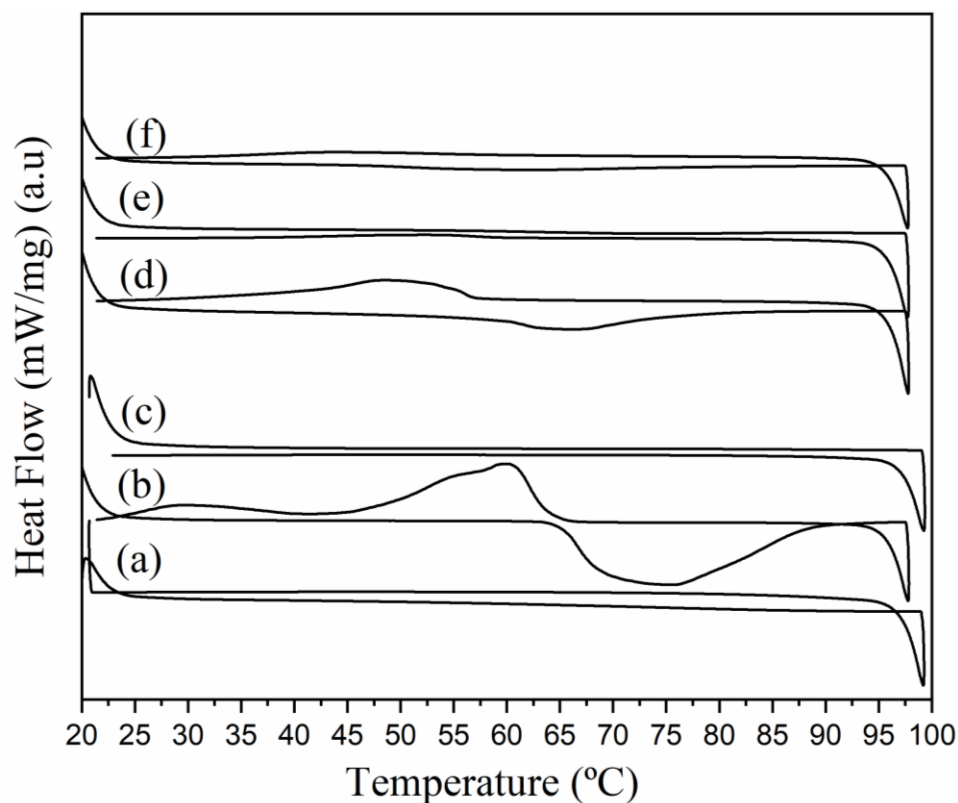


Figure 2-7. DSC curves of product prepared in $scCO_2$ / [EMIM][TF₂N] prepared a) 40 °C, b) 60 °C and c) 80 °C at constant pressure of 27.6 MPa and after one hour annealing. DSC curves of product prepared in $scCO_2$ / [EMIM][TF₂N] prepared at d) 40 °C, e) 60 °C and f) 80 °C at constant pressure of 27.6 MPa and after two hours. Curve b) shows peaks of 60 °C on cooling cycle and 73 °C on heating cycle and curve d) shows peaks at 50 °C on cooling cycle and 66 °C on heating cycle.

Increasing the sol-gel reaction temperature from 40 °C to 60 °C facilitates the formation of crystalline VO₂ (M), probably due to the decrease in viscosity of the IL and enhancing the mass transfer of the system. However, a further increase in the temperature of the reaction would likely decrease the solubility of CO₂ in the IL, slowing down the formation of the final product.

The effect of the sol-gel reaction pressure on phase purity of the final product was studied in the pressure range of 27.6 MPa - 41.4 MPa at a constant temperature of 40 °C for both 1 and 2 h calcination times (Figure 2-8).

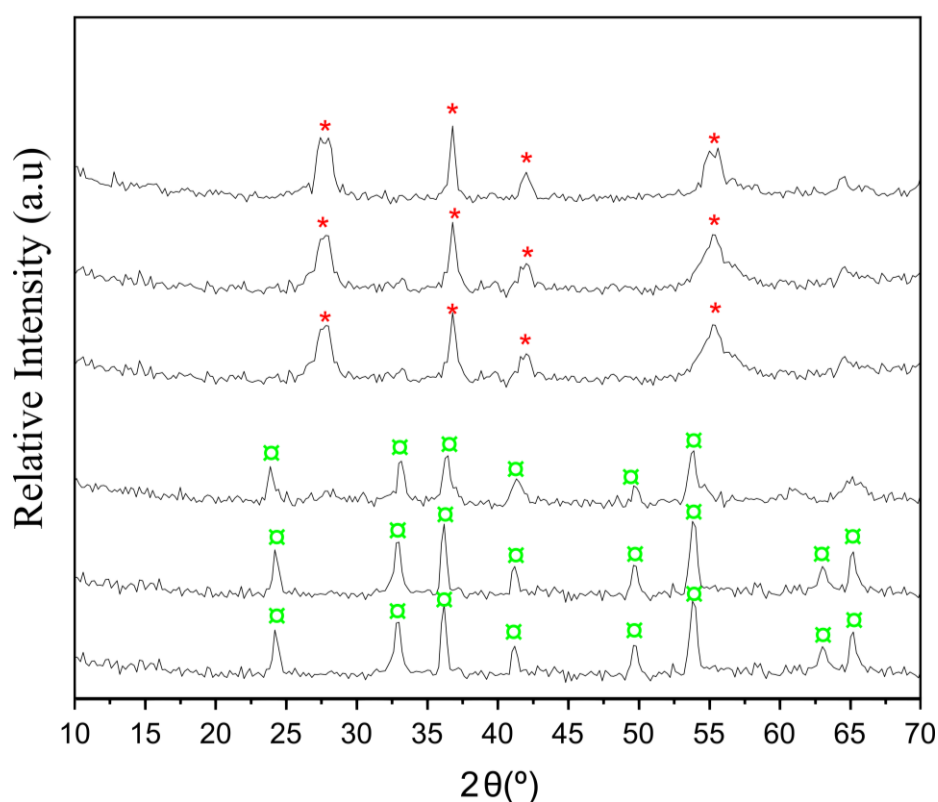


Figure 2-8. XRD pattern of the product prepared in scCO₂/ [EMIM][TF₂N] prepared at a) 27.6 MPa, b) 34.5 MPa and c) 41.4 MPa at a constant temperature of 40 °C and after one-hour annealing. XRD pattern of the product prepared in scCO₂/ [EMIM][TF₂N] prepared at d) 27.6 MPa, e) 34.5 MPa and f) 41.4 MPa at a constant temperature of 40 °C and after two hours. Symbol (◻) represents peaks of V₂O₃ symbol (*) represents peaks of VO₂ (M).

Figure 2-8 shows that by increasing the sol-gel pressure, there is no significant difference in the XRD pattern of the final product after one-hour calcination. However, by increasing the calcination duration to 2 hours, VO₂ (M) was formed but the crystallinity of the sample remains poor. It was previously reported that increasing the pressure of scCO₂/ IL bi-phase reaction slightly decreases the solubility of the CO₂ in the IL [116], which would hinder the formation of the crystalline phase of VO₂.

Figure 2-9 shows the DSC curves of the calcinated products which were prepared at different pressures.

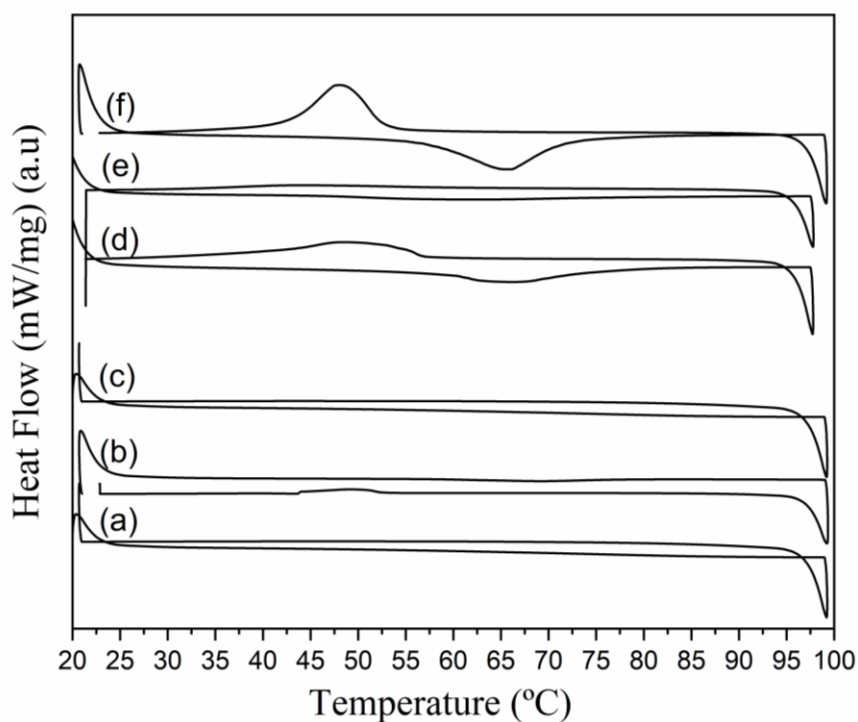


Figure 2-9. DSC curves of product prepared in scCO₂/ [EMIM][TF₂N] prepared at a) 27.6 MPa, b) 34.5 MPa and c) 41.4 MPa at a constant temperature of 40 °C and after one-hour annealing. DSC curves of [EMIM][TF₂N] ionogel prepared at d) 27.6 MPa, e) 34.5 MPa and f) 41.4 MPa at a constant temperature of 40 °C and after two hours. Curve d) shows peaks of 50 °C on the cooling cycle and 66 °C on the heating cycle and curve f) shows peaks at 48 °C on the cooling cycle and 66 °C on the heating cycle.

By extending the annealing time to two hours, transition temperature peaks appear in the DSC curves. By increasing the pressure of the sol-gel reaction, the DSC peaks get sharper and the latent heat of VO₂ improves, verifying an enhancement in the crystallinity of the system.

The effect of temperature and pressure on the sol-gel process was also studied in the absence of the IL in scCO₂ using HAOc as a polycondensation reagent. It seems temperature has more effect on the reaction without IL, compared to the reaction which was performed in biphasic IL/ scCO₂ (Figure 2-10).

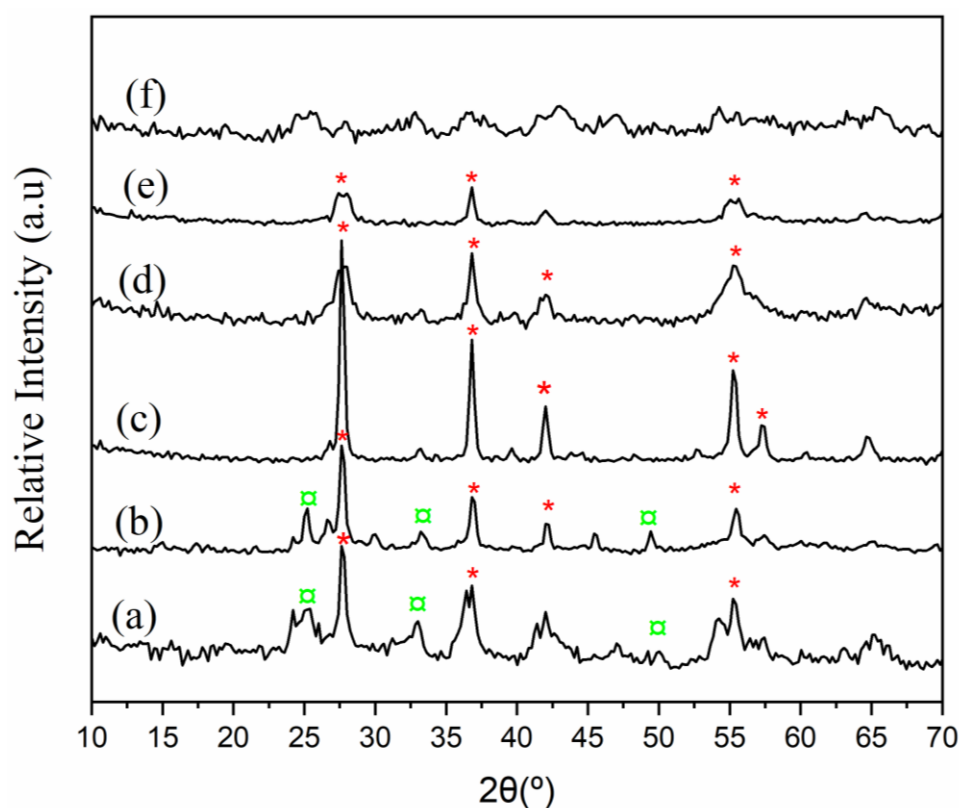


Figure 2-10. XRD pattern of the product prepared in scCO₂ at a) 40 °C, b) 60 °C and c) 80 °C at a constant pressure of 27.6 MPa and after one-hour annealing. XRD pattern of the product prepared in scCO₂ at d) 40 °C, e) 60 °C and f) 80 °C at a constant pressure of 27.6 MPa and after two hours. Symbol (□) represents peaks of V₂O₃, symbol (*) represents peaks of VO₂ (M).

When the sol-gel reaction temperature was raised to 80 °C after 1-hour calcination, good crystalline VO₂ (M) was obtained. We have shown earlier that in order to obtain pure VO₂ (M) in biphasic IL/ scCO₂, a sol-gel temperature of 60 °C and calcination duration of 1h was required.

Increasing the pressure of the sol-gel reaction after calcination leads to the formation of a mixture of VO₂ and V₂O₃ as shown in Figure 2-11. However, even after 2 hours of calcination, it is not possible to form a pure and high crystalline VO₂ (M) product (Figure 2-11).

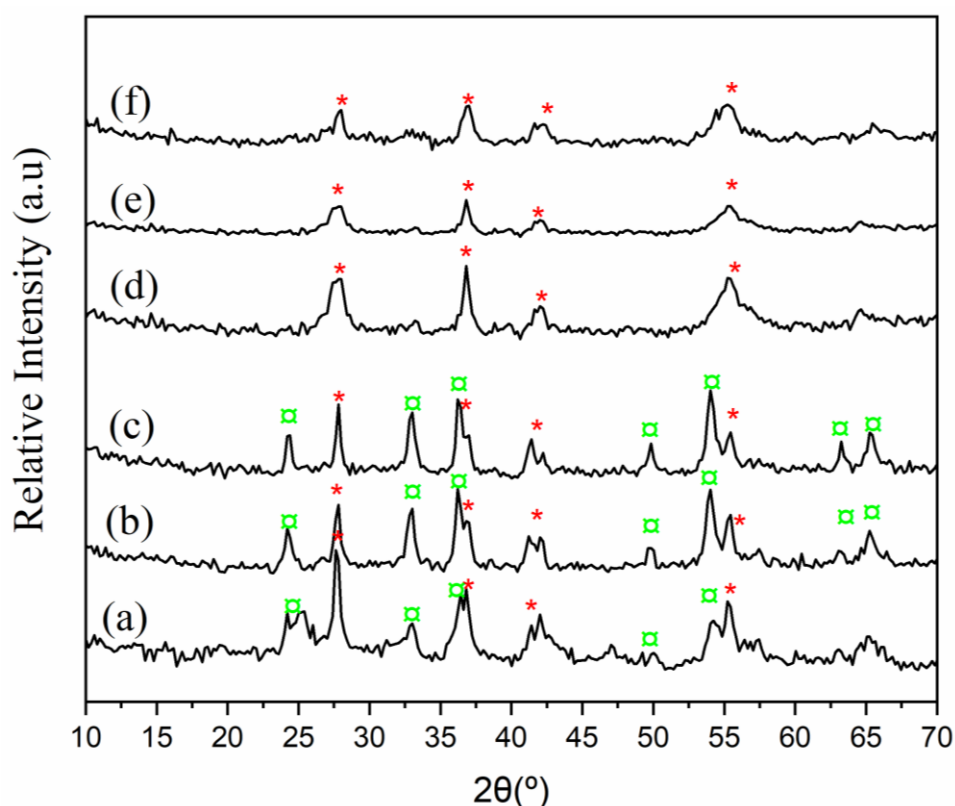


Figure 2-11. XRD pattern of the product prepared in scCO₂ at a) 27.6 MPa, b) 34.5 MPa and c) 41.4 MPa at a constant temperature of 40 °C and after one-hour annealing. XRD patterns of the product prepared in scCO₂ at d) 27.6 MPa, e) 34.5 MPa and f) 41.4 MPa at a constant temperature of 40 °C and after two hours. Symbol (◻) represents peaks of V₂O₃, symbol (*) represents peaks of VO₂ (M).

Table 2-5 summarizes the experimental conditions leading to the formation of pure and crystalline VO₂ (M). When the reaction happens in biphasic [EMIM][TF₂N] IL/ scCO₂, VO₂ (M) can be obtained at 27.6 MPa and 60 °C sol-gel condition and after one-hour calcination. However, in the absence of scCO₂ or by substitution of [EMIM][TF₂N] with [EMIM][TFO], the annealing duration needs to be extended to 2 hours to achieve the same results. The reaction which occurs in the absence of ILs needs a harsher sol-gel condition to result in VO₂ (M).

Table 2-5. Sol-gel conditions to obtain crystalline and pure VO₂ (M)

Sample	IL	CO ₂ (+/-)	Temperature (°C)	Pressure (MPa)	Calcination duration (hr)
1	[EMIM][TF ₂ N]	+	60	27.6	1
2	[EMIM][TF ₂ N]	-	60	-	2
3	-	+	80	27.6	1
4	[EMIM][TFO]	+	60	27.6	2

2.4.5 Morphology Studies by SEM

SEM analysis was performed on the VO₂ (M) samples with good crystallinity and purity (samples 1 to 4 of Table 2-5). The SEM images of samples are shown in Figure 2-12. The morphology of sample 1 which was prepared at biphasic [EMIM][TF₂N]/ scCO₂ shows a nanofiber structure that is slightly larger than sample 3, which was prepared using scCO₂ only. Sample 3 is prepared at a higher supercritical temperature compared to sample 1 and as the total solubility parameter decreased at a higher temperature, the formation of smaller particles is facilitated. Sample 4 which is prepared at biphasic [EMIM][TFO]/ scCO₂ also has a nanofiber structure after calcination very similar to sample 1.

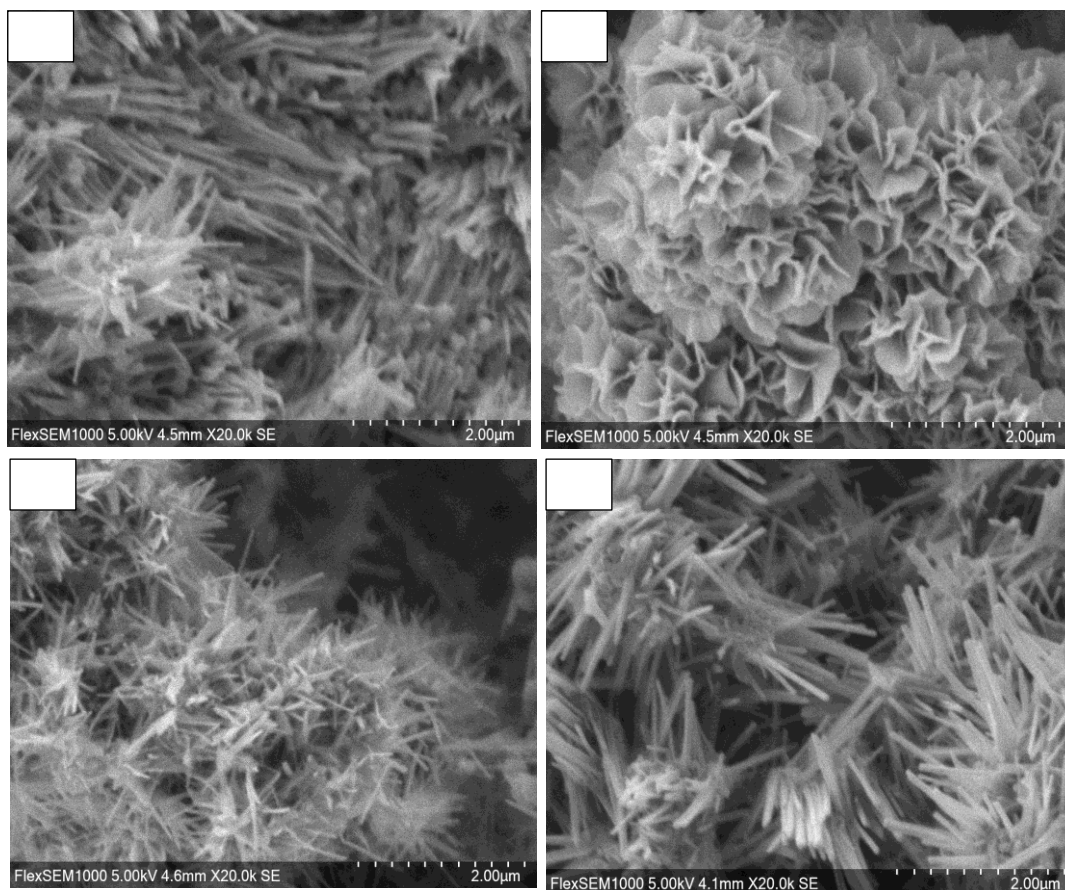


Figure 2-12. SEM images of vanadium oxide prepared in: a) in biphasic [EMIM][TF₂N]/ scCO₂ at 60 °C and 27.6 MPa and after 1 h calcination (sample 1) b) in [EMIM][TF₂N] at 60 °C and ambient pressure and after 2h calcination (sample 2) c) in scCO₂ at 80 °C and 27.6 MPa and 1 h calcination (sample 3) d) in biphasic [EMIM][TFO]/ scCO₂ at 60 °C and 27.6 MPa and after 2 h calcination (sample 4).

The sample which was prepared in IL and in the absence of scCO₂ (sample 2) showed the formation of flower-like porous VO₂ particles as the result of IL extraction and drying under scCO₂ (Figure 2-12- b). Similar results are reported for the formation of silica xerogel after extraction of IL in a sol-gel process [139]. The result confirms the role of supercritical conditions on the formation of nanostructure crystal growth during the sol-gel process. The formation of agglomerated porous structure (sample 4) can negatively affect the optical properties of the VO₂ (M) and limit their use for industrial application.

2.4.6 Optical Properties of the films

VO₂ (M) samples were cast onto glass slides by drop-casting. The UV-Vis-NIR transmittance spectra of the prepared films are characterized at two temperatures of 20 °C and 90 °C. The following equation is used for measuring the integrated luminescence transmittance (380 nm ≤ T_{lum} ≤ 780 nm) and integrated solar transmittance (250 nm ≤ T_{sol} ≤ 2500 nm) for all prepared films.

$$T_i = \int \varphi_i(\lambda)T(\lambda)d\lambda/\varphi_i(\lambda)d\lambda \quad (1)$$

where $T(\lambda)$ is the transmittance at wavelength λ , is lum or sol for the calculation, φ_{lum} is the luminescence efficiency of the human eye, and φ_{sol} is the solar irradiance spectrum corresponding to the sun standing 37° above the horizon. $\Delta T_{lum/IR/sol}$ is obtained by $\Delta T_{lum/IR/sol} = T_{lum/IR/sol,20^\circ C} - T_{lum/IR/sol,80^\circ C}$. Figure 2-13 and Table 2-6 show the solar modulation efficiency and luminescence transmittance of the films. T_{lum} of sample 2 was prepared at the ambient pressure is 15.1 % at 25 °C and 19.7% at 90 °C. The ΔT_{lum} is -4.67 % exhibiting higher transmittance at a higher temperature. This reverse transmittance causes undesirable minus modulation for solar energy which deteriorates the whole efficiency of the film. This reverse transmittance might be attributed to the light scattered by agglomerated VO₂ particles. T_{sol} of the sample is 26.0 % and 25.3 % at 25 °C and 90 °C ($\Delta T_{sol} = 0.76$ %) which is a weak solar modulation ability.

Table 2-6. Solar transmittance and luminescence transmittance differences of VO₂ films at 25 °C and 90 °C.

	T_{sol} (%) (250 nm-2500nm)			T_{lum} (%) (380 nm-780nm)		
	25 °C	90 °C	ΔT_{sol}	25 °C	90 °C	ΔT_{lum}
Sample 1	39.8	34.5	5.3	37.1	37.9	-0.7
Sample 2	26.0	25.3	0.8	15.0	19.7	-4.7
Sample 3	55.7	51.7	7.9	55.2	51.7	3.5
Sample 4	55.7	50.9	4.8	51.7	50.9	0.8

On the other hand, samples 1, 3, and 4 which were prepared using scCO_2 , show a significantly improved solar modulation and luminous transmittance compared to sample 2, which was prepared at ambient pressure. ΔT_{sol} of sample 1, 3 and 4 are 5.31 %, 7.98 %, and 4.81 % respectively. The optical properties of the sample which are prepared in scCO_2 are slightly better than samples prepared in the presence of IL, likely due to the smaller nanofiber size. The integrated luminescence transmittance and solar modulation of the films are very close to the most typical reported single-layer VO_2 film (T_{lum} : 41 % and ΔT_{sol} : 6.7 %).

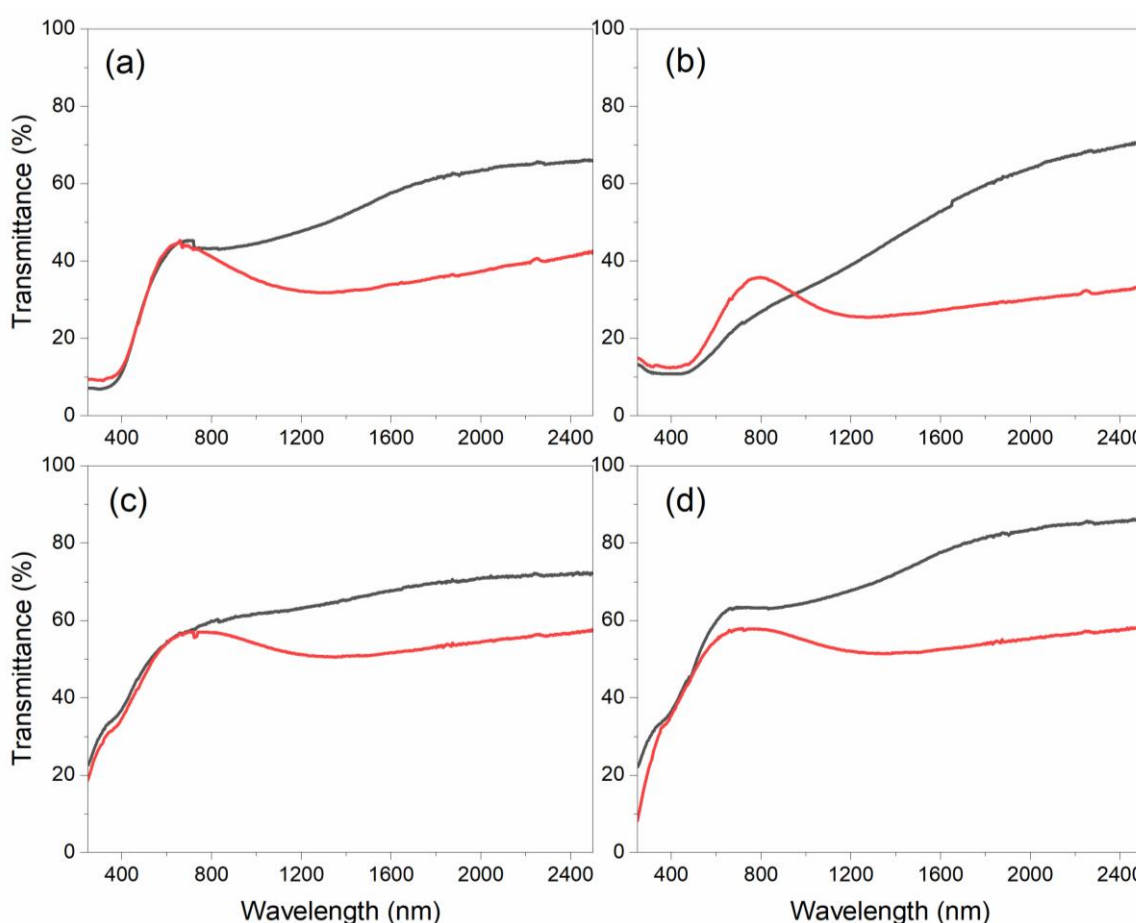


Figure 2-13. UV-Vis-NIR transmittance spectra of (a) Sample 1 (b) Sample 2 (c) Sample 3 (d) Sample 4, at the measurement temperature of 25 °C (black line), and at 90 °C (red line)

2.5 Conclusions

In the present study, the gelation of VTIP as a vanadium precursor is investigated in the presence of $scCO_2$, $scCO_2/IL$ ([EMIM][TF₂N], [EMIM][TFO], [EMIM][AcO], and [EMIM][HSO₄]) biphasic system and in IL only. It has been shown that ILs with a fluorinated anion counterpart such as [EMIM][TF₂N] and [EMIM][TFO] can be used as a substitute for HOAc as an acidic polycondensation reaction. The reaction which is happened in the biphasic system of [EMIM][TF₂N]/ $scCO_2$ showed 78 % gelation yield which is comparable with the 80 % yield which is gained from using a conventional catalytic reagent, HOAc, in $scCO_2$. The gelation yield drops to 39 % when the reaction is carried out in [EMIM][TF₂N] IL in the absence of $scCO_2$ indicating the role of $scCO_2$ in facilitating the gelation process. Characterization of aerogels and ionogels by TGA illustrated that ILs are incorporated into the structure of the dried gel and are not washed out during the drying procedure. Furthermore, BET results indicated that adding IL to the $scCO_2$ system deteriorates the surface area of the obtained gel compared to the ones prepared in the only $scCO_2$. It is also shown that the temperature of the sol-gel process and the calcination posttreatment condition have main effects on the formation of pure and high crystalline VO₂ (M). The pressure of the $scCO_2$ does not play a crucial role in the improvement of purity or crystallinity of the final product. When the reaction happens in [EMIM][TF₂N]/ $scCO_2$ biphasic, milder sol-gel and post-treatment conditions are needed for the formation of pure and high crystalline VO₂ (M) compared to other reactions media mentioned in the papers. Morphology studies on the final samples showed that how choosing different sol-gel conditions can affect the morphology of the products. The optical properties of the samples were analyzed using a UV-Vis-NIR instrument. The results confirmed that using ILs during sol-gel affects the optical properties of the VO₂ film negatively because of the formation of a bigger nano-size VO₂ structure.

Chapter 3

3 Stabilizing vanadyl acetylacetonate using imidazolium ionic liquids for VO₂ thermochromic thin films

***S. Nazari, P. Charpentier, Journal of Thin Film (725), 138640**

Abstract: This study examines the role of different imidazolium ionic liquids (ILs) on the stabilization of vanadyl acetylacetonate, VO(acac)₂, as a vanadium precursor by using UV-Vis spectroscopy. The possible stabilization mechanisms of VO(acac)₂ in IL solution were investigated. Furthermore, a fabrication method is proposed to prepare monoclinic vanadium oxide VO₂ (M) thin films using a mixture of ionic liquid and poly-ionic liquid (PIL). The ILs 1-ethyl 3-vinyl imidazolium bis(trifluoromethanesulfonylimide) ([EVIM][TFSI]), 1-ethyl 3-methyl imidazolium trifluoromethanesulfonate ([EMIM][TFO]) and 1-ethyl 3-methyl imidazolium acetate ([EMIM][AcO]) were investigated. It is shown that ([EVIM][TFSI]) has the best coordinating ability to VO(acac)₂ for protecting the central vanadium atom from oxidation. For thermochromic film formation, the effect of annealing temperature (250 °C – 400 °C) and time (10 minutes - 120 minutes) on crystallization was studied using X-ray diffraction. The possible role of PIL decomposition on the formation and crystallization of VO₂ (M) is discussed. The prepared films showed excellent thermochromic properties with 20.3 % solar modulation efficiency.

3.1 Introduction

Vanadium dioxide (VO_2) has received considerable attention due to its reversible metal-insulator transitions (MIT) at $68\text{ }^\circ\text{C}$ [101,108,140]. This transition is accompanied by a structural transformation between a low-temperature monoclinic phase and a high-temperature rutile phase. VO_2 (M) is an insulator and IR transparent while when above the MIT, VO_2 (M) is changed to VO_2 (R) which is metallic and highly IR reflective. The MIT transition involves drastic changes in the optical properties in the near-IR region, making VO_2 a potential candidate for smart window applications [140,141].

There are several synthetic methods to synthesize monoclinic vanadium oxide (VO_2 (M)) including magnetron sputtering [142], pulsed laser deposition [143], chemical vapor deposition (CVD)[144], and sol-gel processing [108,113]. However, to have an economical and environmentally friendly process, synthesis at low temperatures and durations using inexpensive and nontoxic precursors is paramount for potential scale-up. Vanadyl (IV) acetylacetonate $\text{VO}(\text{acac})_2$ is known as a relatively cheap and non-toxic precursor for the synthesis of vanadium oxide using a sol-gel method. The vanadium valance of $\text{VO}(\text{acac})_2$ is four, so a reduction of V^{5+} to V^{4+} is not required to prepare VO_2 (M) [145]. However, $\text{VO}(\text{acac})_2$ will be oxidized to a vanadium (V) complex in many solvents including water and alcohol [146] during sol-gel processing. On the other hand, the long-term duration of aging to prepare VO_2 (M) with reasonable thermochromic properties is time-consuming and economically inefficient. There is a report on accelerating the aging to 7 days by refluxing the sol solution at $80\text{ }^\circ\text{C}$ [147] which is still long for commercial application [147] R. Lipson et al. [148] suggested an allylic alcoholic solution containing β -methallyl alcohol to inhibit the oxidization of $\text{VO}(\text{acac})_2$ in solution by the involvement of an allylic group which coordinates to the central vanadium atom. However, β -methallyl alcohol is too costly to be considered as a solvent for the sol-gel process. There are also reports on the synthesis of VO_2 (M) by direct confined space combustion of an alcohol solution of $\text{VO}(\text{acac})_2$ [149,150].

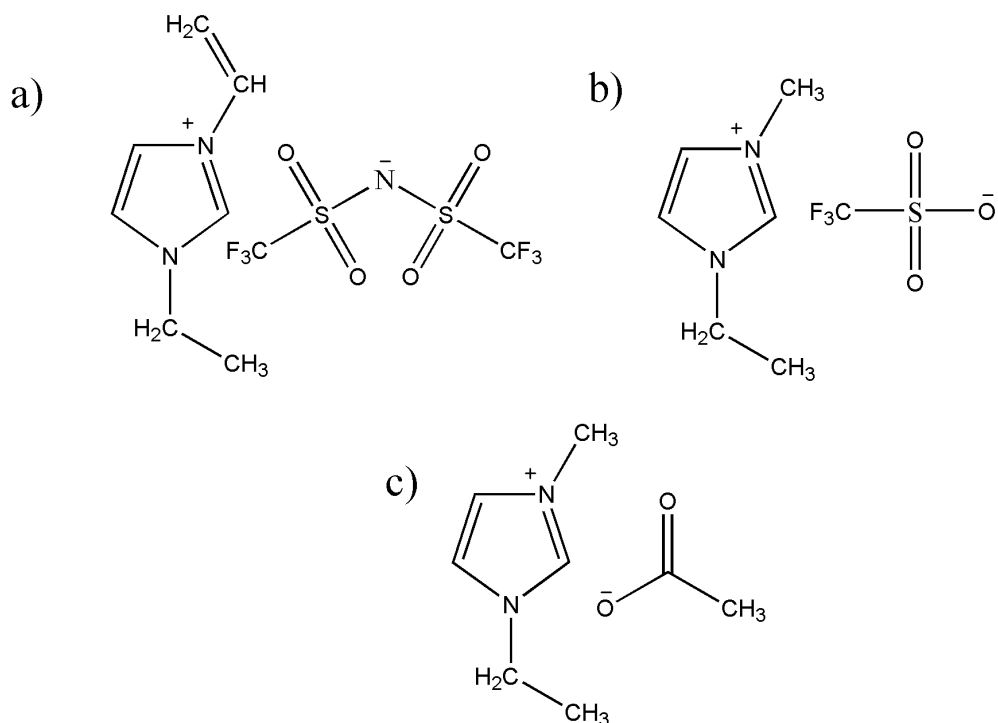
Recently, ionic liquids (ILs) have received considerable attention due to their unique properties and applications including the tunability of their solvent properties by changing their anion or cation counterpart [39,151,152]. In this study, the effect of different

imidazolium ionic liquids on the stability of VO(acac)₂ methanol solution was investigated by UV-Vis spectroscopy. We have tried to shorten the aging process by stabilizing the sol VO(acac)₂ solution using different imidazolium ionic liquids. Although ILs are normally considered non-coordinating, if used in excess, the anion counterpart containing extra electrons might interact with a metal center to some extent [153]. There are also a few reports on the coordination of imidazolium ionic liquids to transition metal complexes including VO(acac)₂ [154,155]. As previously shown, this type of organic bond coordination to central vanadium can inhibit the oxidation of VO(acac)₂ in solution [148]. The coordination ability of the ILs depends mainly on the basicity of their anion counterpart [153]. The ILs with acidic protons were not chosen for this study as the proton can interact with vanadyl oxygen, leaving the coordination position free for oxidation [153]. The ionic liquids chosen for this study are [EVIM][TFSI], [EMIM][TFO] and [EMIM][AcO]. Furthermore, we have developed a novel sol-gel method for the preparation of VO₂ (M) thin films with high thermochromic properties from a sol prepared with imidazolium IL. The effect of annealing parameters on the formation of pure VO₂ (M) is also investigated.

3.2 Experimental

3.2.1 Materials

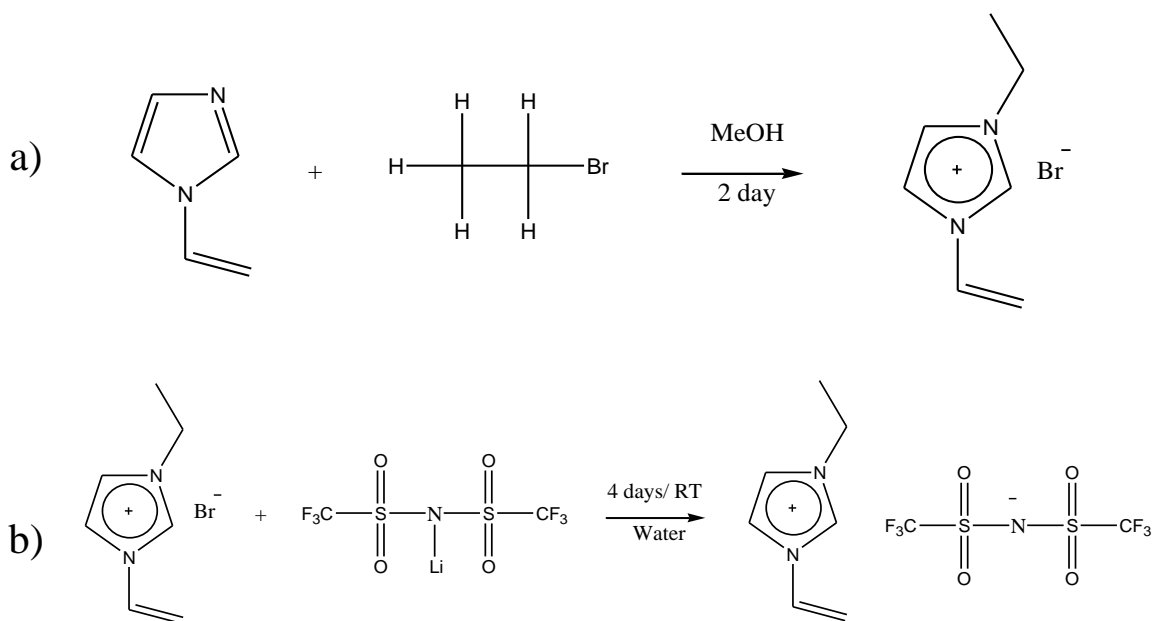
As vanadium precursor, vanadyl (IV) acetylacetonate VO(acac)₂ (98%, Sigma-Aldrich) was used as received. The ionic liquids 1-ethyl 3-methyl imidazolium acetate ([EMIM][AcO]) (97%, Alfa Aesar), 1-ethyl 3-methyl imidazolium trifluoromethanesulfonate ([EMIM][TFO]) (98%, Alfa Aesar) were purchased and used without further purification. 1-ethyl-3-vinyl imidazolium bis (trifluoromethanesulfonylimide) ([EVIM][TFSI]) ionic liquid was synthesized in the lab using T. Inoue et al. procedure [156]. The structure and purity of the ionic liquid were confirmed by ¹HNMR. Chemical structures of the ionic liquids used in this study are shown in Scheme 3-1



Scheme 3-1. Chemical structure of ILs examined in this work: a) 1-ethyl 3 vinyl imidazolium bis (trifluoromethanesulfonylimide) ([EVIM][TFSI]), b) 1-ethyl 3-methyl imidazolium trifluoromethanesulfonate ([EMIM][TFO]), c) 1-ethyl 3-methyl imidazolium acetate ([EMIM][AcO]).

3.2.2 Synthesis of 1-ethyl-3-vinylimidazolium bis (trifluoromethanesulfonylimide) ionic liquid

11.6 g of 1-vinylimidazole (Alpha-Aesar 99%) was added to 27 g of bromoethane (Alpha - Aesar 98%) in 8 mL of methanol. The mixture was heated to 50 °C for 2 days under vigorous stirring. Then, the excess methanol and unreacted bromoethane were evaporated from the solution to obtain 1-ethyl-3-vinylimidazolium bromide as an intermediate product (Scheme 3-2-a).



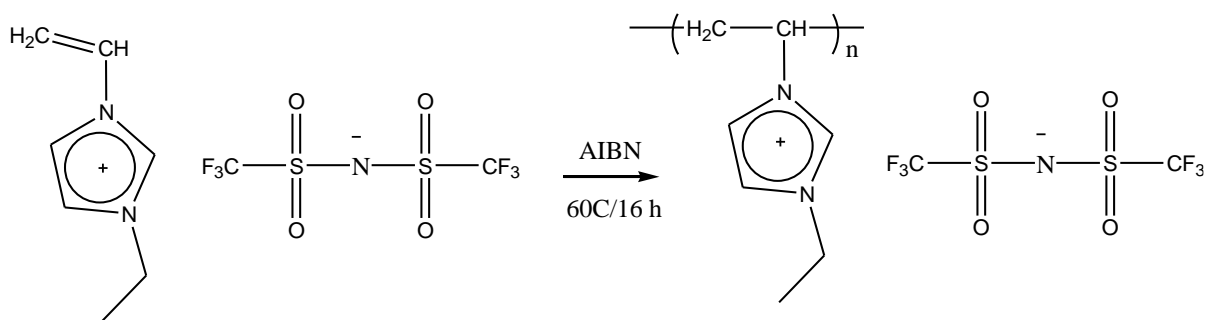
Scheme 3-2. a) procedure to prepare 1-ethyl-3-vinyl imidazolium bromide b) to prepare 1-ethyl-3-vinyl imidazolium bis(trifluoromethanesulfonylimide)

The collected sample was dried under a vacuum at 70 °C (yield of 99 %). 24.8 g of 1-ethyl-3-vinyl imidazolium and 44.2 g of 3-bis (trifluoromethane) sulfonimide lithium (Sigma Aldrich) was dissolved in 60 mL aqueous solution with the mixture stirred for 4 days at room temperature. The resultant ionic liquid phase of 1-ethyl-3-vinyl imidazolium bis(trifluoromethanesulfonyl)imide was separated from the aqueous phase and washed with water three times. The remaining ionic liquid was dried under vacuum at 50 °C resulting in an 80 % yield (Scheme 3-2-b). The structure of the product was confirmed by ^1H NMR (600 MHz) in DMSO- d_6 (Appendix).

3.2.3 Preparation of Poly (1-Ethyl-3-Vinylimidazolium bis (trifluoromethanesulfonylimide))

Poly (1-ethyl-3-vinyl imidazolium bis(trifluoromethanesulfonylimide)) was synthesized via free radical polymerization of 1-ethyl-3-vinyl imidazolium bis(trifluoromethanesulfonyl)imide ionic liquid [156]. The reaction was initiated by AIBN in DMSO anhydrous at 60 °C for 16 hours. The molar ratio of monomer to initiator was

200 and the volume ratio of the monomer to the solvent was 10. After the reaction, the polymer was precipitated by adding excess ethanol to the solution (Scheme 3-3). The precipitation was repeated by dissolving the polymer in acetone and precipitating in ethanol. The PIL sample was characterized using $^1\text{H NMR}$ (600 MHz) in acetone- d_6 (Appendix).



Scheme 3-3. Polymerization procedure to prepare poly (1-ethyl-3-vinylimidazolium bis(trifluoromethanesulfonylimide))

3.2.4 Stability of vanadium acetylacetonate in different ionic liquids

Vanadium acetylacetonate was purchased from Sigma Aldrich (98 %) and used without further purification. The mixture of $\text{VO}(\text{acac})_2$ and methanol 0.05 M were prepared to study the stability of the precursor using various volumetric amounts of IL as the stabilizer at room temperature. All the solutions were sonicated for 2 hours and they were aged for different time intervals. The solutions then were tested using a UV-Vis spectrometer (Shimadzu 3600) in the range of (400 - 900) nm.

3.2.5 Preparation of VO_2 thin film in IL/ MeOH solution

To prepare $\text{VO}_2(\text{M})$ thermochromic films, solutions of 0.05 M $\text{VO}(\text{acac})_2$ in methanol/IL (1 volume ratio) were prepared. To increase the viscosity of the sample, 2.5 w% of PIL was added to the solution and sonicated at 60 °C for 10 minutes and left for aging for 1 day. Subsequently, the glass substrate (VMR microscopic glass slides (25 × 25 × 2 mm) was ultrasonicated in the solution of 0.5 M HCl, deionized water, and ethanol for 30 minutes and dried in a vacuum oven.

The solution was deposited on a glass slide using a spin coater (Laurel Spin Coater-Model WS400BZ) at 400 rpm for 6 seconds and 1000 rpm for 20 seconds. The prepared thin films were annealed at different temperatures for a pre-set time using a tubular furnace (Barnstead Thermolyne Tube furnace 21100) under a constant nitrogen flow. The thermochromic properties of the film were tested by UV-Vis spectrometry. The annealing films were removed from the glass slide for subsequent characterization by XRD and DSC. The SEM of the removed film was shown in the Appendix.

3.3 Results and Discussion

3.3.1 Stability of vanadium acetylacetonate in MeOH solution

$\text{VO}(\text{acac})_2$ molecule has a C_2V geometry [157] as shown in Figure 3-1-a. The central vanadium atom in this complex is chemically accessible to coordinate with different solvent molecules. Furthermore, the solvent molecule in the coordination sphere can be replaced with an oxygen molecule, which will help convert vanadium (IV) to vanadium (V) in many solvents such as water or methanol.

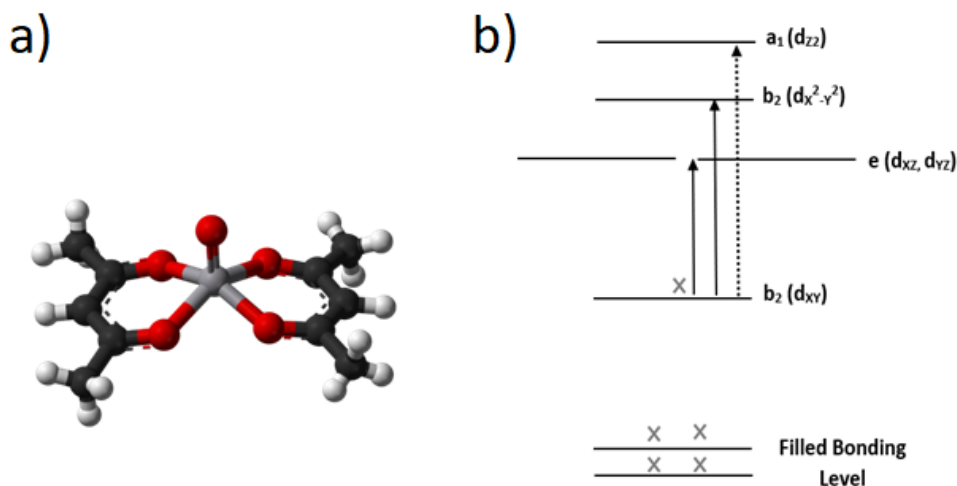


Figure 3-1. a) Chemical structure of vanadium acetylacetonate, $\text{VO}(\text{acac})_2$, b) Electronic energy level of vanadium acetylacetonate, $\text{VO}(\text{acac})_2$.

Figure 3-1-b shows the electronic energy levels of vanadyl (IV) complex with C_2V symmetry for the square pyramid: $b_2 (d_{xy})$, $e (d_{xz}, d_{yz})$, $b_1 (x^2-y^2)$, $a_1 (d_z^2)$. As b_2 is

considered pure vanadium ($3d_{xy}$ orbital) and e (d_{xz}, d_{yz}) is a combination of vanadium and oxygen orbitals, a transition from b_2 (d_{xy}) to e (d_{xz}, d_{yz}) having the lowest transition energy should be the one most sensitive to axial solvent perturbations.[153,157,158] The (d_{xy} to d_z^2) and (d_{xy} to $d_{xz, yz}$ and $d_x^2-d_y^2$) transitions in $\text{VO}(\text{acac})_2$ structure will appear as two peaks at 570 nm and 780 nm in a UV-Vis spectrum. Therefore, UV-Vis can be used as a useful tool to study the oxidation of $\text{VO}(\text{acac})_2$ in solution.

Figure 3-2 shows the UV-Vis spectrum of $\text{VO}(\text{acac})_2$ solution in methanol at day 1 (black line) and after aging for, 3, 7, and 25 days (red, blue, and green lines).

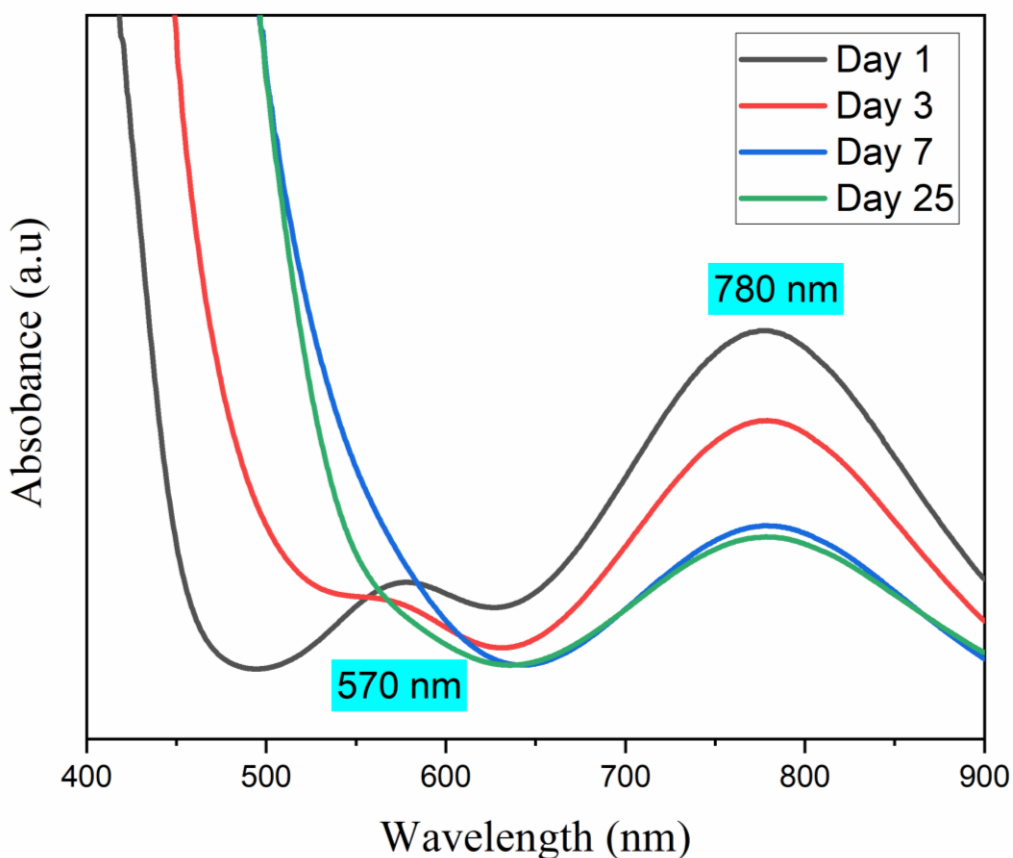
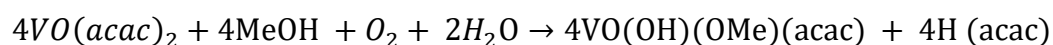


Figure 3-2. UV-Vis spectrum of $\text{VO}(\text{acac})_2$ in methanol solution after different aging times.

The color of the fresh $\text{VO}(\text{acac})_2$ solution in MeOH is dark blue, which gradually will change to orange by aging when exposed to air. The color change is attributed to the

oxidation of V(IV) to V(V) of the central vanadium atom of VO(acac)₂. As shown in Figure 3-2, the peak at 780 nm decreases in intensity with increasing time and the transition peak at 570 nm disappears with increasing time, indicating the oxidation of vanadium. Furthermore, there is a redshift in the charge transfer peak which is located near the UV region (<500 nm). The half-filled orbital of V(IV) atom consequently involves repulsion energy and the repulsion will be removed in the V(V) atom when oxidation occurs, resulting in the observed redshift in the transition peak. The oxidation of VO(acac)₂ by molecular oxygen in methanol was investigated by R. Grybos et al. [146] as follows:



Their study indicated the formation of VO(OH)(OMe)(acac), hydroxometoxooxo (pentane-2,4 dionato) vanadium (V) [146]. The red/orange appearance of the solution is attributed to the formation of this complex. The complete conversion of VO(acac)₂ to VO(OH)(OMe)(acac) was shown to take 50 days [147] at room temperature. The VO(OH)(OMe)(acac) complex needs to be reduced during an annealing process to synthesize VO₂(M). It has been shown that the full conversion of VO(acac)₂ to VO(OH)(OMe)(acac) is necessary to obtain VO₂(M) with reasonable thermochromic properties. However, as the vanadium valance of VO(acac)₂ is already four, a prolonged aging and annealing process is inefficient for VO₂(M) formation.

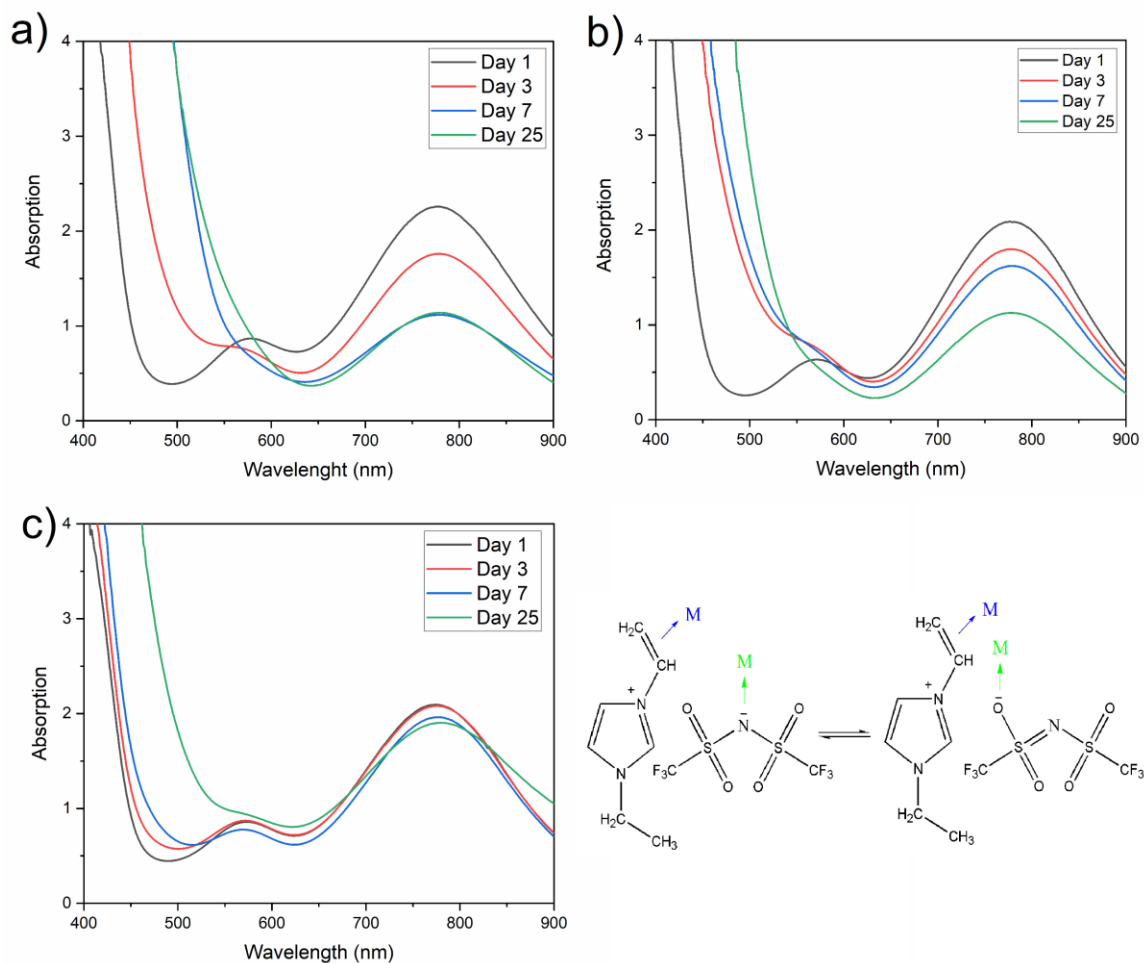


Figure 3-3. UV-Vis spectrums of VO(acac)₂ methanol solution with a) volume ratio of MeOH: [EVIM][TFSI]= 20, b) volume ratio of MeOH: [EVIM][TFSI]= 1, c) volume ratio of MeOH: [EVIM][TFSI]= 0.2.

Figure 3-3 shows the UV-Vis spectrums of VO(acac)₂ in methanol solution after adding different concentrations of [EVIM][TFSI] during different aging time intervals. As shown, when the volume ratio of the MeOH: [EVIM][TFSI] is 20, the solution is still undergoing oxidation by aging. When the volume ratio of MeOH: [EVIM][TFSI] was decreased to 1, there is a smaller decrease in intensity of the first d-d transition peak at 780 nm, even after 25 days of aging. However, there is still a redshift in the charge transfer band after 3 days. This overlaps with the peak at 570 nm which is related to the other d-d transition. By decreasing the volume ratio of MeOH: [EVIM][TFSI] to 0.2, there is a very small decrease

in d-d transition peaks, and a slight red shift is observed by aging. The color of the precursor solution was not changed for over a month. As shown in Figure 3-3, [EVIM][TFSI] can stabilize the precursor by the vinyl bond of imidazolium cation or through a range of nitrogen or oxygen binding modes of its anion counterpart, depending on the electronic and steric demands of the metal center.

Figure 3-4 shows the UV-Vis spectrum of $\text{VO}(\text{acac})_2$ methanol solution with the addition of different [EMIM][TFO] concentrations.

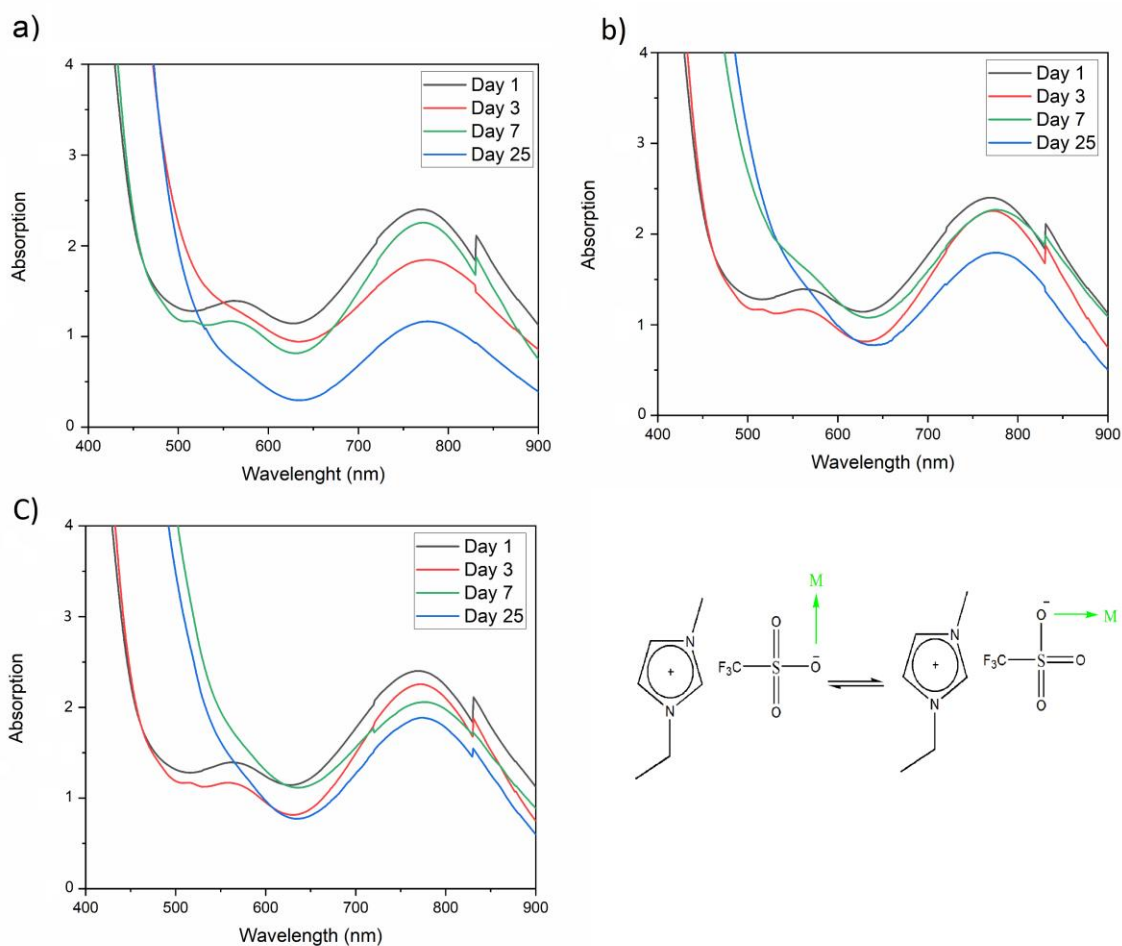


Figure 3-4. UV-Vis spectrums of $\text{VO}(\text{acac})_2$ methanol solution with a) volume ratio of MeOH: [EMIM][TFO] = 20, b) volume ratio of MeOH: [EMIM][TFO] = 1, c) volume ratio of MeOH: [EMIM][TFO] = 0.2.

The stability of $\text{VO}(\text{acac})_2$ in methanol solution increases with increasing concentration of $[\text{EMIM}][\text{TFO}]$. However, by comparing the results without IL in MeOH and when using $[\text{EMIM}][\text{TFO}]$, $[\text{EVIM}][\text{TFSI}]$ has a better coordination ability. The Lewis basicity of TFSI is lower than TFO and it is a bulkier anion. Therefore, its better coordination ability is likely to be due to the high charge distribution via four distinct binding modes: monodentate nitrogen or oxygen coordination and/or bidentate oxygen–oxygen or nitrogen–oxygen coordination [153]. There is another reason for the high coordination ability of $[\text{EVIM}][\text{TFSI}]$, which is not attributed to its anion but its cation. The vinyl bond on the imidazolium cation can have a role in its coordination ability of the ionic liquid because of the π -system (Figure 3-3). The high coordination ability of $[\text{EVIM}][\text{TFSI}]$ leads to the stabilization of $\text{VO}(\text{acac})_2$ solution and oxidation inhibition [148]. It has been previously reported that the π -system of the unsaturated vinyl bond of the solvent can stabilize $\text{VO}(\text{acac})_2$ solution for longer times aging [148].

Figure 3-5 shows the UV-Vis spectrum of $\text{VO}(\text{acac})_2$ methanol solution with the addition of different concentrations of $[\text{EMIM}][\text{AcO}]$. When the volume ratio of MeOH: $[\text{EMIM}][\text{AcO}]$ is 20, the solution is going through oxidation after 3 days and there is also a dramatic decrease in the peak at 780 nm. After 7 days of aging, the peak at 780 nm has disappeared as a result of complete oxidation. When the volume ratio of MeOH: $[\text{EMIM}][\text{AcO}]$ was decreased to 1 and 0.2, the rate of oxidation significantly increased. The results confirm that the acetate anion shows weak coordination ability to vanadium atoms of $\text{VO}(\text{acac})_2$. The spectrum also shows that increasing the concentration of $[\text{EMIM}][\text{AcO}]$ enhances the oxidation process of $\text{VO}(\text{acac})_2$ in solution. It has been shown before that acetate anions in $[\text{EMIM}][\text{AcO}]$ form close contact with the imidazolium cation through C-H \cdots O hydrogen bonding [159] (Figure 3-3). This strong hydrogen bonding decreases the coordination ability of acetate anions to the central vanadium atom of $\text{VO}(\text{acac})_2$. There are also reports showing that ILs with AcO anion counterparts have promoted other oxidation reactions[160].

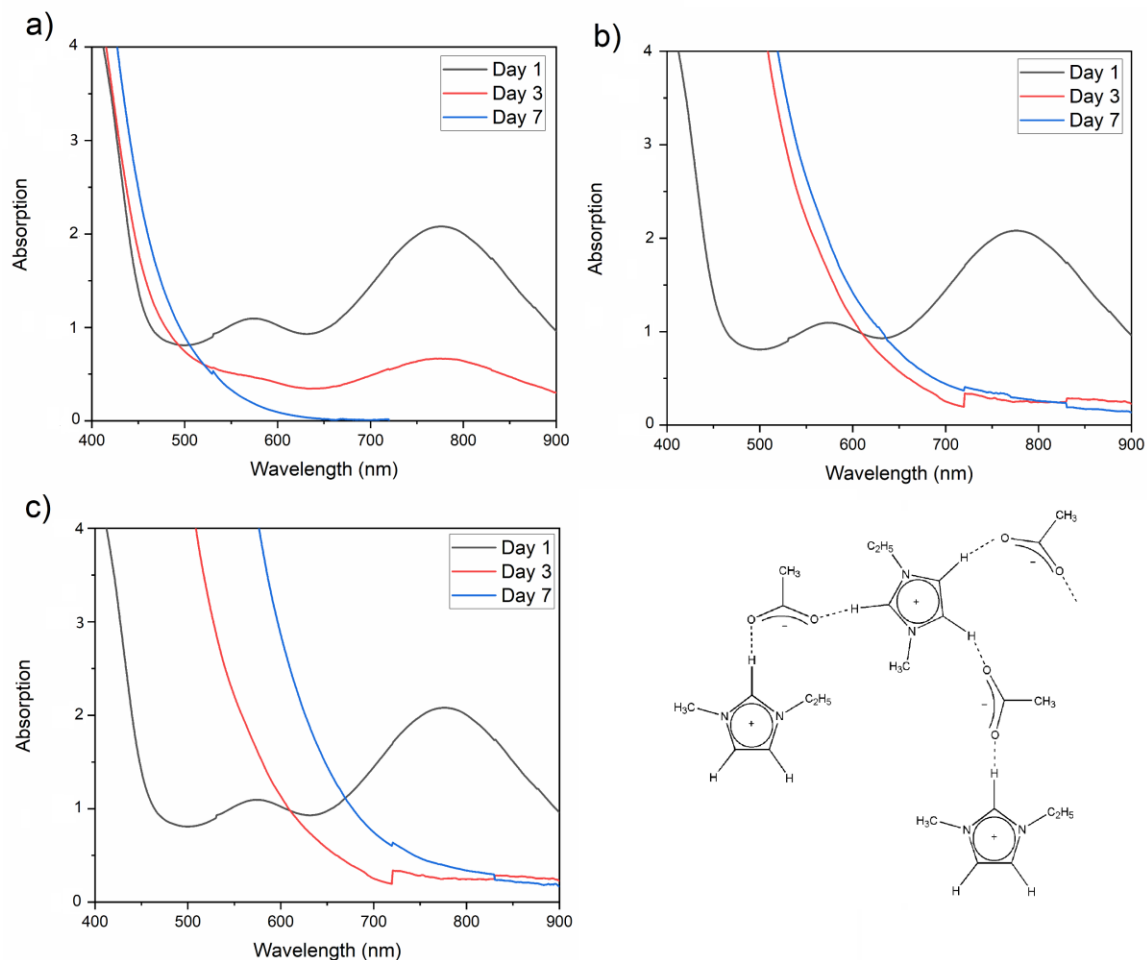


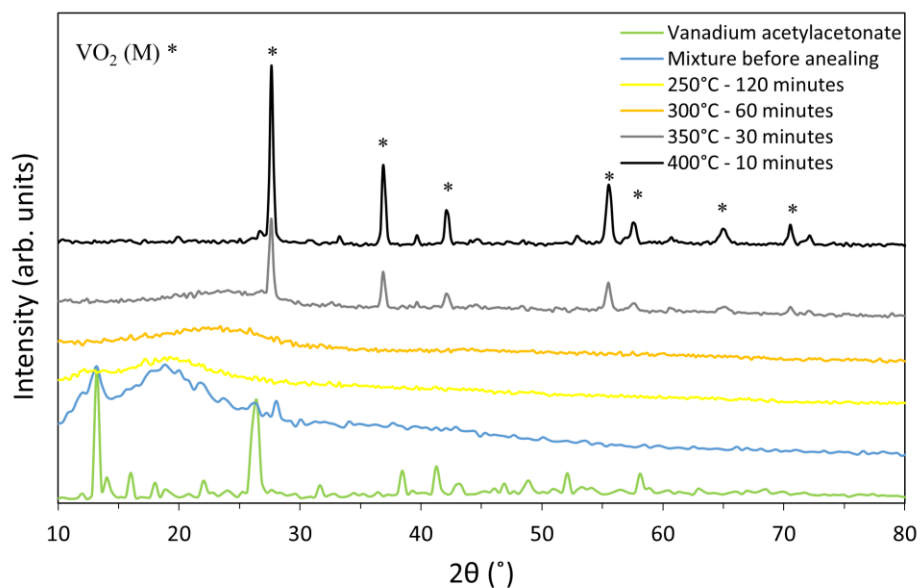
Figure 3-5. UV-Vis spectrums of $\text{VO}(\text{acac})_2$ methanol solution with a) volume ratio of $\text{MeOH}:\text{[EMIM][AcO]} = 20$, b) volume ratio of $\text{MeOH}:\text{[EMIM][AcO]} = 1$, c) volume ratio of $\text{MeOH}:\text{[EMIM][AcO]} = 0.2$

These results show that some imidazolium ILs with high coordination ability can be used to inhibit oxidation of $\text{VO}(\text{acac})_2$ in the MeOH solution. Lewis basicity and a high number of coordination sites have the main effect in the stabilization of $\text{VO}(\text{acac})_2$. In the next section, a precursor sol solution that has been stabilized with $[\text{EVIM}][\text{TFSI}]$ will be used as a casting solution for the preparation of VO_2 thin film to examine the utility of this approach.

3.3.2 Preparation of VO₂ thin film

To prepare VO₂(M) thermochromic films, solutions of VO(acac)₂ in methanol/[EVIM][TFSI] (volume ratio: 1) were prepared. To increase the viscosity of the sample, 2.5 w % of PIL was added to the solution and sonicated at 60 °C for 10 minutes and left for 3 days aging. The fresh sol without aging did not adhere well to the substrate. However, aging for 3 days enhanced adhesivity to the SiO₂ of the glass slide which is attributed to the formation of VO(OH)(OMe)(acac).[161] The hydroxyl –OH groups of the precursor will interact with silanol –Si–OH groups of the Si-substrate and improve the adhesion at the deposition of the VO(acac)₂–methanol sol films onto the substrate.[145,147] The precursor sol solution was cast onto the glass slides and annealed at different temperatures and duration. Figure 3-6-a shows the XRD patterns of prepared vanadium film samples after annealing.

a)



b)

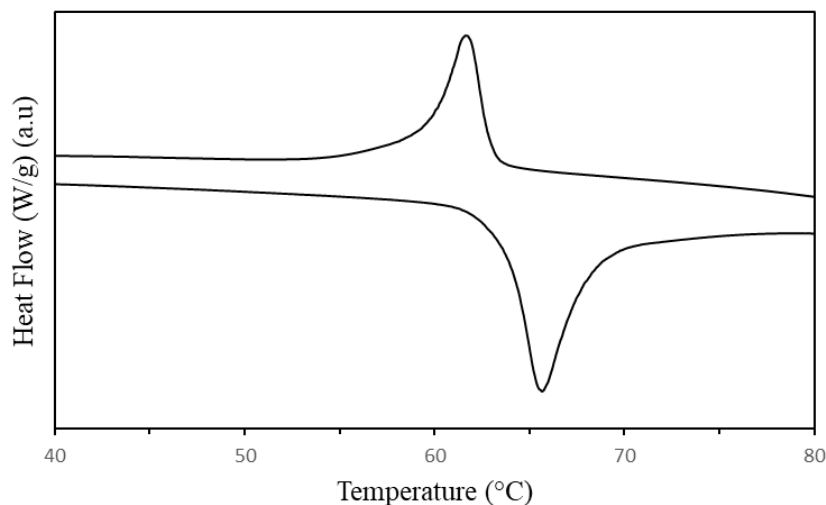


Figure 3-6. a) XRD patterns of samples before and after annealing at different temperatures and duration, b) DSC Curve of the sample after annealing at 400°C for 10 minutes.

When the annealing temperature was lower than 350 °C, no crystalline sample was formed, even by extending the annealing duration to 60 minutes. Crystalline VO₂ (JCPDS72-0514, P21/c, a=0.5743 nm, b=0.4517 nm, c=0.5375 nm, and $\beta=122.61^\circ$) was formed at 350°C after 30 minutes and by increasing the temperature to 400 °C, a better crystalline sample with sharper XRD peaks was formed after 10 minutes. The DSC curve of the film sample annealed at 400 °C for 10 mins also confirms the formation of VO₂(M), showing the transition temperature of 66 °C and 62 °C at the heating and cooling cycle respectively (Figure 3-6). The hysteresis loop width of the transition is quite small ($\Delta T = 4$ °C), indicating the fast response of the product to the temperature change[162]. The annealing temperature and duration of the reaction are much lower than previously reported, leading to a simple and economical method for the production of VO₂ (M). Furthermore, the stability of VO(acac)₂ in IL solution and during the process provides a convenient method for the synthesis of VO₂ (M).

One concern that might arise during the annealing process is that the annealing temperature of 400 °C can partially decompose the PIL and IL. The PIL degree of decomposition by time at each annealing temperature (250 °C, 300 °C, 350 °C, and 400 °C) was investigated using TGA (Table 3-1). It has been shown that 40% of the poly-ionic liquid decomposes at 400 °C after 10 minutes. However, it seems the decomposition of the polymer likely induces the formation of the VO₂ monoclinic phase. Similar results have been reported

regarding the influence of decomposition of poly- vinyl pyrrolidone (PVP) on the formation and crystallization of VO₂ (M) by annealing at 600 °C [47]. The authors suggested that the release of reductive gases can prevent vanadium (IV) from oxidation and facilitate the formation of VO₂ (M) phase. If degradation of the polymer happens at the same temperature with VO₂ crystallization, this potentially helps facilitate the formation of VO₂(M). Nevertheless, at a lower temperature, the influence of polymer decomposition and the reductive gases prevents the crystallization of VO₂.

Table 3-1. Decomposition percentage of PIL at different temperatures.

Temperature (°C)	Time (Minutes)	Decomposition percentage (%)
250	120	4
300	60	9
350	30	27
400	10	40

The thermochromic and optical properties of the prepared VO₂ thin films were evaluated using UV- Vis- NIR instrument at two temperatures of 30 °C and 85 °C (Figure 3-7). The solar modulation (T_{sol}) and the integral luminous transmittance (T_{lum}) were obtained using the following equation:

$$T_{lum,sol} = \frac{\int \varphi_{lum,sol}(\lambda)T(\lambda)d\lambda}{\int \varphi_{lum,sol}(\lambda)d\lambda}$$

where λ is the wavelength of light, φ_{lum} is the luminescence efficiency of the human eye, and φ_{sol} is the solar irradiance spectrum corresponding to the sun standing 37° above the horizon and T is the transmission of the VO₂ thin film at different temperatures. The solar transmittance of the film is 79.1 % at 30°C and 58.3% at 85 °C.

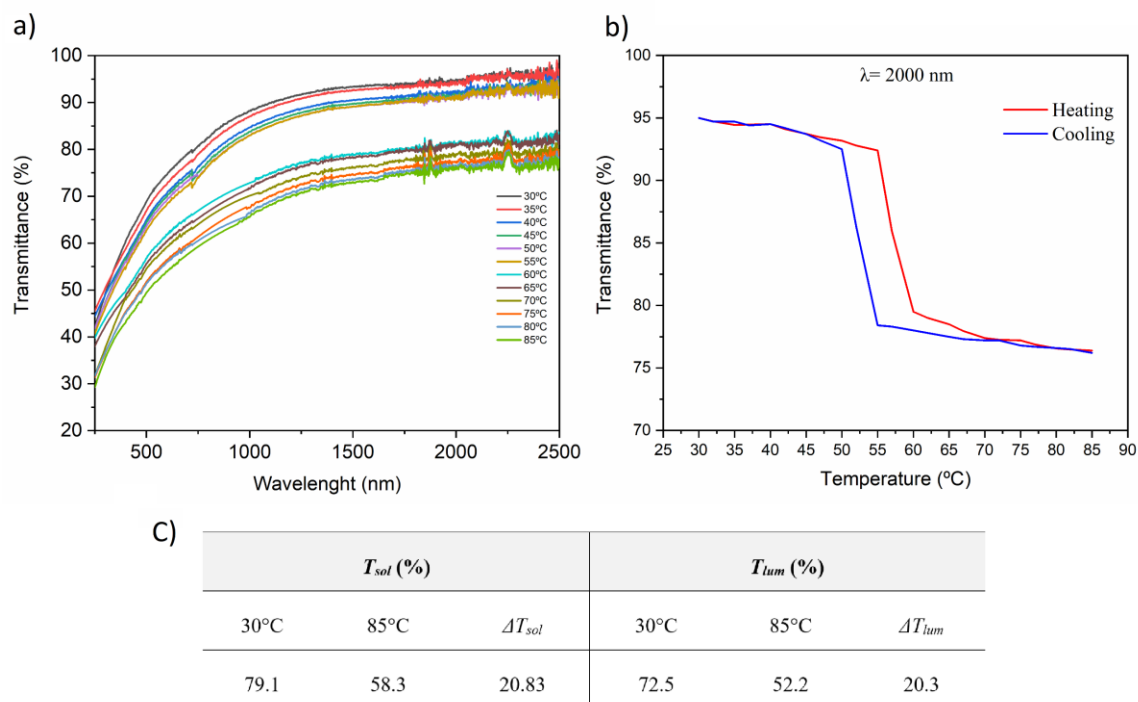


Figure 3-7. a) Transmission spectra of VO₂ film at 30°C and 85°C b) Hysteresis loop characteristic analysis of VO₂ film c) Optical calculations of VO₂ film

As a result, we can calculate a solar modulation efficiency (20.8 %) which is usually used to determine the thermochromic properties of VO₂ films. The result is encouraging as the solar modulation value is much higher than 6.7 % [163] for a single-layered VO₂ film, 14.7 % for nano-porous VO₂ [55], 13.6 % for VO₂/SiO₂ [42]. The modulation efficiency of 20.8% is obtained at luminescence transmittance of 72.5 % and 52.2 % at 30 °C and 85°C respectively ($\Delta T_{lum} = 20.3$ %) (Figure 3-7-c). However, there was also a drop in the UV-Vis range when increasing the temperature. This indicates a possible role for PIL in the switching properties of VO₂.

The hysteresis width of the transmittance as a function of temperature can be calculated during the metal-insulator transition of heating/cooling cycles, as shown in Figure 3-7. The hysteresis width of the film is calculated as 5 °C (Figure 3-7-c) which is close to the DSC data. However, it seems the transition temperature range is between (55 - 60) °C in the heating cycle, which is 5 °C lower than the transition temperature which is observed for the VO₂ powder in DSC data. It has been reported before that the transition temperature

drops when the VO₂ is dispersed in polymer coating as it can inhibit the agglomeration of VO₂ particles. Therefore, the energy needed for VO₂ particles in polymer film to do the transition from monoclinic to tetragonal rutile face is reduced, leading to a lower transition temperature [164].

3.4 Conclusion

In this study, [EVIM][TFSI], [EMIM][TFO] and [EMIM][AcO] imidazolium ionic liquids were used to investigate the stability of the VO(acac)₂ methanol solution for extended periods of aging time. It has been shown that sol solution in the presence of 1-ethyl-3-vinyl imidazolium bis (trifluoromethanesulfonylimide), [EVIM][TFSI] showed the highest stability compared to [EMIM][TFO] and [EMIM][AcO]. This is justified because of the high coordination ability of [TFSI] anion and the existence of the vinyl bond on the cation counterpart of the IL. [EMIM][AcO] showed a reverse effect on the stability of the precursor solution. By increasing the concentration of [EMIM][AcO], oxidation was accelerated. This can be justified by the fact that there is high internal hydrogen bonding between cation and anion counterpart of [EMIM][AcO], weaken its coordination ability. It has been also shown before that ILs with AcO anions can promote the oxidation process.

The mixture of [EVIM][TFSI] IL/PIL/ methanol and VO(acac)₂ was explored for the sol-gel process to fabricate thermochromic films. After annealing at 400 °C for 10 minutes, the film was formed very crystalline and pure VO₂ (M) with narrow hysteresis of 4 °C. We have proposed that the decomposition of the IL/PIL can induce the formation of the VO₂ monoclinic by preventing vanadium (IV) from oxidation. The VO₂ (M) film showed great thermochromic properties with 20.3 % solar modulation properties of 20.3 %. However, the luminous transmittance of the film dropped within the UV-Vis region probably which enhanced the solar modulation efficiency. Furthermore, using IL/PIL in the sol-gel solution promoted the formation of flower-like morphology which consists of a large number of uniform VO₂ nano-sheets.

Chapter 4

4 Novel Fabrication Methods Vanadium Dioxide Using Polymerized Ionic Liquid

Abstract: Various intelligent thermochromic coatings have been investigated as optical switches for smart window applications. Vanadium oxide (VO_2) coatings in particular have garnered significant attention since they show automatic solar/heat control in response to environmental temperature changes without using any external switching device. In this study, VO_2 nanostructures are synthesized using a hydrothermal method, following by calcination treatment. It is shown that the calcination conditions can influence the crystallinity, hysteresis width, and latent heat of the VO_2 nanostructures as well as their size and morphology. The role of VO_2 loading on the optical properties of the films is investigated by integrating the nanostructures into a ethylene-vinyl acetate (EVA) polymer coating. Furthermore, the VO_2 nanostructures are Mo-doped to decrease their transition temperature. The role of calcination on the morphology and size of the Mo-doped nanostructures is investigated. Moreover, improving the optical properties of the VO_2 nanostructures is followed by coating them with amorphous SiO_2 coatings. The role of TEOS volume on the optical properties of the film is investigated. Two complementary methods for the fabrication of VO_2 and VO_2/SiO_2 nanostructures are suggested using poly-ionic liquid (PIL) as a dielectric host: 1) solution casting 2) UV-Curing. The optical properties of the resulting films showed prominent solar modulation using the UV-Curing method. VO_2/SiO_2 composite film prepared by UV-curing shows entrapped nanostructures in the polymer matrix by strong hydrogen bonding which can lead to better dispersion and great optical properties of the final film.

4.1 Introduction

Vanadium oxide (VO_2) has gained considerable attention because of its reversible first order metallic-insulator transition (MIT) at a transition temperature of $68\text{ }^\circ\text{C}$ [101,102,165]. The MIT is followed by a crystallographic transformation from semiconductor to monoclinic phase, VO_2 (M), at low temperatures to a metallic tetragonal rutile phase, VO_2 (R), at high temperatures. The structure transformation can cause drastic changes in the physical properties of VO_2 , such as electric, optical and magnetic properties, etc., which makes it a potential candidate for a variety of applications such as thermochromic window coatings[105,140], light modulators, and storage media[166]. However, there are three main challenges to prepare thermochromic coatings for smart windows applications. The ideal transition temperature for intelligent glazing is between $20\text{-}25\text{ }^\circ\text{C}$ [3] while the critical temperature of VO_2 , $68\text{ }^\circ\text{C}$, is considered too high for this application. Furthermore, it is very challenging to prepare pure phase VO_2 (M/R) with a shape-controlled nanostructure with sharp and narrow hysteresis loops for practical application in smart thermochromic devices[162,167,168]. Moreover, thermochromic VO_2 coatings have the drawback of low luminescence transmittance (T_{lum}) and low solar modulating ability (ΔT_{sol}) and there is a great challenge to improve both properties simultaneously[105,106]. There are several reports which have tried to achieve optical enhancement by introducing special dopant ions (Mg^{2+} , F^-)[141,169] into the VO_2 crystal lattice or depositing anti-reflection (AR) coatings such as TiO_2 [170,171] and SiO_2 [43,103] layers to enhance both the T_{lum} and ΔT_{sol} . There is a report[172] about developing a VO_2 /hydrogel hybrid which resulted in ultra-high thermochromic performance; however, the translucent appearance at higher temperatures limited its full application. For the fabrication of thermochromic VO_2 coatings, it is important to have a matrix to absorb as much heat and light from sunlight as possible to accelerate the optical switching process. Consequently, different polymers have been already used as solar absorbing materials. Specific heat capacity is one of the factors indicating the quantity of heat which can be absorbed by one mole of a substance to raise its temperature by one degree centigrade. Imidazolium-based ILs are molten salts which have a melting point below $100\text{ }^\circ\text{C}$. They also have a large specific heat capacity value ($\sim 570\text{ J/mol}\cdot\text{K}$) compared to the polymers which have been used in the existing coatings materials for fabrication of VO_2 [72–74].

Furthermore, studies on the optical properties of imidazolium based ILs have shown that they are transparent in most of the UV region and in the visible and near IR region[75,76]. Therefore, the high heat capacity and transparency of ILs make them a potential candidate to be used as a coating modifier for thermochromic window application. On the other hand, IL is an ionic compound with a relatively high dielectric constant which has dipolar as well as ionic contribution[78,79]. VO₂ nanoparticles in dielectric hosts show enhanced luminescence transmittance and solar energy transmittance based on effective medium theory[173]. Like other properties of ILs, their dielectric constants can be tuned over a wide range of cations and anions. Replacement of highly symmetric anions with some dipolar anions can enhance the dielectric constant. Despite the ILs' great properties as a potential coating for thermochromic materials, their liquid nature limits their application as a coating. Poly Ionic Liquids (PILs), which also called polymerized ILs, are a new class of polymeric materials that feature IL species in each monomer repeating unit. PILs are attracting great interest not only because of the combination of the unique properties of ILs with the macromolecular architecture, but also a matter of amplifying the properties of ILs[86,87].

In this study, all three challenges of preparing thermochromic coatings for smart glazing are examined. The hydrothermal process with a controlled calcination process was used to prepare VO₂ (M), Mo-doped VO₂, and VO₂/SiO₂ nanostructures with high purity and small hysteresis width (0 °C - 4 °C). Furthermore, nanostructures incorporated in poly (1-ethyl-3-vinyl imidazolium bis (trifluoromethanesulfonylimide)) by different fabrication methods including solution-based spin coating and UV-curing. The thermochromic properties of the films were measured and compared by UV-Vis-NIR spectroscopy.

4.2 Experimental

4.2.1 Synthesis of nanorod VO₂ (M)

VO₂ nanorods were prepared following the procedure proposed by Y. Li's[41] group. V₂O₅ (Sigma Aldrich Reagent) and oxalic acid powder (H₂C₂O₄.2H₂O, Sigma Aldrich) were dissolved in 200 mL of deionized water (the molar ratio of oxalic acid and vanadium pentoxide 1:2). The resultant solution was stirred for 24 h at room temperature. Then,

40 mL of the suspension was transferred into a 100-mL Teflon lined autoclave and heated between 200 °C -250 °C for a preset time. After the hydrothermal procedure, the autoclave was cooled down to room temperature. The resulting black precipitate was washed three times with deionized water and alcohol alternatively, and then collected by filtration and dried at 60 °C in air overnight. The resulting precipitates were post-treated by annealing the powder at 400 °C -500 °C for a preset time to obtain crystalline VO₂ (M) nanorods. The crystal structure of the synthesized VO₂ (M) sample was collected by a Bruker benchtop X-ray diffractometer using Cu K α radiation (λ for K α = 1.54 059 Å) at 30 kV and 10 mA. Scanning Electron Microscopy (SEM-LEO 1540XB) was used to study the surface morphology of the samples. Each sample osmium sputtered by an Edwards Auto500 unit at 15 mA/min for the 90 s to achieve a 5 nm - 7 nm osmium layer. All images were taken at 3 kV at different magnifications. The phase transition behavior of the prepared samples was measured by differential scanning calorimetry (DSC-SDT Q600) over the temperature of 10 °C to 90 °C. The heating rate and cooling rate were set at 10 °C/min and 5 °C/min respectively.

4.2.2 Synthesis of Mo-nanorod VO₂ (M)

V_{1-x}Mo_xO₂ (x = 0.3 1.2, 2.4 at. %) nanowires were prepared by the hydrothermal reduction of V₂O₅ by oxalic acid in the presence of molybdcic acid within a Teflon-lined autoclave vessel, heated at 250 °C for 48 h. The solid black residue was recovered by filtration and washed three times by deionized water and alcohol alternatively and dried at 60 °C in air overnight. The resulting precipitates were post-treated by annealing the powder at 500 °C for 1 h. The Mo - doped VO₂ (M) samples were characterized by a Bruker benchtop X-ray diffractometer and Differential Scanning Calorimetry. The elemental composition of doped samples was confirmed and quantified using the energy dispersive X-ray detection (EDX) feature of the SEM.

4.2.3 Synthesis of VO₂/SiO₂ Nanorods

A modified Stober method was used for the preparation of amorphous silica shells on VO₂ nanostructures. A solution of 24 mg of VO₂ nanostructures in 4:1 (v/v) ethanol: water was ultrasonicated to obtain a homogeneous dispersion. Then, 400 μ L of ammonium hydroxide

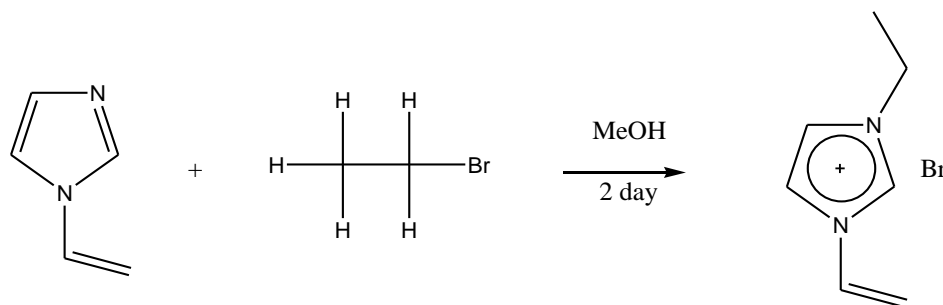
(NH₄OH) (0.25 M final solution) was added to the solution. Subsequently, 200-800 μ L tetra-ethylorthosilicate (TEOS) was added to this dispersion (0.02 M concentration of TEOS). The reaction was carried out for 25 minutes at room temperature and then the solution was centrifuged to collect VO₂/SiO₂ nanostructures.

4.2.4 Preparation of EVA ThermoChromic Films Using Solution Casting

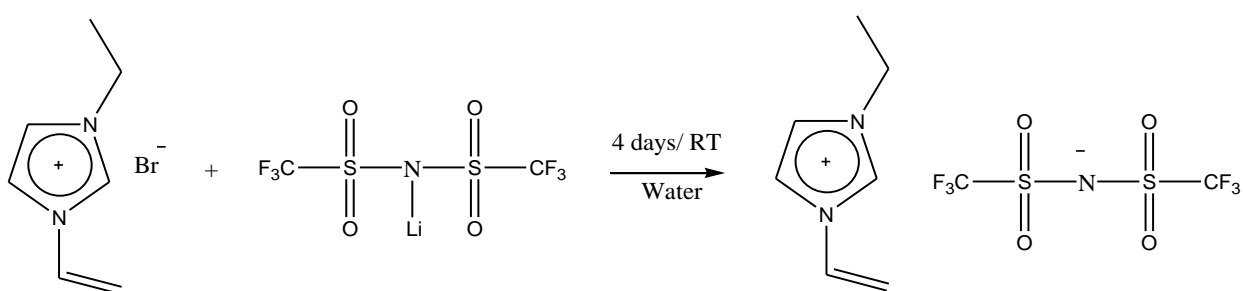
EVA solution (10 wt %) was prepared using chloroform as the solvent. Different loadings of VO₂ (2, 4, 6, and 8 mg/ mL) nanostructures were dispersed in the solution using a sonication bath for 4 hours. The solution is casted on the glass slides (VMR microscopic glass slides (25 mm \times 25 mm \times 2 mm) using a spin coater (Laurel Spin Coater- Model WS400BZ) at 400 rpm for 6 S and 2000 rmp for 30 s.

4.2.5 Preparation of 1-Ethyl-3-Vinylimidazolium bis(trifluoromethanesulfonylimide)

The ionic liquid is prepared using Inoue et al.'s method[156]. 11.6 g of 1-vinyl imidazole (Alpha-Aesar 99%) was added to 27 g of bromoethane (Alpha-Aesar 98%) in 8 mL of methanol. The mixture was heated to 50 °C for 2 days under vigorous stirring. Then, the excess methanol and unreacted bromoethane were evaporated from the solution to obtain 1-ethyl-3vinylimidazolium bromide as an intermediate product (Scheme 4-1). The collected sample was dried under vacuum at 70 °C (yield of 99%). 24.8 g of 1-ethyl-3-vinyl imidazolium and 44.2 g of 3-bis(trifluoromethane) sulfonimide lithium (Sigma Aldrich) was dissolved in 60 mL aqueous solution. The mixture was stirred for 4 days at room temperature. The resultant ionic liquid phase of 1-ethyl-3- vinyl imidazolium bis(trifluoromethanesulfonyl)imide was separated from the aqueous phase and washed with water three times. The remaining ionic liquid was dried under vacuum at 50 °C resulting in 80 % product yield as determined (Scheme 4-2). The structure of the product was confirmed by ¹H NMR (600 MHz) in DMSO-d₆ (Appendix).



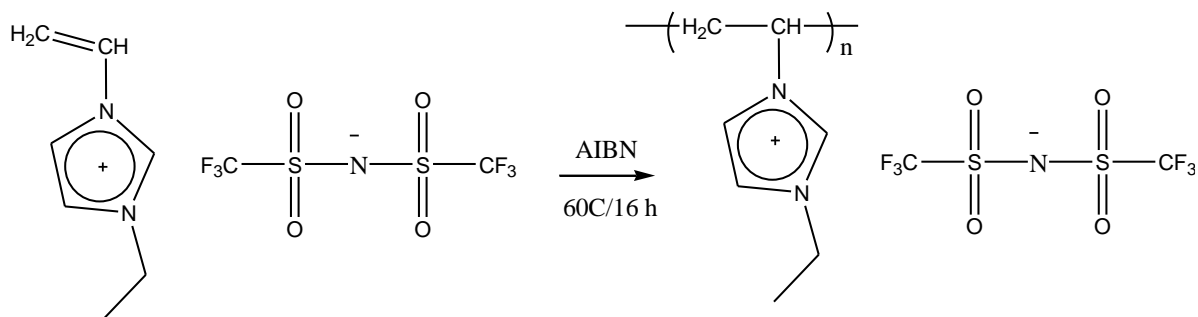
Scheme 4-1. Reaction scheme to prepare 1-ethyl-3-vinyl imidazolium bromide.



Scheme 4-2. Reaction scheme to prepare 1-ethyl-3-vinyl imidazolium bis(trifluoromethanesulfonylimide).

4.2.6 Preparation of Poly (1-Ethyl-3-Vinylimidazolium bis (trifluoromethanesulfonylimide)):

Poly (1-ethyl-3-vinyl imidazolium bis(trifluoromethanesulfonylimide)) was synthesized via free radical polymerization of 1-ethyl-3-vinyl imidazolium bis(trifluoromethanesulfonylimide) ionic liquid[156] as shown in Scheme 4-1.



Scheme 4-3. Reaction scheme to prepare poly (1-ethyl-3-vinyl imidazolium bis(trifluoromethanesulfonylimide)).

The reaction was initiated by AIBN in DMSO anhydrous solvent at 60 °C for 16 hours. The molar ratio of monomer to initiator and the volume ratio of the monomer to the solvent was examined to result in different PIL molecular weights. After the reaction, the polymer was precipitated by adding excess ethanol to the solution. The precipitation was repeated by dissolving the polymer in acetone and then re-precipitating in ethanol two more times. PIL sample was characterized using ^1H NMR (600 MHz) in acetone- d_6 (Appendix). The viscosity of the polymers was measured using a Ubbelohde dilution viscometer.

4.2.7 Preparation of PIL Thermo-chromic Composite Films Using Solution Casting

PIL solution (10 wt %) was prepared using acetonitrile as the solvent. Then, VO_2 or VO_2/SiO_2 nanostructure (4 mg/ mL) was dispersed in the solution using a sonication bath at 60 °C for 4 h. The well-dispersed solutions were cast onto glass slides (VMR microscopic glass slides (25 mm \times 25 mm \times 2 mm) using a spin coater (Laurel Spin Coater- Model WS400BZ) at 400 rpm for 1 minute. The optical properties of the coated film were measured using a UV-Vis Spectrometer (Shimadzu 3600) in the range of 250-2500 nm. The morphology of the samples was investigated using Scanning Electron Microscopy (SEM-LEO 1540XB). A Veeco diMultiMode V atomic force microscope (AFM, Veeco, Plainview, NY, USA) was used to measure the thickness of the films via the Nanoscope V7.30 program software.

4.2.8 Preparation of PIL Thermochromic Films Using UV-Curing

The solution mixture of IL monomer and VO₂ or VO₂/ SiO₂ nanostructure (4 mg/ mL) was sonicated for 4 hours at 60 °C. Then, 2.5 wt % hydroxy-2-methylpropiophenon (Sigma Aldrich-97 %) was added to the solution as the photo-initiator. The 0 to 2.5 and 7.2 molar percentage of divinylbenzene (Sigma Aldrich- 80 %) was also added as crosslinker while purging the solution with Argon. The obtained viscous and homogenous solution was cast onto VMR microscopic glass slides (25 × 25 × 2 mm)) by dip coating. The Teflon plate was placed under a 365 nm UV-lamp (Fischer Black-Ray B100AP high-intensity UV-lamp -100W) for 10-40 minutes. The prepared films' optical properties were tested using a UV-Vis spectrometer (Shimadzu 3600) in the range of 250-2500 nm.

4.3 Results and Discussion

4.3.1 Effect of Calcination Condition on Synthesis of VO₂ (M)

The hydrothermal method was used as the first step of the reaction leading to the formation of VO₂ (M) by reducing V₂O₅ as the precursor. Normally, the hydrothermal process forms the products of metastable and non-thermochromic phases rather than pure VO₂ (M). XRD is used as the analysis method to characterize the hydrothermal process products (Figure 4-1). The XRD results indicate the formation of V₃O₅ at 250 °C after 24 hours of reaction time from the oxidation of the V₂O₅ starting material. The XRD pattern of the V₃O₅ powder can be assigned to a monoclinic structure within the P2/c space group (JCPDS card 72-0977). Extending the reaction time to 48 hours and 72 hours does not show any significant changes. However, when the temperature is 200 °C, VO₂ (B) appears after 48 hours of reaction time. The peaks were indexed to VO₂ (B) with space group C2/m, lattice parameters a = 12.0417(3) Å, b = 3.6892(8) Å, c = 6.4312(2) Å, and β = 106.965(2) Å; which match with JCPDS Card No. 01-081-2392.

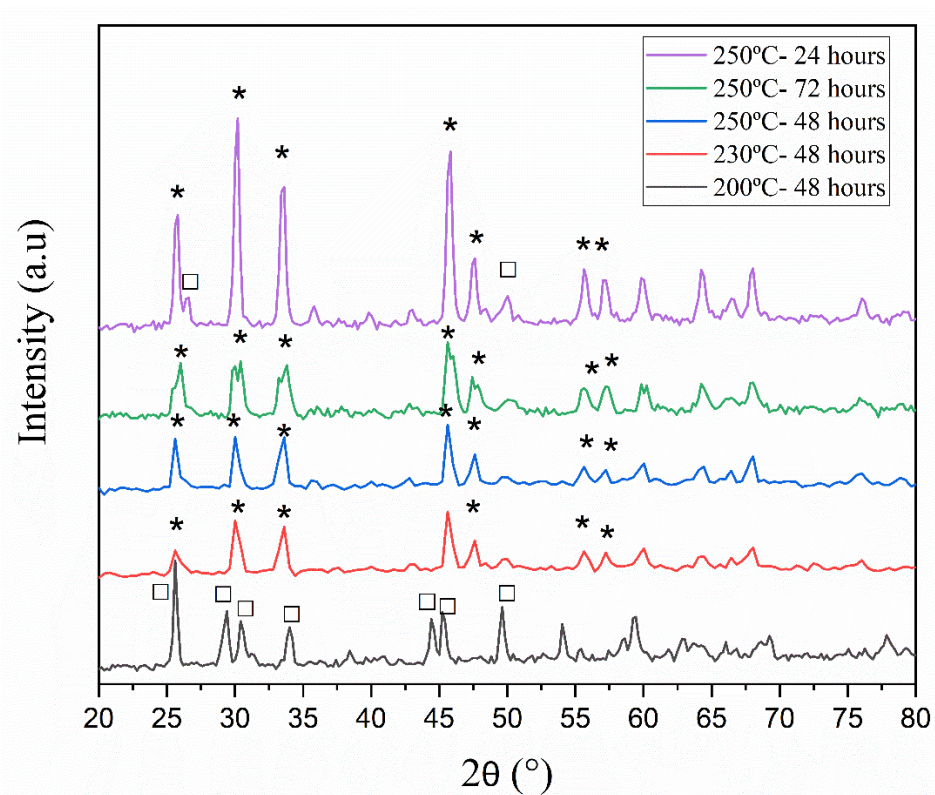


Figure 4-1. XRD patterns of hydrothermal samples prepared at 200 °C -250 °C for different reaction times. (*) symbol represents V₃O₅ and symbol (□) represents VO₂ (B).

To obtain the pure monoclinic phase (M1) of VO₂, the sample which was collected from the hydrothermal reaction at 200 °C after 48 hours was annealed at various annealing temperatures and time. As shown in Figure 4-2, samples annealed at 500°C exhibit diffraction peaks which can be assigned to the pure monoclinic VO₂ (JCPDS72-0514, P21/c, a=0.5743 nm, b=0.4517 nm, c=0.5375 nm, and b=122.61°). The intensities of the diffraction peaks are improved significantly as the annealing time increases to one hour, indicating an enhancement in the crystallinity of the sample. As shown in Figure 4-2, the conversion to VO₂ (M) does not happen at temperature 400 °C, even though the annealing time was increased to 4 hours.

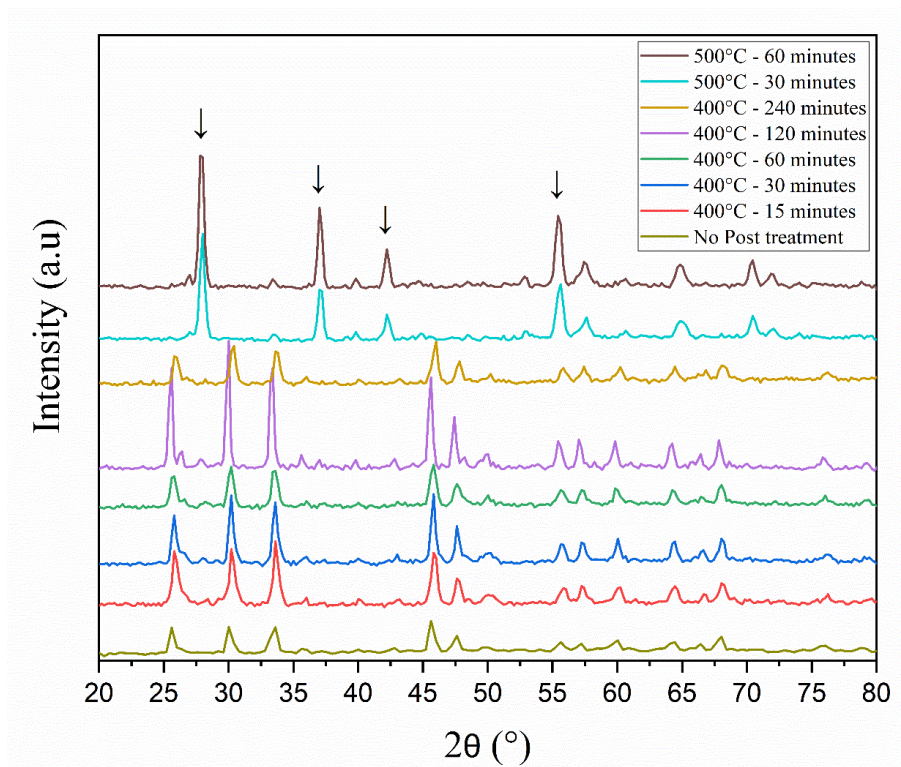


Figure 4-2. XRD patterns of samples at different annealing conditions; the annealing temperature varies from 400 °C to 500 °C and the annealing time varies from 30 minutes to 4 hours. Symbol (↓) represents VO₂ (M).

To investigate the influence of annealing temperature and duration on the transition temperature, hysteresis width, and latent heat (J/g) of VO₂ (M), measurements were done using differential scanning calorimetry (DSC). Figure 4-3. DSC curves of samples after various annealing conditions.

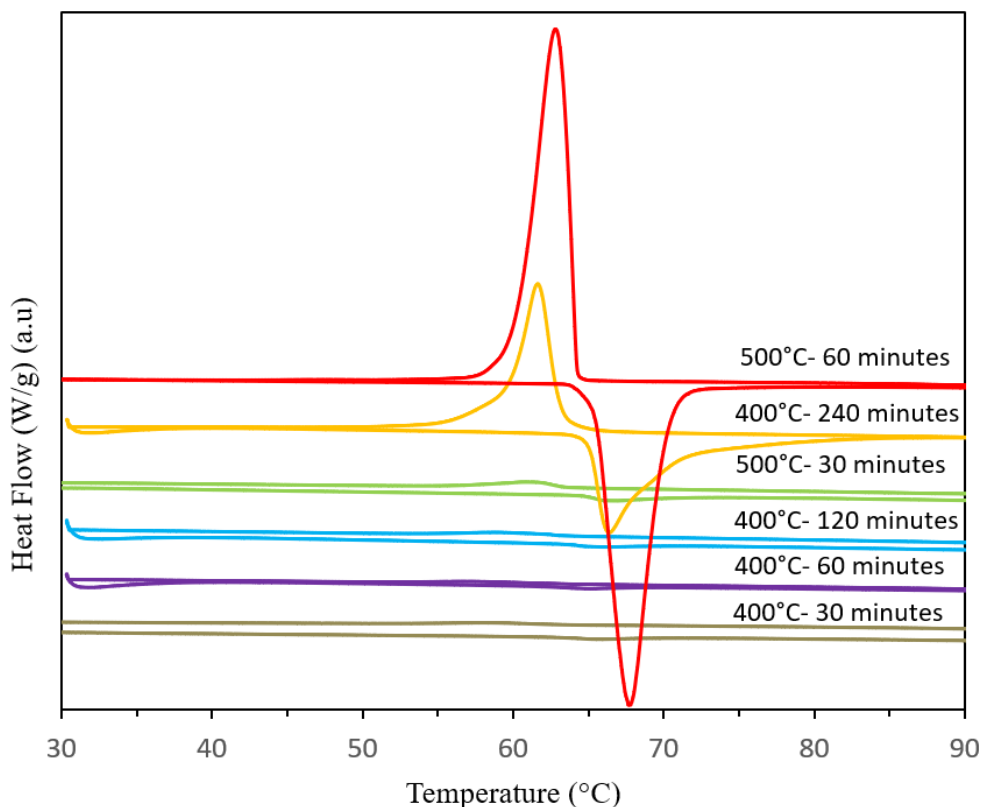


Figure 4-3. DSC curves of samples after various annealing conditions.

The latent heat of the phase transition (which is calculated as the area under heating) indicates the thermochromic properties of VO₂ (M) nanostructure and corresponds to the value of solar energy modulation ability of VO₂ (M)[174]. The thermal hysteresis width is defined as the difference between T_c in the heating cycle and T_c in the cooling cycling[168]. The hysteresis loop width should be as narrow as possible and the transition gradient should be sharp as possible to have a quick metal to insulator and insulator to metal transition to make it applicable for smart glazing[162,168]. It has been shown that ideal thermochromic glazing acts as an energy effective solar system when the hysteresis loop is sharp and narrow (between 0 °C -4 °C).

As shown in Figure 4-3 and Table 4-1, by optimizing the annealing parameters, the latent heat of metal to insulator and insulator to metal transition in VO₂ increases dramatically due to the high crystallinity of the sample. When the sample was calcinated at 500 °C for 1 hour, the latent heat is 3.25 j/g. However, by decreasing the temperature or the duration

of the calcination, the latent heat decreased due to the poor crystallinity of the samples. The hysteresis width as well as the DSC peak sharpness is improved by increasing the calcination temperature or duration (Table 4-1, Figure 4-3). The hysteresis of the sample which is calcinated at 500 °C for 1 hour is as low as 4.5 °C indicates a fast response and high sensitivity of the VO₂ to the temperature changes and this may be associated with the high crystallinity at high annealing temperatures. There is another method which is recently reported in the literature for reducing the hysteresis width of VO₂ samples which involves dehydration of a new intermedium, VO₂ (M). 0.15H₂O[167] or VO₂ (M). 0.25H₂O[175]. The hysteresis width of 4.3 °C[167] and 3.4 °C[175] are reported using this method.

Table 4-1 DSC results for the heating and cooling cycles of samples obtained at different calcination conditions.

Annealing Temperature (°C)	Annealing Duration (Min)	$T_{c-heating}$ (°C)	$T_{c-cooling}$ (°C)	Hysteresis Width (°C)	Latent Heat (J/g)
500	60	67.6	63.1	4.5	3.25
400	240	66.3	61.8	4.5	1.75
500	30	67.7	61.6	6.1	1.11
400	120	66.4	60.0	6.4	0.80
400	60	65.6	58.4	7.2	0.36
400	30	66.0	58.5	7.5	0.32

Scanning Electron Microscopy (SEM) was used to study the morphology of the samples. Figure 4-4 indicates the formation of nanorods after calcination. The SEM study shows the role of calcination conditions on the size of the nanostructure. By improving the calcination conditions, the average diameter of the nanorods changes from 330 nm for the sample calcinated at 400 °C for 120 minutes, to 152 nm for the sample prepared at 500 °C for 60 minutes (Table 4-2). As shown in Figure 4-4, the calcination condition does not affect the nanostructure shape.

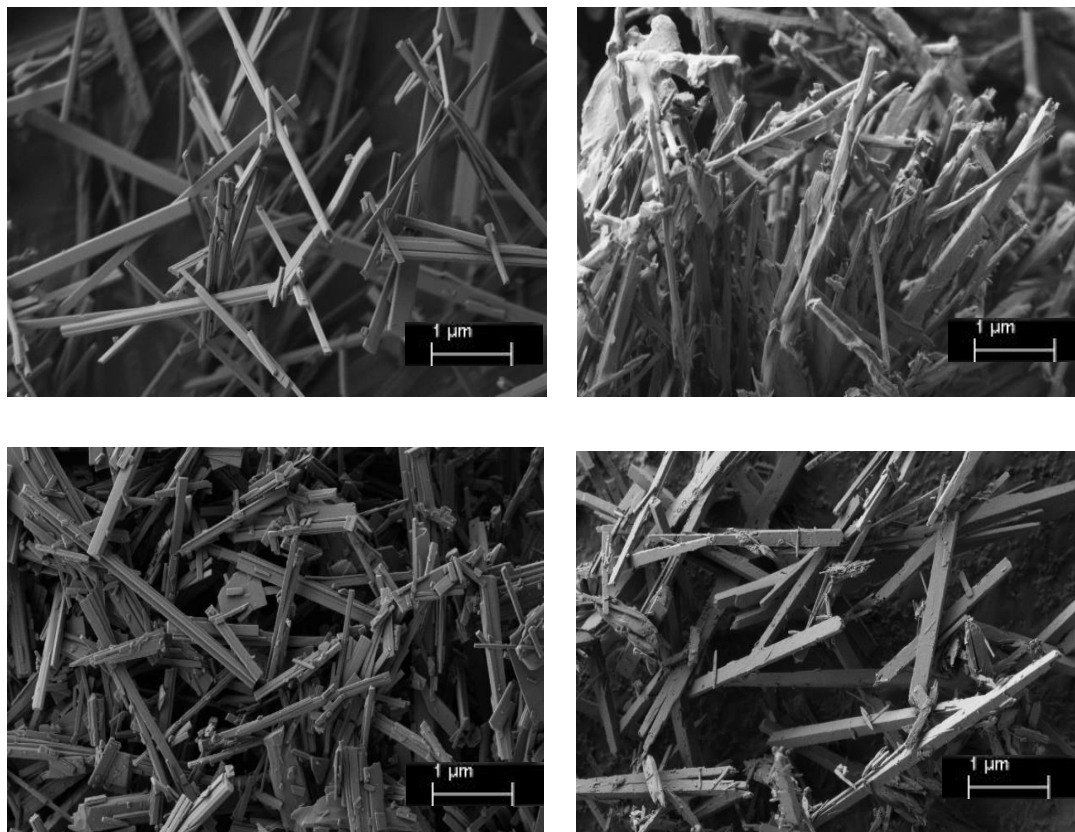


Figure 4-4. SEM images of samples after annealing a) at 500 °C for 60 minutes b) at 500 °C for 30 minutes c) at 400 °C after 120 minutes d) at 400 °C after 240 minutes

Table 4-2. Nanostructure size and shape by changing the calcination temperature and duration.

Annealing Temperature (°C)	Annealing Duration (Min)	nanostructure size	nanostructure shape
500	60	152	nanorods
400	240	255	nanorods
500	30	178	nanorods
400	120	330	nanorods

The VO₂ nanostructure were collected after annealing at 500 °C for 60 minutes then dispersed into a EVA polymer solution at different VO₂ loadings and cast onto glass slides. The following equation is used for measuring the integrated visible transmittance (380 nm ≤ T_{vis} ≤ 780 nm) and integrated solar transmittance (280 nm ≤ T_{sol} ≤ 2500 nm) for all prepared films:

$$T_i = \int \varphi_i(\lambda)T(\lambda)d\lambda/\varphi_i(\lambda)d\lambda$$

where $T(\lambda)$ is the transmittance at wavelength λ , is lum or sol for the calculation, φ_{lum} is the luminescence efficiency of the human eye, and φ_{sol} is the solar irradiance spectrum corresponding to the sun standing 37° above the horizon. $\Delta T_{lum/IR/sol}$ is obtained by $\Delta T_{lum/IR/sol} = T_{lum/IR/sol,20^\circ C} - T_{lum/IR/sol,80^\circ C}$. The solar modulation efficiency and luminescence transmittance of the films are evaluated and compared in Table 4-3.

Table 4-3. Optical properties of EVA films with different loadings of VO₂

Nanostructure Load in Composite	T_{lum} (%)			T_{sol} (%)		
	25 °C	90 °C	ΔT_{lum} (%)	25 °C	90 °C	ΔT_{sol} (%)
2 mg	42.3	37.0	5.3	50.4	43.7	6.7
4 mg	39.8	34.8	5.0	51.7	42.8	8.9
6 mg	37.1	37.8	-0.7	39.8	34.5	5.3
8 mg	15.0	19.6	-4.6	38.1	37.4	0.7

To have a thermochromic film in practical window application, it is necessary to find an optimal balance between the luminous transmittance and solar modulation ability by finding an optimal loading of VO₂ in the film[176]. Table 4-3 indicates that for the 2 mg/mL dispersion, solar modulation of 6.7 % is obtained at a visible light transmittance of 42.3 %. Increasing the active particle loading to 4 mg/mL increases the solar modulation to 8.9 %; however, the visible light transmittance is decreased to 39.8 %. Further increasing the

nanostructure loading to 6 mg/10 mL or 8 mg/10 mL negatively affects the luminous transmittance of the film.

4.3.2 Effect of Mo-doping on VO₂ (M)

To decrease the transition temperature of the VO₂ (M), molybdenum with 0.3, 1.2, and 2.1 atm % is doped into the crystal structure of the vanadium oxide. Substitutional doping with molybdenum usually induces a 12 °C/ atm % -15 °C/ atm % decrease of the transition temperature[22]. However, we have observed ~20.5 °C/ atm % Mo-doped VO₂ nanorods synthesized by the hydrothermal method (Figure 4-5). As it is shown in the DSC curve, the transition temperature is decreased to 20 °C- 24 °C by 2.1 at% Mo-doping.

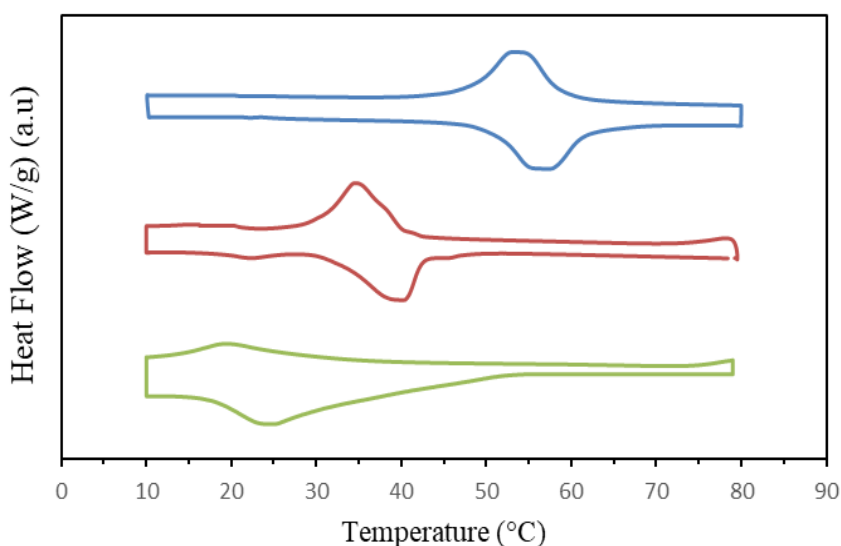


Figure 4-5. DSC curves of VO₂ nanorods samples with 0.3, 1.2, and 2.1 atm% Mo

In the previously reported value for Mo-doped nanowires, 2.5 at% of Mo is used to reach 20 °C -25 °C of transition temperature while the hysteresis width between metal to insulator phase and insulator to metal phase is reported approximately 12 °C according to the DSC curve [22]. Nevertheless, we have observed unprecedented small hysteresis ($\Delta T \sim 4$ °C) for our synthesized Mo-doped VO₂ nanostructure samples. EDX spectrum of the Mo-doped samples confirms the dopant atom percentage of the VO₂ sample (Figure 4-6).

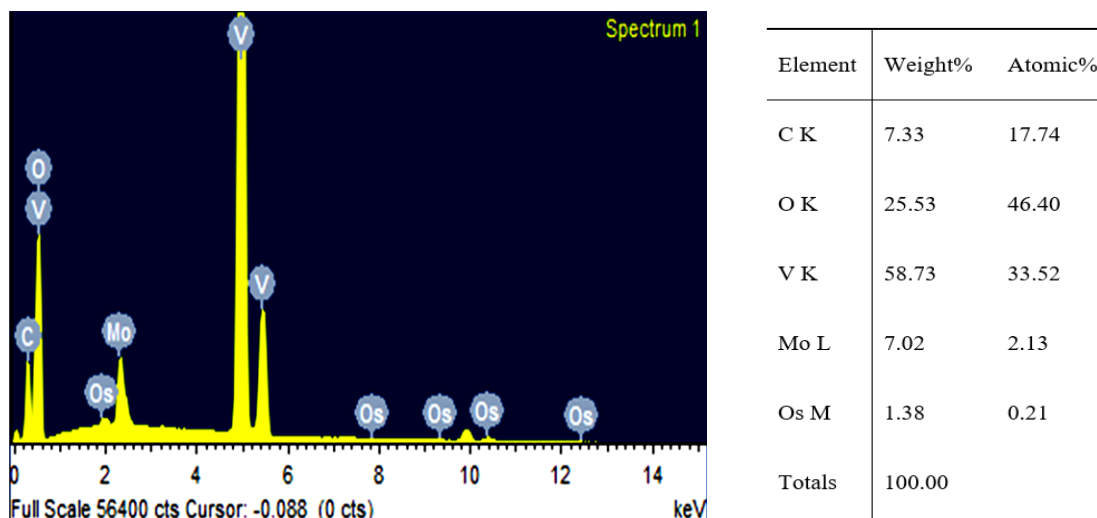


Figure 4-6. EDX of Mo-doped VO₂ (M)

Figure 4-7 indicates the morphology of the doped samples before and after the annealing treatment. Studies have shown that incorporation of atoms into host lattices as a dopant can manipulate various crystal growth behaviors of nanomaterials. As shown in Figure 4-6-a and Figure 4-7-c, doping the VO₂ samples promotes the formation of “snowflake” morphology along with hexagonal particles in micro-scales. Snowflake morphology for VO₂ (M) and Mo-doped VO₂ (M) has been reported by different authors[35,177]. However, it should be noted that VO₂ particles with snowflake morphologies can limit particle dispersion, transparency, and overall application to smart windows[10]. Consequently, the Mo-doped samples were post-treated by annealing at 500 °C for 1 hour. The morphology of the annealed samples shows nanoscale particles indicating the rule of an annealing treatment in obtaining nanoscale particles in Mo-doped VO₂ (Figure 4-7-b and Figure 4-7-d).

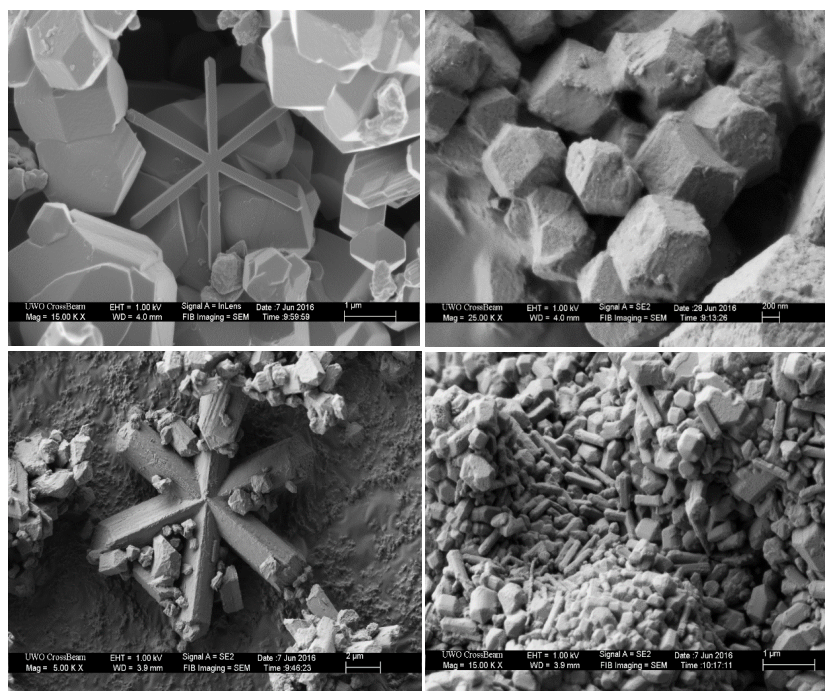


Figure 4-7. SEM images of a) VO₂ (M) with 0.6 atm% Mo before annealing treatment b) VO₂ (M) with 0.6 atm% Mo after annealing treatment c) VO₂ (M) with 0.3 atm% before annealing treatment d) VO₂ (M) with 2.13 atm% after annealing treatment.

4.3.3 Effect of SiO₂ coating on optical properties of VO₂

To improve the optical properties of the VO₂ films, they were coated with a SiO₂ antireflection layer. This layer can modulate the refractive index (RI) of the composite and decrease the scattering caused by inconsistent RI between the nanostructure and the polymer matrix[43]. Figure 4-8 shows the XRD patterns of VO₂/SiO₂ nanostructures with different TEOS volume. It is shown that all the nanostructures exhibit the typical diffraction peaks of M1 phase VO₂. Since the synthesized VO₂/SiO₂ nanostructures were not annealed, the SiO₂ remained amorphous.

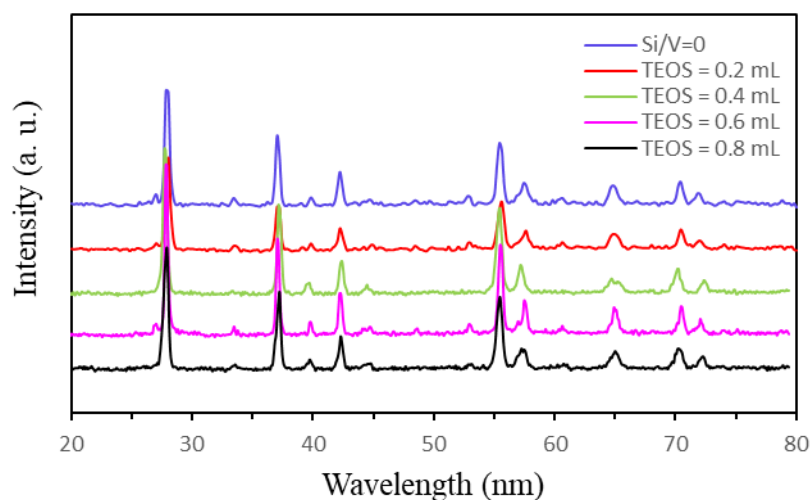


Figure 4-8. XRD patterns of VO₂-SiO₂ nanostructures upon increasing the different volume of the TEOS.

The VO₂/SiO₂ nanostructures were collected and well dispersed into EVA polymer film solution and cast onto glass slides for optical properties study. Table 4-4 depicts the change in the optical properties of the film in response to the variation of TEOS volume.

Table 4-4. Optical properties of EVA films with the different TEOS volume ratio

TEOS (V/ μ)	T_{lum} (%)			T_{sol} (%)		
	25 °C	90 °C	ΔT_{lum} (%)	25 °C	90 °C	ΔT_{sol} (%)
0	39.8	34.8	5.0	51.7	42.8	8.9
200	45.7	36.8	7.9	62.0	52.4	9.6
400	44.2	36.3	8.9	51.9	41.9	10.0
600	50.8	45.1	5.7	56.8	44.0	12.8
800	50.5	42.3	8.2	56.0	44.6	11.4

As shown, the visible transmittance of the film enhances greatly (from T_{sol} 39.8 % to 50.8 %) by increasing the TEOS proportion from 200 μL to 600 μL due to the increase in the thickness of SiO_2 shell layer[103]. The higher SiO_2 proportion also improved the optical performance with a larger solar modulation ability from ΔT_{sol} of 8.9 % to 12.8 %. However, a further increase in TEOS volume did not improve the optical properties significantly. Similar improvement in optical properties is previously reported [43] when Si/V molar ratio is increased in VO_2 - SiO_2 composite films using a different synthesis approach.

4.3.4 PIL Solution Casting method for fabrication of VO_2

The polymerized ionic liquid was synthesized via free radical polymerization of [EVIM][TF₂N] as shown in Scheme 4.3 Polymerization was initiated by AIBN in DMSO using different molar ratio of the monomer to initiator M/I and volume ratio of the monomer to the solvent M/S at 60 °C for 16 h (Table 4-5). As shown in Table 4-5, by increasing the M/I and M/S, the viscosity and subsequently the molecular weight of the polymer increased. The viscosity and molecular weight of the prepared polymers are comparable with the results reported by Inoue et. al[156].

Table 4-5. Viscosity (η) and molecular weight (M_w) of PIL by changing volume ratio of the monomer to the solvent (M/S) and the molar ratio of the monomer to the initiator (M/I).

M/I	M/S	η ($\text{cm}^3 \cdot \text{g}^{-1}$)	$M_w/ 10^3$
25	3.0	44.6	201
100	3.2	60.1	325
200	9.8	74.2	457

The viscosity (η) of the poly-ionic liquid was measured using a rotational viscometer and the molecular weight (M_w) is calculated by employing the Mark-Houwink_Sakurada equation $[\eta] = KM_v^a$ with parameters of $K = 2.3 \times 10^{-2} \text{ cm}^3 \cdot \text{g}^{-1}$ and $a = 0.62$. These parameters were determined in a polystyrene/MEK solution at 30 °C. To have a targeted VO_2 - polymer composite, the find the best molecular weight of the polymer is important

for full coverage of the VO₂ particles. 4 mg loading of VO₂ particles dispersed in acetonitrile and 10 wt % PIL with different molecular weights, then the solution was casted onto the glass slides using a spin coater using different spin coating speeds. The optical properties of the obtained films are calculated as shown in Table 4-6.

Table 4-6. The thickness and optical properties of the VO₂-PIL films using PIL with different molecular weight and using various spin-coating speeds.

Mw/10 ³	Spin Coating Speed (rpm)	Thickness (nm)	T_{lum} (%)	ΔT_{sol} (%)
220	400	700	45.4	9.5
	1000			
360	400	971	28.7	10.3
	1000			
480	400	1203	15.9	12.6
	1000			
220	400	680	54.6	8.5
	2000			
360	400	879	35.8	11.0
	2000			
480	400	1093	19.1	11.4
	2000			
220	400	540	56.2	8.3
	3000			
360	400	717	39.4	9.6
	3000			
480	400	971	25.3	10.2
	3000			

By increasing the molecular weight of the polymer used in the solution, the viscosity of the solution is enhanced, and the thickness of the film increased accordingly. The approximate

thickness of the films is measured using AFM. However, the visible transmittance of the film at 25 °C decreased by increasing the molecular weight of the polymer as the color of the polymer matrix became deeper. Therefore, PILs with higher molecular weights are not considered suitable based on the luminous transmittance being lower than 40 % at 25 °C. The results show that when the polymer with $M_w = 220 \times 10^3$ is used at 1000 rpm coating speed, it results in good solar modulation of 9.5 % while keeping the high luminous transmittance of 45.4 %.

4.3.5 UV-curing method for fabrication of VO₂

The UV-curing method was examined for the in-situ incorporation of VO₂ in the polymer structure for more uniform dispersion. VO₂ nanostructure is well dispersed in the monomer solution, deep coated on the glass, and been polymerized under UV irradiation. The degrees of conversion of vinyl polymerizable groups from cross-linker mixtures (0, 2.5, 7.2 molar %) to PIL based films were assessed using Fourier transform infrared (FTIR) analysis (Figure 4-9). By increasing the crosslinker content in the mixture from 0 to 2.5 and 7.2 molar %, the reaction time decreases from 40 minutes to 25 minutes and 10 minutes, respectively.

The characteristic infrared absorbance bands were used to monitor the disappearance of the vinyl monomer at 1662 cm⁻¹ (stretching vibration in C=C) and 995 cm⁻¹ (out of plane bending of the -CH=groups). Simultaneously, the asymmetrical stretching vibrations of the -CH₂- groups become more noticeable on PILs samples (2960 cm⁻¹- 2850 cm⁻¹). To prepare the casting solution, 4 mg loading of VO₂ or VO₂/ SiO₂ was dispersed in 10 mL of monomer and a mixture of 7.2 % of crosslinker and initiator. The glass is then dip-coated in the casting solution and then UV-cured for 10 minutes. The optical properties of the film are determined and compared with the previous method in the next section.

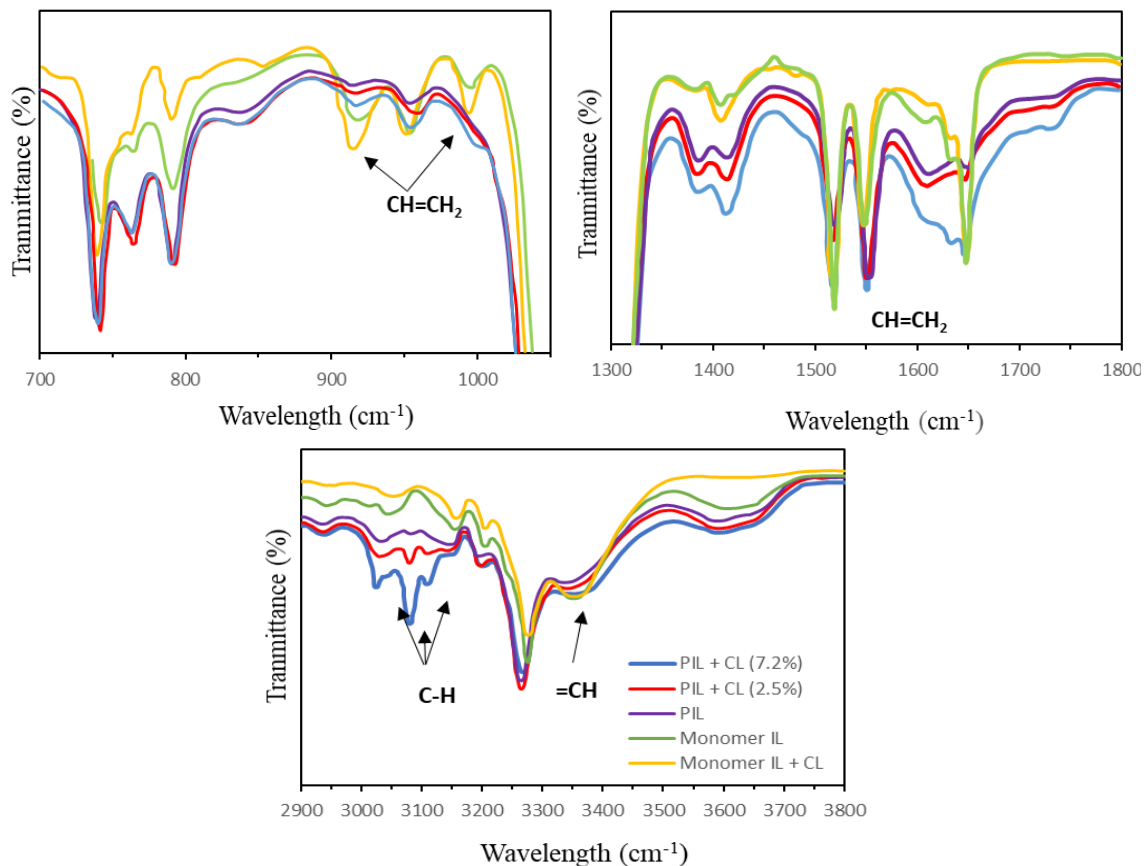


Figure 4-9. FTIR spectra of monomer IL, monomer and crosslinker (CL) and PIL samples as a function of the crosslinker molar percentage.

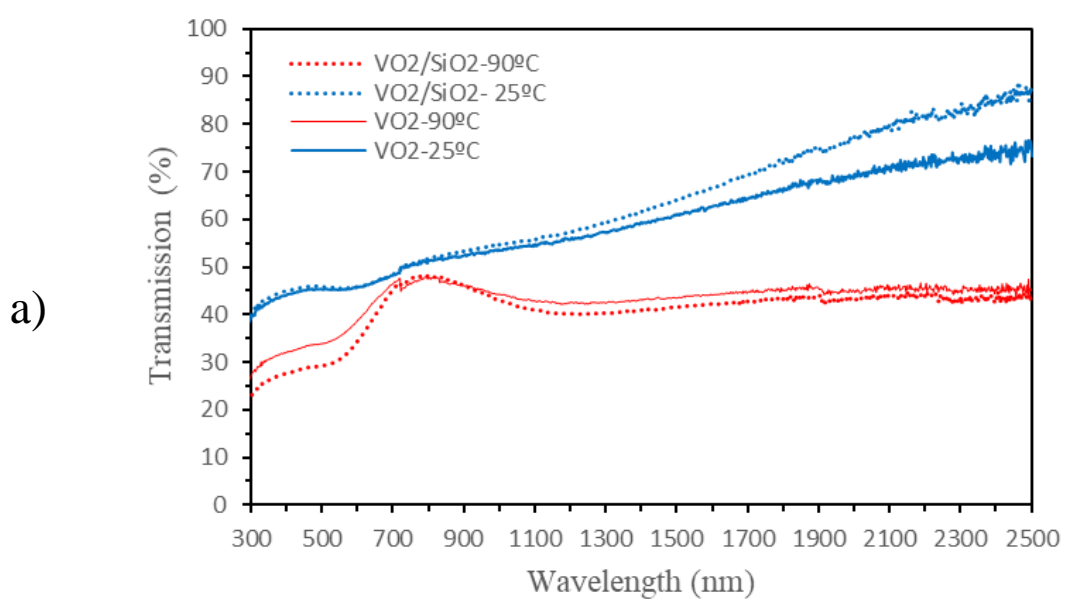
4.3.6 Comparison of optical properties of the films prepared by solution casting and UV-curing

VO₂ and VO₂/SiO₂ nanostructures were integrated into a PIL film using solution casting of final polymer and UV-curing of the IL monomer. The optical properties of the film were determined and compared to each other. T_{lum} of the VO₂-PIL film, which was prepared by solution casting, is 45.40 % at 25 °C and 36.52 % at 90 °C, and the T_{sol} are 50.51 % at 25 °C and 40.99 %. The ΔT_{lum} is 8.89 % and ΔT_{sol} is 9.52 %. The one-layer sample of VO₂-PIL, which was also made by solution casting, presents an excellent thermochromic property with a reasonable integrated visible transmittance of as high as 45 %, while a good solar modulation ability of 9.52 % was retained. The integrated luminescence transmittance and solar modulation of this film are the best among the most typical single-layer VO₂

(T_{lum} : 41 % and ΔT_{lum} : 6.7 %)[163] indicating the role of PIL as a dielectric matrix with high heat capacity.

Table 4-7. Comparison of optical properties of various VO₂ films.

Sample	T_{lum} (%)			T_{sol} (%)		
	25 °C	90 °C	ΔT_{lum} (%)	25 °C	90 °C	ΔT_{sol} (%)
VO ₂ -PIL Solution Casted	45.4	36.5	8.9	50.5	41.0	9.5
VO ₂ /SiO ₂ -PIL Solution Casted	45.7	31.9	13.8	51.7	38.5	13.2
VO ₂ -PIL UV-Cured	64.9	46.8	18.2	65.3	47.1	18.2
VO ₂ /SiO ₂ -PIL UV-Cured	83.6	52.9	30.7	84.5	53.8	30.7



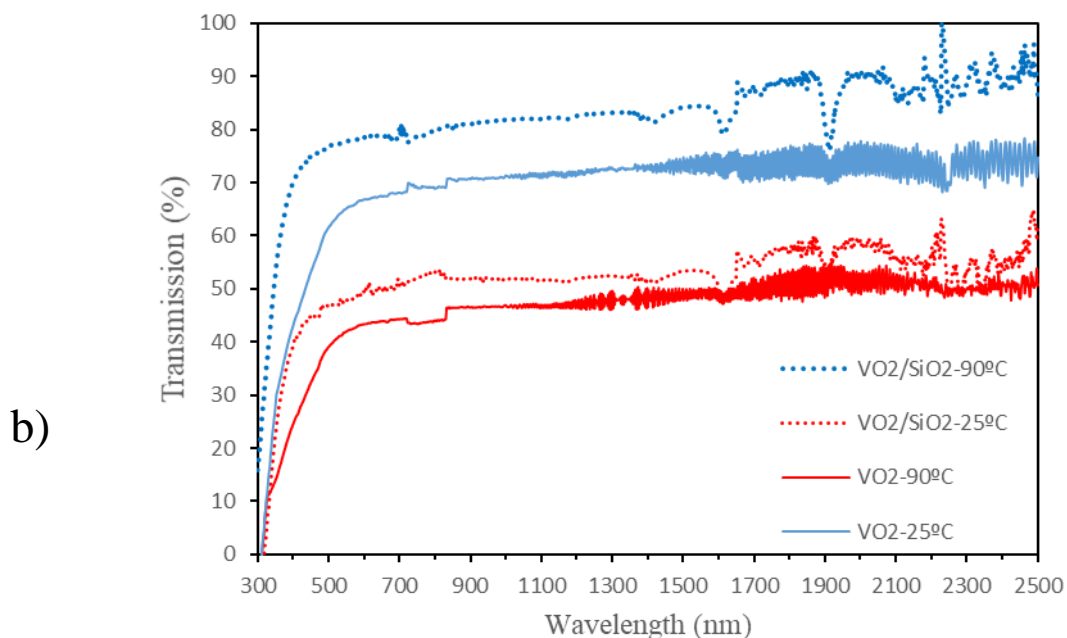


Figure 4-10. UV-Vis-NIR transmittance spectra of a) VO₂-PIL and VO₂/SiO₂- PIL prepared by solution casting b) VO₂-PIL and VO₂/SiO₂- PIL prepared by UV-curing.

By modifying the surface of VO₂ nanostructured with amorphous SiO₂, the solar modulation of the film increased to 13.2 % with maintaining the luminescence transmittance of 45.7%. The solar modulation and luminance transmittance of the VO₂-SiO₂ film is significantly improved compared to the one which was prepared with a similar method but without PIL (ΔT_{sol} of 7.5, T_{lum} of 55.3 %). Additionally, ΔT_{lum} is enhanced compared to the VO₂/SiO₂ which was reported before[42,103]. Furthermore, the thermochromic properties of the composite films which were prepared by in-situ UV-curing polymerization are evaluated. T_{lum} of the VO₂-PIL film is 64.9 % at 25 °C and 46.8 % at 90 °C and the T_{sol} are 62.3 % at 25 °C and 47.1 %. The ΔT_{lum} is 18.2 % and ΔT_{sol} is 18.2 %. The solar modulation efficiency increased to 30.7% with luminescence transmittance of 83 % at 25 °C and 52.9 % at 85 °C. The T_{lum} result is much higher than the T_{lum} of the best reported VO₂ sample (83 % versus 45 % at 25 °C, 52.9 % versus 40 %) which gives approximately 30 % ΔT_{lum} . This large difference in transmittance in the visible range spectrum leads to a great enhancement of ΔT_{sol} . Similar results were reported by Y.

Zhou et al.[172] on the formation of VO₂ hydrogel hybrid thermochromic films with the highest ΔT_{sol} reported of 35 % at with 79 % of T_{lum} at 25 °C. Additionally, compared with the solution casting method, the VO₂- PIL film prepared by UV-curing exhibited a higher T_{lum} at 25 °C. This is attributed to the VO₂ nanostructures being dispersed in the polymer matrix with a minimum scattering of light which leads to improved solar transmittance.

By looking at UV-Vis- NIR spectrum of VO₂/SiO₂ composite film prepared by UV-curing (Figure 4-10 b), there are three peaks at approximately 1420 cm⁻¹, 1610 cm⁻¹ and 1910 cm⁻¹. Two peaks at 1420 cm⁻¹ and 1910 cm⁻¹ indicate typical absorption of water due to O-H stretching and a combination of O-H and H-O-H bending, respectively[172]. The FTIR spectrum of the films are examined for further investigation (Figure 4-11). The peak at 1610 cm⁻¹ is also observed in FTIR spectrum. During the UV-curing process, VO₂/SiO₂ can be trapped in the IL network by coordination through the strong hydrogen bond between hydroxide on silica shell and nitrogen or oxygen of TFSI anion. The peak at 1610 cm⁻¹ increased in intensity by increasing the temperature, indicating a weakened hydrogen bond at elevated temperature.

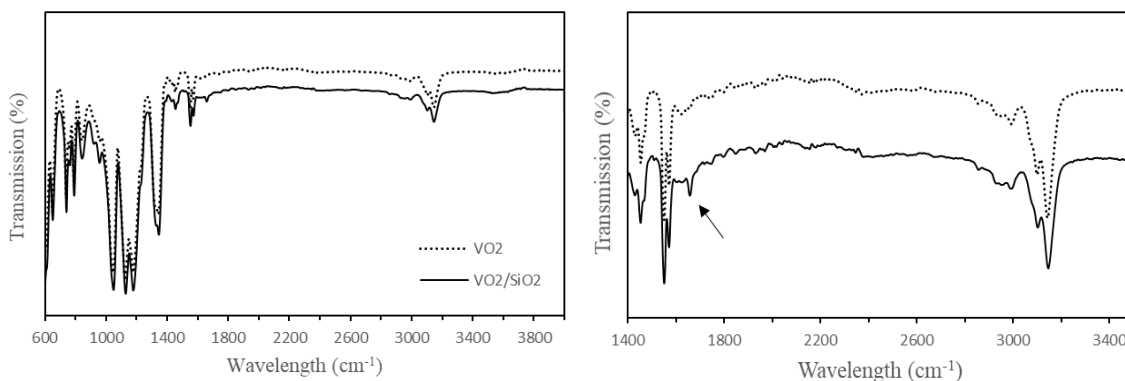


Figure 4-11. FTIR of UV-Cured film in range of a) 600 cm⁻¹ - 4000 cm⁻¹ b) 1400 cm⁻¹ - 3500 cm⁻¹ (Zoomed in).

The results confirm that the casting method has a large effect on the optical properties of the films. The films that were prepared by UV-curing present a superior solar modulation efficiency compared to the films prepared by solution casting. However, the luminescence transmittance of the UV-cured samples decreases by increasing the temperature which

shows the involvement of VO₂/SiO₂-PIL composite film in thermochromicity. On the other hand, the films which were prepared by solution casting with a similar thickness and W % ratio did not show the transparency in the visible range compared to the one prepared by UV-Curing. This indicates enhanced dispersion of VO₂ and VO₂/SiO₂ nanostructures in UV-cured composite film.

4.4 Conclusion

VO₂ nanostructures were synthesized using the hydrothermal method following by calcination treatment. The results showed the best crystallinity and hysteresis width were obtained for calcination conditions at 500 °C for 60 minutes. The VO₂ nanostructures were Mo-doped with 2.1 atm% molybdenum to decrease the transition temperature of the VO₂ nanostructure to ideal room temperature (20 °C – 24 °C). The role of calcination on the morphology and size of the Mo-doped VO₂ nanostructures were investigated using SEM. Furthermore, VO₂ nanostructures were coated with amorphous SiO₂ for improving the optical properties of the thermochromic films. A TEOS volume of 600 μL gave the best solar modulation along with the higher luminescence transmittance. Two novel casting methods were examined to prepare a thermochromic film with higher optical properties using PIL as a dielectric host: 1) solution casting 2) UV-curing. In the solution casting method, the role of polymer molecular weight and spin coater speed were studied to optimize the optical properties in this method. In the UV-curing method, the role of the crosslinker in the reaction time is investigated. The optical properties of VO₂ and VO₂/SiO₂ nanostructures incorporated in PIL coatings were investigated. The results showed that the solar modulation efficiency increased to 30.7 % with luminescence transmittance of 83 % at 25 °C when VO₂/ SiO₂ nanostructures were integrated into PIL film using the UV-Curing method. This observation might be attributed to entrapped VO₂/ SiO₂ in the film as the result of strong hydrogen bonding between N- and F- atoms in the anion counterpart of PIL and SiO₂.

Chapter 5

5 Conclusion and future work

In this doctoral project, we have proposed different methodologies for using ionic liquids in preparation of vanadium dioxide nanocomposites to overcome previous obstacles limiting the large-scale implementation of thermochromic VO₂ smart windows:

- 1) Finding green and convenient methodology for the synthesis of VO₂ under mild synthesis conditions.
- 2) Improving the solar modulation efficiency, ΔT_{sol} which is the key factor for the evaluation of smartness of a window.
- 3) Decreasing the phase transition temperature close to the ambient temperature (25 °C).
- 4) Finding a suitable polymeric matrix and a dielectric host for long term stabilization of VO₂ nanostructures.

In Chapter 2, different imidazolium ionic liquids were used in a combination with supercritical CO₂ (scCO₂) system as green binary solvents to synthesize VO₂ at low temperatures. [EMIM][Tf₂N], [EMIM][TFO], [EMIM][AcO] and [EMIM][HSO₄] were the selected imidazolium ionic liquids with different counter anions. It was shown that ILs with a fluorinated anion counterpart such as [EMIM][Tf₂N] and [EMIM][TFO] could be effectively used as a substitute for HOAc as an acidic catalyst in the sol-gel process. The reactions in the biphasic system of [EMIM][Tf₂N]/scCO₂ showed similar gelation yield to the ones using a conventional catalytic reagent, HOAc, in scCO₂. The mechanism of ionic liquid catalytic involvement in the gelation process of the vanadium precursor was investigated. In the absence of scCO₂ from the system, the gelation yield dropped significantly showing the role of scCO₂ in catalyzing the gelation process. Characterization of ionogels and aerogels illustrated that ILs were incorporated into the structure of the dried gel and are not washed out during the drying procedure and deteriorated the surface area of the obtained gel compared to ones prepared in the only scCO₂. Furthermore, the role of temperature and pressure during the gelation process was investigated. It was shown that

the calcination posttreatment temperature and duration had a crucial role in the improvement of purity or crystallinity of the final product. When the reaction happened in [EMIM][TF₂N] /scCO₂ biphasic conditions, milder sol-gel, and posttreatment conditions were needed for the formation of pure and high crystalline VO₂ (M). Morphology studies on the final samples showed that how choosing different sol-gel conditions can affect the morphology of the products. The optical properties of the samples were analyzed using a UV-Vis-NIR instrument. The results confirmed that using ILs during sol-gel affects the optical properties of the VO₂ film negatively because of the formation of a bigger nano-size VO₂ structure.

In Chapter 3, imidazolium ionic liquids including [EVIM][TFSI], [EMIM][TFO], and [EMIM][AcO] imidazolium ionic liquids were used to investigate the stability of the VO(acac)₂ methanol solution for extended periods of aging time. The highest stability achieved by using -ethyl-3-vinyl imidazolium bis (trifluoromethanesulfonylimide), [EVIM][TFSI] as the result of the high coordination ability of [TFSI] anion and the existence of the vinyl bond on the cation counterpart of the IL. It has been shown that ILs with AcO anions can promote the oxidation process. The mixture of [EVIM][TFSI] IL/PIL/methanol and VO(acac)₂ was explored for the sol-gel process to fabricate thermochromic films. After annealing at 400 °C for 10 minutes, the film was formed very crystalline and pure VO₂ (M) with narrow hysteresis of 4 °C. We have proposed that the decomposition of the IL/PIL can induce the formation of the VO₂ monoclinic by preventing vanadium (IV) from oxidation. The VO₂ (M) film showed great thermochromic properties with 20.3 % solar modulation properties. Furthermore, using IL/PIL in the sol-gel solution promoted the formation of flower-like morphology which consists of a large number of uniform VO₂ nano-sheets.

In Chapter 4, it was shown that the annealing parameters have a crucial role in the obtained morphology, size, and crystallinity of the synthesized VO₂ samples. The synthesized VO₂ nanostructures showed sharp and narrow hysteresis width between (0 - 4) °C. The VO₂ nanostructures were Mo-doped with 2.1 atm% molybdenum to decrease the transition temperature to ideal room temperature. The role of calcination on the morphology and size of the Mo-doped VO₂ nanostructures was investigated using SEM. Furthermore, VO₂

nanostructures were coated with amorphous SiO₂ for improving the optical properties of the thermochromic film. Two novel casting methods were examined to prepare thermochromic films with higher optical properties using PIL as a dielectric host: 1) solution casting 2) UV-Curing. In the solution casting method, the role of polymer molecular weight and spin coater speed were studied to optimize the optical properties in this method. In the UV-curing method, the role of the crosslinker in the reaction time is investigated. The optical properties of VO₂ and VO₂/SiO₂ nanostructures incorporated in PIL coatings were investigated. The results showed that the prominent solar modulation efficiency of 30.70 % with luminescence transmittance of 83 % at 25 °C when VO₂/ SiO₂ nanostructures were integrated into PIL film using the UV-Curing method. This observation might be attributed to entrapped VO₂/ SiO₂ in the film as the result of strong hydrogen bonding between N- and F- atoms in the anion counterpart of PIL and SiO₂.

Some challenges remained and need more detailed investigation which can be addressed in the future:

- ❖ Surface-Enhanced Raman Spectroscopy (SERS) could be used to measure the dielectric properties of VO₂ oriented nanostructures, which have shown a high plasmonic effect in the visible region.¹⁶ The unique vibrational information contained within Raman spectra makes SERS one of the most powerful analytical techniques for high spatial resolution and characterization including monitoring structural changes of molecules and molecular dynamics.
- ❖ Both refractive index dispersion and absorption spectra should be measured using refractometers and ellipsometry instruments. To measure n and k coefficients for a given layer structure as a function of temperature, the complex dielectric function, and the individual layer thickness must be known. Commercial software (ATSOS) will be used which is based on the matrix formalism in connection with the Fresnel equations to model refractive and reflective behavior of multilayer optical systems.
- ❖ Anti-Oxidation Properties: to explore whether VO₂-PIL composite coating will improve the oxidation resistance of the as-prepared VO₂ particles, the prepared

composite film can be annealed in air at elevated temperature for different time intervals and at a certain heating rate to study the stability of the film at the abused condition. VO_2 film will readily oxidize into V_3O_7 or V_2O_5 at a high temperature which can be detected by XRD measurements. The long-term stability of VO_2 film is also will be studied by exposing the film to the air at room temperature for over 6 months. We are proposing that PIL can act as an effective barrier layer for the diffusion of oxygen into the VO_2 lattice.

- ❖ To have better dispersion of nanostructure, novel ionogel materials can be formed by infusing ILs in a solid phase of VO_2 as the metal-oxide host. The modified IL tethered VO_2 can be uniformly dispersed in a polymer matrix. Furthermore, the interaction between the IL and its host can be adjusted by modifying the cation and anion counterpart of the ILs. The ionic liquid- tethered SiO_2 nanostructure [178] and ionic liquid-tethered TiO_2 nanoparticle/poly (ionic liquid) [179] are prepared in the literature.

References

- [1] A.A.M. Sayigh, World Renewable Energy Congress VI: Renewables: The Energy for the 21st Century, 2000.
- [2] B.P. Jelle, S.E. Kalnæs, T. Gao, Low-emissivity materials for building applications: A state-of-the-art review and future research perspectives, *Energy Build.* 96 (2015) 329–356.
<https://doi.org/http://dx.doi.org/10.1016/j.enbuild.2015.03.024>.
- [3] L. Long, H. Ye, How to be smart and energy efficient: A general discussion on thermochromic windows, *Sci. Rep.* 4 (2014) 6427.
<http://dx.doi.org/10.1038/srep06427>.
- [4] M. Kamalisarvestani, R. Saidur, S. Mekhilef, F.S. Javadi, Performance, materials and coating technologies of thermochromic thin films on smart windows, *Renew. Sustain. Energy Rev.* 26 (2013) 353–364.
<https://doi.org/http://dx.doi.org/10.1016/j.rser.2013.05.038>.
- [5] M.E.A. Warwick, R. Binions, Advances in thermochromic vanadium dioxide films, *J. Mater. Chem. A.* 2 (2014) 3275–3292.
<https://doi.org/10.1039/C3TA14124A>.
- [6] A. Tiwari, A.K. Mishra, H. Kobayashi, A.P.F. Turner, *Intelligent Nanomaterials*, n.d.
- [7] S.-Y. Li, G.A. Niklasson, C.G. Granqvist, Thermochromic fenestration with VO₂-based materials: Three challenges and how they can be met, *Thin Solid Films.* 520 (2012) 3823–3828. <https://doi.org/http://dx.doi.org/10.1016/j.tsf.2011.10.053>.
- [8] I.P. Parkin, T.D. Manning, Intelligent Thermochromic Windows, *J. Chem. Educ.* 83 (2006) 393. <https://doi.org/10.1021/ed083p393>.
- [9] A. Seeboth, D. Löttsch, *Thermochromic and Thermotropic Materials*, 2013.
- [10] Y. Gao, C. Cao, L. Dai, H. Luo, M. Kanehira, Y. Ding, Z.L. Wang, Phase and

- shape controlled VO₂ nanostructures by antimony doping, *Energy Environ. Sci.* 5 (2012) 8708–8715. <https://doi.org/10.1039/C2EE22290F>.
- [11] G. Stefanovich, A. Pergament, D. Stefanovich, Electrical switching and Mott transition in VO₂, *J. Phys. Condens. Matter.* 12 (2000) 8837–8845. <https://doi.org/10.1088/0953-8984/12/41/310>.
- [12] J.B. Goodenough, The two components of the crystallographic transition in VO₂, *J. Solid State Chem.* 3 (1971) 490–500. [https://doi.org/http://dx.doi.org/10.1016/0022-4596\(71\)90091-0](https://doi.org/http://dx.doi.org/10.1016/0022-4596(71)90091-0).
- [13] S. Shin, S. Suga, M. Taniguchi, M. Fujisawa, H. Kanzaki, A. Fujimori, H. Daimon, Y. Ueda, K. Kosuge, S. Kachi, Vacuum-ultraviolet reflectance and photoemission study of the metal-insulator phase transitions in VO₂, V₆O₁₃, V₂O₃ *Phys. Rev. B.* 41 (1990) 4993–5009.
- [14] A. Krammer, O. Bouvard, A. Schüler, Study of Si doped VO₂ thin films for solar thermal applications, *Energy Procedia.* 122 (2017) 745–750. <https://doi.org/https://doi.org/10.1016/j.egypro.2017.07.390>.
- [15] J.F.P. and H.J.G. J. B. MacChesney, *J. Electrochem. Soc.*, *J. Electrochem. Soc.* 115 (1968) 52–55.
- [16] E. Lugscheider, S. Bärwulf, C. Barimani, Properties of tungsten and vanadium oxides deposited by MSIP–PVD process for self-lubricating applications, *Surf. Coatings Technol.* 120–121 (1999) 458–464. [https://doi.org/http://dx.doi.org/10.1016/S0257-8972\(99\)00467-3](https://doi.org/http://dx.doi.org/10.1016/S0257-8972(99)00467-3).
- [17] T.D. Manning, I.P. Parkin, M.E. Pemble, D. Sheel, D. Vernardou, Intelligent Window Coatings: Atmospheric Pressure Chemical Vapor Deposition of Tungsten-Doped Vanadium Dioxide, *Chem. Mater.* 16 (2004) 744–749. <https://doi.org/10.1021/cm034905y>.
- [18] N. Wang, S. Magdassi, D. Mandler, Y. Long, Simple sol–gel process and one-step annealing of vanadium dioxide thin films: Synthesis and thermochromic properties, *Thin Solid Films.* 534 (2013) 594–598. <https://doi.org/http://dx.doi.org/10.1016/j.tsf.2013.01.074>.

- [19] D. Li, M. Li, J. Pan, Y. Luo, H. Wu, Y. Zhang, G. Li, Hydrothermal Synthesis of Mo-Doped VO₂/TiO₂ Composite Nanocrystals with Enhanced Thermochromic Performance, *ACS Appl. Mater. Interfaces*. 6 (2014) 6555–6561. <https://doi.org/10.1021/am500135d>.
- [20] L. Whittaker, T.-L. Wu, C.J. Patridge, G. Sambandamurthy, S. Banerjee, Distinctive finite size effects on the phase diagram and metal-insulator transitions of tungsten-doped vanadium(iv) oxide, *J. Mater. Chem.* 21 (2011) 5580–5592. <https://doi.org/10.1039/C0JM03833D>.
- [21] Y. Jiazhen, Z. Yue, H. Wanxia, T. Mingjin, Effect of Mo-W Co-doping on semiconductor-metal phase transition temperature of vanadium dioxide film, *Thin Solid Films*. 516 (2008) 8554–8558. <https://doi.org/http://dx.doi.org/10.1016/j.tsf.2008.05.021>.
- [22] C.J. Patridge, L. Whittaker, B. Ravel, S. Banerjee, Elucidating the Influence of Local Structure Perturbations on the Metal–Insulator Transitions of V_{1-x}Mo_xO₂ Nanowires: Mechanistic Insights from an X-ray Absorption Spectroscopy Study, *J. Phys. Chem. C*. 116 (2012) 3728–3736. <https://doi.org/10.1021/jp2091335>.
- [23] L. Whittaker, C.J. Patridge, S. Banerjee, Microscopic and Nanoscale Perspective of the Metal–Insulator Phase Transitions of VO₂: Some New Twists to an Old Tale, *J. Phys. Chem. Lett.* 2 (2011) 745–758. <https://doi.org/10.1021/jz101640n>.
- [24] Y.-T. Wang, C.-H. Chen, Facile Growth of Thermochromic VO₂ Nanostructures with Greatly Varied Phases and Morphologies, *Inorg. Chem.* 52 (2013) 2550–2555. <https://doi.org/10.1021/ic302562j>.
- [25] J.N. and R.F.H. Jr, Synthesis of vanadium dioxide thin films and nanoparticles, *J. Phys. Condens. Matter*. 20 (2008) 264016. <http://stacks.iop.org/0953-8984/20/i=26/a=264016>.
- [26] Y.D. and X.N. and Z.J. and Z. Xiulin, Vanadium dioxide films with good electrical switching property, *J. Phys. D. Appl. Phys.* 29 (1996) 1051.
- [27] J.-H. Cho, Y.-J. Byun, J.-H. Kim, Y.-J. Lee, Y.-H. Jeong, M.-P. Chun, J.-H. Paik, T.H. Sung, Thermochromic characteristics of WO₃-doped vanadium dioxide thin

- films prepared by sol–gel method, *Ceram. Int.* 38, Supple (2012) S589–S593.
<https://doi.org/http://dx.doi.org/10.1016/j.ceramint.2011.05.104>.
- [28] M. Maaza, K. Bouziane, J. Maritz, D.S. McLachlan, R. Swanepool, J.M. Frigerio, M. Every, Direct production of thermochromic VO₂ thin film coatings by pulsed laser ablation, *Opt. Mater. (Amst)*. 15 (2000) 41–45.
[https://doi.org/http://dx.doi.org/10.1016/S0925-3467\(99\)00104-4](https://doi.org/http://dx.doi.org/10.1016/S0925-3467(99)00104-4).
- [29] J.B.K. Kana, J.M. Ndjaka, P.O. Ateba, B.D. Ngom, N. Manyala, O. Nemraoui, A.C. Beye, M. Maaza, Thermochromic VO₂ thin films synthesized by rf-inverted cylindrical magnetron sputtering, *Appl. Surf. Sci.* 254 (2008) 3959–3963.
<https://doi.org/http://dx.doi.org/10.1016/j.apsusc.2007.12.021>.
- [30] G. V Jorgenson, J.C. Lee, Doped vanadium oxide for optical switching films, *Sol. Energy Mater.* 14 (1986) 205–214. [https://doi.org/http://dx.doi.org/10.1016/0165-1633\(86\)90047-X](https://doi.org/http://dx.doi.org/10.1016/0165-1633(86)90047-X).
- [31] Y. Takahashi, M. Kanamori, H. Hashimoto, Y. Moritani, Y. Masuda, Preparation of VO₂ films by organometallic chemical vapour deposition and dip-coating, *J. Mater. Sci.* 24 (n.d.) 192–198. <https://doi.org/10.1007/BF00660953>.
- [32] D. Barreca, L.E. Depero, E. Franzato, G.A. Rizzi, L. Sangaletti, E. Tondello, U. Vettori, Vanadyl Precursors Used to Modify the Properties of Vanadium Oxide Thin Films Obtained by Chemical Vapor Deposition, *J. Electrochem. Soc.* . 146 (1999) 551–558.
- [33] J.-H. Son, J. Wei, D. Cobden, G. Cao, Y. Xia, Hydrothermal Synthesis of Monoclinic VO₂ Micro- and Nanocrystals in One Step and Their Use in Fabricating Inverse Opals, *Chem. Mater.* 22 (2010) 3043–3050.
<https://doi.org/10.1021/cm903727u>.
- [34] J. Zhu, Y. Zhou, B. Wang, J. Zheng, S. Ji, H. Yao, H. Luo, P. Jin, Vanadium Dioxide Nanoparticle-based Thermochromic Smart Coating: High Luminous Transmittance, Excellent Solar Regulation Efficiency, and Near Room Temperature Phase Transition, *ACS Appl. Mater. Interfaces.* 7 (2015) 27796–27803. <https://doi.org/10.1021/acsami.5b09011>.

- [35] R. Chen, L. Miao, H. Cheng, E. Nishibori, C. Liu, T. Asaka, Y. Iwamoto, M. Takata, S. Tanemura, One-step hydrothermal synthesis of $V_{1-x}W_xO_2(M/R)$ nanorods with superior doping efficiency and thermochromic properties, *J. Mater. Chem. A*. 3 (2015) 3726–3738. <https://doi.org/10.1039/C4TA05559D>.
- [36] R. Sui, A.S. Rizkalla, P.A. Charpentier, Formation of Titania Nanofibers: A Direct Sol–Gel Route in Supercritical CO_2 , *Langmuir*. 21 (2005) 6150–6153. <https://doi.org/10.1021/la0505972>.
- [37] R. Sui, A.S. Rizkalla, P.A. Charpentier, Synthesis and Formation of Silica Aerogel Particles By a Novel Sol–Gel Route in Supercritical Carbon Dioxide, *J. Phys. Chem. B*. 108 (2004) 11886–11892. <https://doi.org/10.1021/jp036973d>.
- [38] R. Sui, P. Charpentier, Synthesis of Metal Oxide Nanostructures by Direct Sol–Gel Chemistry in Supercritical Fluids, *Chem. Rev.* 112 (2012) 3057–3082. <https://doi.org/10.1021/cr2000465>.
- [39] Z.K. Donato, L. Matějka, S.R. Mauler, K.R. Donato, Recent Applications of Ionic Liquids in the Sol-Gel Process for Polymer–Silica Nanocomposites with Ionic Interfaces, *Colloids and Interfaces*. 1 (2018). <https://doi.org/10.3390/colloids1010005>.
- [40] Ž. Knez, M. Pantić, D. Cör, Z. Novak, M. Knez Hrnčič, Are supercritical fluids solvents for the future?, *Chem. Eng. Process. - Process Intensif.* 141 (2019) 107532. <https://doi.org/https://doi.org/10.1016/j.cep.2019.107532>.
- [41] Y. Li, S. Ji, Y. Gao, H. Luo, M. Kanehira, Core-shell $VO_2@TiO_2$ nanorods that combine thermochromic and photocatalytic properties for application as energy-saving smart coatings, *Sci. Rep.* 3 (2013) 1370. <http://dx.doi.org/10.1038/srep01370>.
- [42] Y. Gao, S. Wang, H. Luo, L. Dai, C. Cao, Y. Liu, Z. Chen, M. Kanehira, Enhanced chemical stability of VO_2 nanoparticles by the formation of SiO_2/VO_2 core/shell structures and the application to transparent and flexible VO_2 -based composite foils with excellent thermochromic properties for solar heat control, *Energy Environ. Sci.* 5 (2012) 6104–6110. <https://doi.org/10.1039/C2EE02803D>.

- [43] L. Zhao, L. Miao, C. Liu, C. Li, T. Asaka, Y. Kang, Y. Iwamoto, S. Tanemura, H. Gu, H. Su, Solution-Processed VO₂-SiO₂ Composite Films with Simultaneously Enhanced Luminous Transmittance, Solar Modulation Ability and Anti-Oxidation property, *Sci. Rep.* 4 (2014) 7000. <http://dx.doi.org/10.1038/srep07000>.
- [44] H.-K. Chen, H.-C. Hung, T.C.-K. Yang, S.-F. Wang, The preparation and characterization of transparent nano-sized thermochromic VO₂-SiO₂ films from the sol-gel process, *J. Non. Cryst. Solids.* 347 (2004) 138-143. <https://doi.org/http://dx.doi.org/10.1016/j.jnoncrysol.2004.07.065>.
- [45] R. Li, S. Ji, Y. Li, Y. Gao, H. Luo, P. Jin, Synthesis and characterization of plate-like VO₂(M)@SiO₂ nanoparticles and their application to smart window, *Mater. Lett.* 110 (2013) 241-244. <https://doi.org/http://dx.doi.org/10.1016/j.matlet.2013.05.051>.
- [46] X. Cao, M.N. Thet, Y. Zhang, S.C. Joachim Loo, S. Magdassi, Q. Yan, Y. Long, Solution-based fabrication of VO₂ (M) nanoparticles via lyophilisation, *RSC Adv.* 5 (2015) 25669-25675. <https://doi.org/10.1039/C4RA16840B>.
- [47] L. Kang, Y. Gao, H. Luo, A Novel Solution Process for the Synthesis of VO₂ Thin Films with Excellent Thermochromic Properties, *ACS Appl. Mater. Interfaces.* 1 (2009) 2211-2218. <https://doi.org/10.1021/am900375k>.
- [48] Y. Zhou, Y. Cai, X. Hu, Y. Long, VO₂/hydrogel hybrid nanothermochromic material with ultra-high solar modulation and luminous transmission, *J. Mater. Chem. A.* 3 (2015) 1121-1126. <https://doi.org/10.1039/C4TA05035E>.
- [49] G.A.N. and S.-Y.L. and C.G. Granqvist, Thermochromic vanadium oxide thin films: Electronic and optical properties, *J. Phys. Conf. Ser.* 559 (2014) 12001. <http://stacks.iop.org/1742-6596/559/i=1/a=012001>.
- [50] G. Wyszecski, Photometry, in: *Color Sci. Concepts Methods, Quant. Data Formulae*, 1982: pp. 723-33.
- [51] NoASTM G173-03 Standards Tables of Reference Solar Spectral Irradiances: Direct Normal and Hemispherical on 37 Tilted Surface, in: *Annu. B. ASTM Stand.*, American Society for Testing and Materials, Philadelphia, PA, USA, 2003.

- [52] J. Zhou, Y. Gao, X. Liu, Z. Chen, L. Dai, C. Cao, H. Luo, M. Kanahira, C. Sun, L. Yan, Mg-doped VO₂ nanoparticles: hydrothermal synthesis{, } enhanced visible transmittance and decreased metal-insulator transition temperature, *Phys. Chem. Chem. Phys.* 15 (2013) 7505–7511. <https://doi.org/10.1039/C3CP50638J>.
- [53] L. Dai, S. Chen, J. Liu, Y. Gao, J. Zhou, Z. Chen, C. Cao, H. Luo, M. Kanahira, F-doped VO₂ nanoparticles for thermochromic energy-saving foils with modified color and enhanced solar-heat shielding ability, *Phys. Chem. Chem. Phys.* 15 (2013) 11723–11729. <https://doi.org/10.1039/C3CP51359A>.
- [54] S.-Y. Li, G.A. Niklasson, C.G. Granqvist, Nanothermochromics: Calculations for VO₂ nanoparticles in dielectric hosts show much improved luminous transmittance and solar energy transmittance modulation, *J. Appl. Phys.* 108 (2010). <https://doi.org/http://dx.doi.org/10.1063/1.3487980>.
- [55] X. Cao, N. Wang, J.Y. Law, S.C.J. Loo, S. Magdassi, Y. Long, Nanoporous Thermochromic VO₂ (M) Thin Films: Controlled Porosity, Largely Enhanced Luminous Transmittance and Solar Modulating Ability, *Langmuir*. 30 (2014) 1710–1715. <https://doi.org/10.1021/la404666n>.
- [56] Y. Gao, L. Kang, Z. Chen, H. Luo, Solution Processing of Nanoceramic VO₂ Thin Films for Application to Smart Windows, in: *NanoFabrication*, n.d. <https://doi.org/10.5772/39017>.
- [57] M.-H. Lee, J.-S. Cho, Better thermochromic glazing of windows with anti-reflection coating, *Thin Solid Films*. 365 (2000) 5–6. [https://doi.org/http://dx.doi.org/10.1016/S0040-6090\(99\)01112-8](https://doi.org/http://dx.doi.org/10.1016/S0040-6090(99)01112-8).
- [58] G. Xu, P. Jin, M. Tazawa, K. Yoshimura, Optimization of antireflection coating for VO₂-based energy efficient window, *Sol. Energy Mater. Sol. Cells*. 83 (2004) 29–37. <https://doi.org/http://dx.doi.org/10.1016/j.solmat.2004.02.014>.
- [59] N.R. Mlyuka, G.A. Niklasson, C.G. Granqvist, Thermochromic multilayer films of VO₂ and TiO₂ with enhanced transmittance, *Sol. Energy Mater. Sol. Cells*. 93 (2009) 1685–1687. <https://doi.org/http://dx.doi.org/10.1016/j.solmat.2009.03.021>.
- [60] P.J. and G.X. and M.T. and K. Yoshimura, A VO₂ -Based Multifunctional

- Window with Highly Improved Luminous Transmittance, *Jpn. J. Appl. Phys.* 41 (2002) L278.
- [61] C.G. Granqvist, O. Hunderi, Optical properties of ultrafine gold particles, *Phys. Rev. B.* 16 (1977) 3513–3534.
- [62] J.C.M. Garnett, Colours in Metal Glasses and in Metallic Films, *Philos. Trans. R. Soc. London A Math. Phys. Eng. Sci.* 203 (1904) 385–420.
- [63] S. Nazari, S. Cameron, M.B. Johnson, K. Ghandi, Physicochemical properties of imidazo-pyridine protic ionic liquids, *J. Mater. Chem. A.* 1 (2013) 11570–11579. <https://doi.org/10.1039/C3TA12022H>.
- [64] M. Cai, Y. Liang, M. Yao, Y. Xia, F. Zhou, W. Liu, Imidazolium Ionic Liquids As Antiwear and Antioxidant Additive in Poly(ethylene glycol) for Steel/Steel Contacts, *ACS Appl. Mater. Interfaces.* 2 (2010) 870–876. <https://doi.org/10.1021/am900847j>.
- [65] M. Ivanova, S. Kareth, M. Petermann, Supercritical carbon dioxide and imidazolium based ionic liquids applied during the sol–gel process as suitable candidates for the replacement of classical organic solvents, *J. Supercrit. Fluids.* 132 (2018) 76–82. <https://doi.org/https://doi.org/10.1016/j.supflu.2017.07.005>.
- [66] A. Vioux, L. Viau, S. Volland, J. Le Bideau, Use of ionic liquids in sol-gel; ionogels and applications, *Comptes Rendus Chim.* 13 (2010) 242–255. <https://doi.org/https://doi.org/10.1016/j.crci.2009.07.002>.
- [67] M. Ivanova, S. Kareth, E.T. Spielberg, A. V Mudring, M. Petermann, Silica ionogels synthesized with imidazolium based ionic liquids in presence of supercritical CO₂, *J. Supercrit. Fluids.* 105 (2015) 60–65. <https://doi.org/https://doi.org/10.1016/j.supflu.2015.01.014>.
- [68] I. Osada, H. de Vries, B. Scrosati, S. Passerini, Ionic-Liquid-Based Polymer Electrolytes for Battery Applications, *Angew. Chemie Int. Ed.* 55 (2016) 500–513. <https://doi.org/10.1002/anie.201504971>.
- [69] G.-R. Zhang, M. Munoz, B.J.M. Etzold, Boosting Performance of Low Temperature Fuel Cell Catalysts by Subtle Ionic Liquid Modification, *ACS Appl.*

- Mater. Interfaces. 7 (2015) 3562–3570. <https://doi.org/10.1021/am5074003>.
- [70] H. Lin, J. Peng, V. Suryanarayanan, D. Velayutham, K. Ho, Perfluoro anion based binary and ternary ionic liquids as electrolytes for dye-sensitized solar cells, *J. Power Sources*. 311 (2016) 167–174. <https://doi.org/http://dx.doi.org/10.1016/j.jpowsour.2016.02.029>.
- [71] D.R. MacFarlane, N. Tachikawa, M. Forsyth, J.M. Pringle, P.C. Howlett, G.D. Elliott, J.H. Davis, M. Watanabe, P. Simon, C.A. Angell, Energy applications of ionic liquids, *Energy Environ. Sci.* 7 (2014) 232–250. <https://doi.org/10.1039/C3EE42099J>.
- [72] Y.U. Paulechka, A.G. Kabo, A. V Blokhin, G.J. Kabo, M.P. Shevelyova, Heat Capacity of Ionic Liquids: Experimental Determination and Correlations with Molar Volume, *J. Chem. Eng. Data*. 55 (2010) 2719–2724. <https://doi.org/10.1021/je900974u>.
- [73] J. Troncoso, C.A. Cerdeiriña, Y.A. Sanmamed, L. Romaní, L.P.N. Rebelo, Thermodynamic Properties of Imidazolium-Based Ionic Liquids: Densities, Heat Capacities, and Enthalpies of Fusion of [bmim][PF₆] and [bmim][NTf₂], *J. Chem. Eng. Data*. 51 (2006) 1856–1859. <https://doi.org/10.1021/je060222y>.
- [74] A. Diedrichs, J. Gmehling, Measurement of heat capacities of ionic liquids by differential scanning calorimetry, *Fluid Phase Equilib.* 244 (2006) 68–77. <https://doi.org/http://dx.doi.org/10.1016/j.fluid.2006.03.015>.
- [75] A. Paul, P.K. Mandal, A. Samanta, How transparent are the imidazolium ionic liquids? A case study with 1-methyl-3-butylimidazolium hexafluorophosphate, [bmim][PF₆], *Chem. Phys. Lett.* 402 (2005) 375–379. <https://doi.org/http://dx.doi.org/10.1016/j.cplett.2004.12.060>.
- [76] A. Paul, P.K. Mandal, A. Samanta, On the Optical Properties of the Imidazolium Ionic Liquids, *J. Phys. Chem. B*. 109 (2005) 9148–9153. <https://doi.org/10.1021/jp0503967>.
- [77] D. Liu, C. Zhong, Modeling of the Heat Capacity of Polymers with the Variable Connectivity Index, *Polym J.* 34 (2002) 954–961.

<http://dx.doi.org/10.1295/polymj.34.954>.

- [78] M.-M. Huang, Y. Jiang, P. Sasisanker, G.W. Driver, H. Weingärtner, Static Relative Dielectric Permittivities of Ionic Liquids at 25 °C, *J. Chem. Eng. Data.* 56 (2011) 1494–1499. <https://doi.org/10.1021/je101184s>.
- [79] M. Mizoshiri, T. Nagao, Y. Mizoguchi, M. Yao, Dielectric permittivity of room temperature ionic liquids: A relation to the polar and nonpolar domain structures, *J. Chem. Phys.* 132 (2010). <https://doi.org/http://dx.doi.org/10.1063/1.3419906>.
- [80] J. Robertson, High dielectric constant oxides, *Eur. Phys. J. - Appl. Phys.* 28 (2004) 265–291. <https://doi.org/10.1051/epjap:2004206>.
- [81] Z. He, P. Alexandridis, Nanoparticles in ionic liquids: interactions and organization, *Phys. Chem. Chem. Phys.* 17 (2015) 18238–18261. <https://doi.org/10.1039/C5CP01620G>.
- [82] K. Richter, A. Birkner, A.-V. Mudring, Stabilizer-Free Metal Nanoparticles and Metal–Metal Oxide Nanocomposites with Long-Term Stability Prepared by Physical Vapor Deposition into Ionic Liquids, *Angew. Chemie Int. Ed.* 49 (2010) 2431–2435. <https://doi.org/10.1002/anie.200901562>.
- [83] C. Vollmer, C. Janiak, Naked metal nanoparticles from metal carbonyls in ionic liquids: Easy synthesis and stabilization, *Coord. Chem. Rev.* 255 (2011) 2039–2057. <https://doi.org/http://dx.doi.org/10.1016/j.ccr.2011.03.005>.
- [84] H.S. Schrekker, M.A. Gelesky, M.P. Stracke, C.M.L. Schrekker, G. Machado, S.R. Teixeira, J.C. Rubim, J. Dupont, Disclosure of the imidazolium cation coordination and stabilization mode in ionic liquid stabilized gold(0) nanoparticles, *J. Colloid Interface Sci.* 316 (2007) 189–195. <https://doi.org/http://dx.doi.org/10.1016/j.jcis.2007.08.018>.
- [85] A.S. Pensado, A.A.H. Pádua, Solvation and Stabilization of Metallic Nanoparticles in Ionic Liquids, *Angew. Chemie Int. Ed.* 50 (2011) 8683–8687. <https://doi.org/10.1002/anie.201103096>.
- [86] S. Zhang, K. Dokko, M. Watanabe, Porous ionic liquids: synthesis and application, *Chem. Sci.* 6 (2015) 3684–3691. <https://doi.org/10.1039/C5SC01374G>.

- [87] J. Yuan, D. Mecerreyes, M. Antonietti, Poly(ionic liquid)s: An update, *Prog. Polym. Sci.* 38 (2013) 1009–1036.
<https://doi.org/http://dx.doi.org/10.1016/j.progpolymsci.2013.04.002>.
- [88] J. Yuan, M. Antonietti, Poly(ionic liquid)s: Polymers expanding classical property profiles, *Polymer (Guildf)*. 52 (2011) 1469–1482.
<https://doi.org/http://dx.doi.org/10.1016/j.polymer.2011.01.043>.
- [89] K. Nakamura, K. Fukao, T. Inoue, Dielectric Relaxation and Viscoelastic Behavior of Polymerized Ionic Liquids with Various Counteranions, *Macromolecules*. 45 (2012) 3850–3858. <https://doi.org/10.1021/ma300040b>.
- [90] J. Tang, M. Radosz, Y. Shen, Poly(ionic liquid)s as Optically Transparent Microwave-Absorbing Materials, *Macromolecules*. 41 (2008) 493–496.
<https://doi.org/10.1021/ma071762i>.
- [91] S. Bellayer, J.W. Gilman, N. Eidelman, S. Bourbigot, X. Flambard, D.M. Fox, H.C. De Long, P.C. Trulove, Preparation of Homogeneously Dispersed Multiwalled Carbon Nanotube/Polystyrene Nanocomposites via Melt Extrusion Using Trialkyl Imidazolium Compatibilizer, *Adv. Funct. Mater.* 15 (2005) 910–916. <https://doi.org/10.1002/adfm.200400441>.
- [92] K. Vijayakrishna, K.T.P. Charan, K. Manojkumar, S. Venkatesh, N. Pothanagandhi, A. Sivaramakrishna, P. Mayuri, A.S. Kumar, B. Sreedhar, Ni Nanoparticles Stabilized by Poly(Ionic Liquids) as Chemoselective and Magnetically Recoverable Catalysts for Transfer Hydrogenation Reactions of Carbonyl Compounds, *ChemCatChem*. (2016) n/a-n/a.
<https://doi.org/10.1002/cctc.201501313>.
- [93] X. Mu, J. Meng, Z.-C. Li, Y. Kou, Rhodium Nanoparticles Stabilized by Ionic Copolymers in Ionic Liquids: Long Lifetime Nanocluster Catalysts for Benzene Hydrogenation, *J. Am. Chem. Soc.* 127 (2005) 9694–9695.
<https://doi.org/10.1021/ja051803v>.
- [94] D. Mecerreyes, Polymeric ionic liquids: Broadening the properties and applications of polyelectrolytes, *Prog. Polym. Sci.* 36 (2011) 1629–1648.

<https://doi.org/http://dx.doi.org/10.1016/j.progpolymsci.2011.05.007>.

- [95] R. Marcilla, M.L. Curri, P.D. Cozzoli, M.T. Martínez, I. Loinaz, H. Grande, J.A. Pomposo, D. Mecerreyes, Nano-Objects on a Round Trip from Water to Organics in a Polymeric Ionic Liquid Vehicle, *Small*. 2 (2006) 507–512.
<https://doi.org/10.1002/sml.200500373>.
- [96] A. Pourjavadi, S.H. Hosseini, M. Doulabi, S.M. Fakoorpoor, F. Seidi, Multi-Layer Functionalized Poly(Ionic Liquid) Coated Magnetic Nanoparticles: Highly Recoverable and Magnetically Separable Brønsted Acid Catalyst, *ACS Catal.* 2 (2012) 1259–1266. <https://doi.org/10.1021/cs300140j>.
- [97] C.M. Tollan, R. Marcilla, J.A. Pomposo, J. Rodriguez, J. Aizpurua, J. Molina, D. Mecerreyes, Irreversible Thermochromic Behavior in Gold and Silver Nanorod/Polymeric Ionic Liquid Nanocomposite Films, *ACS Appl. Mater. Interfaces*. 1 (2009) 348–352. <https://doi.org/10.1021/am800058x>.
- [98] T.Y. Kim, H.W. Lee, M. Stoller, D.R. Dreyer, C.W. Bielawski, R.S. Ruoff, K.S. Suh, High-Performance Supercapacitors Based on Poly(ionic liquid)-Modified Graphene Electrodes, *ACS Nano*. 5 (2011) 436–442.
<https://doi.org/10.1021/nn101968p>.
- [99] I. Azcune, A. Genua, A.R. Luzuriaga, I. Odriozola, Chapter Poly(Ionic Liquid)s and Nanoobjects BT - Applications of Ionic Liquids in Polymer Science and Technology, in: D. Mecerreyes (Ed.), Springer Berlin Heidelberg, Berlin, Heidelberg, 2015: pp. 323–353. https://doi.org/10.1007/978-3-662-44903-5_12.
- [100] X. Li, X. Ni, Z. Liang, Z. Shen, Synthesis of imidazolium-functionalized ionic polyurethane and formation of CdTe quantum dot–polyurethane nanocomposites, *J. Polym. Sci. Part A Polym. Chem.* 50 (2012) 509–516.
<https://doi.org/10.1002/pola.25058>.
- [101] K. Sun, C.A. Riedel, A. Urbani, M. Simeoni, S. Mengali, M. Zalkovskij, B. Bilenberg, C.H. de Groot, O.L. Muskens, VO₂ Thermochromic Metamaterial-Based Smart Optical Solar Reflector, *ACS Photonics*. 5 (2018) 2280–2286.
<https://doi.org/10.1021/acsp Photonics.8b00119>.

- [102] H. Qi, L. Wan, X. Huiyan, W. Jiawei, Y. Yin, W. Huaiyu, M. Libo, M. Fei, J. Xuchuan, S.O. G., C.P. K., VO₂/TiN Plasmonic Thermochromic Smart Coatings for Room-Temperature Applications, *Adv. Mater.* 30 (2018) 1705421. <https://doi.org/10.1002/adma.201705421>.
- [103] D. Kolenaty, J. Houska, J. Vlcek, Improved performance of thermochromic VO₂/SiO₂ coatings prepared by low-temperature pulsed reactive magnetron sputtering: Prediction and experimental verification, *J. Alloys Compd.* 767 (2018) 46–51. <https://doi.org/https://doi.org/10.1016/j.jallcom.2018.07.093>.
- [104] Q. Hao, W. Li, H. Xu, J. Wang, Y. Yin, H. Wang, L. Ma, F. Ma, X. Jiang, O.G. Schmidt, P.K. Chu, VO₂/TiN Plasmonic Thermochromic Smart Coatings for Room-Temperature Applications, *Adv. Mater.* 30 (2018) 1705421. <https://doi.org/10.1002/adma.201705421>.
- [105] T. Chang, X. Cao, N. Li, S. Long, X. Gao, L.R. Dedon, G. Sun, H. Luo, P. Jin, Facile and Low-Temperature Fabrication of Thermochromic Cr₂O₃/VO₂ Smart Coatings: Enhanced Solar Modulation Ability, High Luminous Transmittance and UV-Shielding Function, *ACS Appl. Mater. Interfaces.* 9 (2017) 26029–26037. <https://doi.org/10.1021/acsami.7b07137>.
- [106] F. Xu, X. Cao, J. Zhu, G. Sun, R. Li, S. Long, H. Luo, P. Jin, Broadband thermochromic VO₂-based composite film with ultra-high solar modulation ability, *Mater. Lett.* 222 (2018) 62–65. <https://doi.org/https://doi.org/10.1016/j.matlet.2018.03.176>.
- [107] Z. Liang, L. Zhao, W. Meng, C. Zhong, S. Wei, B. Dong, Z. Xu, L. Wan, S. Wang, Tungsten-doped vanadium dioxide thin films as smart windows with self-cleaning and energy-saving functions, *J. Alloys Compd.* 694 (2017) 124–131. <https://doi.org/https://doi.org/10.1016/j.jallcom.2016.09.315>.
- [108] W. Lu, G. Zhao, B. Song, J. Li, X. Zhang, G. Han, Preparation and thermochromic properties of sol-gel-derived Zr-doped VO₂ films, *Surf. Coatings Technol.* 320 (2017) 311–314. <https://doi.org/https://doi.org/10.1016/j.surfcoat.2016.12.070>.
- [109] J. Zou, L. Xiao, L. Zhu, X. Chen, One-step rapid hydrothermal synthesis of

- monoclinic VO₂ nanoparticles with high precursors concentration, *J. Sol-Gel Sci. Technol.* 91 (2019) 302–309. <https://doi.org/10.1007/s10971-019-04999-0>.
- [110] H.H. Afify, S.A. Hassan, M. Obaida, A. Abouelsayed, Influence of annealing on the optical properties of monoclinic vanadium oxide VO₂ prepared in nanoscale by hydrothermal technique, *Phys. E Low-Dimensional Syst. Nanostructures.* 114 (2019) 113610. <https://doi.org/https://doi.org/10.1016/j.physe.2019.113610>.
- [111] T.D. Vu, Z. Chen, X. Zeng, M. Jiang, S. Liu, Y. Gao, Y. Long, Physical vapour deposition of vanadium dioxide for thermochromic smart window applications, *J. Mater. Chem. C.* 7 (2019) 2121–2145. <https://doi.org/10.1039/C8TC05014G>.
- [112] B. Rajeswaran, A.M. Umarji, Defect engineering of VO₂ thin films synthesized by Chemical Vapor Deposition, *Mater. Chem. Phys.* 245 (2020) 122230. <https://doi.org/https://doi.org/10.1016/j.matchemphys.2019.122230>.
- [113] M.M. Seyfour, R. Binions, Sol-gel approaches to thermochromic vanadium dioxide coating for smart glazing application, *Sol. Energy Mater. Sol. Cells.* 159 (2017) 52–65. <https://doi.org/https://doi.org/10.1016/j.solmat.2016.08.035>.
- [114] I. Mjejri, A. Rougier, M. Gaudon, Low-Cost and Facile Synthesis of the Vanadium Oxides V₂O₃, VO₂, and V₂O₅ and Their Magnetic, Thermochromic and Electrochromic Properties, *Inorg. Chem.* 56 (2017) 1734–1741. <https://doi.org/10.1021/acs.inorgchem.6b02880>.
- [115] Z. Bingxing, Z. Jianling, H. Buxing, Assembling Metal–Organic Frameworks in Ionic Liquids and Supercritical CO₂, *Chem. – An Asian J.* 11 (2016) 2610–2619. <https://doi.org/10.1002/asia.201600323>.
- [116] S. Keskin, D. Kayrak-Talay, U. Akman, Ö. Hortaçsu, A review of ionic liquids towards supercritical fluid applications, *J. Supercrit. Fluids.* 43 (2007) 150–180. <https://doi.org/https://doi.org/10.1016/j.supflu.2007.05.013>.
- [117] M.P. Singh, R.K. Singh, S. Chandra, Studies on Imidazolium-Based Ionic Liquids Having a Large Anion Confined in a Nanoporous Silica Gel Matrix, *J. Phys. Chem. B.* 115 (2011) 7505–7514. <https://doi.org/10.1021/jp2003358>.
- [118] L. Viau, C. Tourné-Péteilh, J.-M. Devoisselle, A. Vioux, Ionogels as drug delivery

- system: one-step sol–gel synthesis using imidazolium ibuprofenate ionic liquid, *Chem. Commun.* 46 (2010) 228–230. <https://doi.org/10.1039/B913879J>.
- [119] R.K. Donato, M. Lavorgna, P. Musto, K.Z. Donato, A. Jager, P. Štěpánek, H.S. Schrekker, L. Matějka, The role of ether-functionalized ionic liquids in the sol–gel process: Effects on the initial alkoxide hydrolysis steps, *J. Colloid Interface Sci.* 447 (2015) 77–84. <https://doi.org/https://doi.org/10.1016/j.jcis.2015.01.079>.
- [120] R.K. Donato, L. Matějka, H.S. Schrekker, J. Pleštil, A. Jigounov, J. Brus, M. Šlouf, The multifunctional role of ionic liquids in the formation of epoxy-silica nanocomposites, *J. Mater. Chem.* 21 (2011) 13801–13810. <https://doi.org/10.1039/C1JM11752A>.
- [121] M.C. Biesinger, L.W.M. Lau, A.R. Gerson, R.S.C. Smart, Resolving surface chemical states in XPS analysis of first row transition metals, oxides and hydroxides: Sc, Ti, V, Cu and Zn, *Appl. Surf. Sci.* 257 (2010) 887–898. <https://doi.org/https://doi.org/10.1016/j.apsusc.2010.07.086>.
- [122] X. Zhang, S. Heinonen, E. Levänen, Applications of supercritical carbon dioxide in materials processing and synthesis, *RSC Adv.* 4 (2014) 61137–61152. <https://doi.org/10.1039/C4RA10662H>.
- [123] Ž. Knez, D. Cör, M. Knez Hrnčič, Solubility of Solids in Sub- and Supercritical Fluids: A Review 2010–2017, *J. Chem. Eng. Data.* 63 (2018) 860–884. <https://doi.org/10.1021/acs.jced.7b00778>.
- [124] C. Liu, L. Shaw, Nanoparticulate Materials and Core/Shell Structures Derived from Wet Chemistry Methods, in: 2015: pp. 1–21. https://doi.org/10.1007/978-94-007-6178-0_100906-1.
- [125] J. Livage, M. Henry, C. Sanchez, Sol-gel chemistry of transition metal oxides, *Prog. Solid State Chem.* 18 (1988) 259–341. [https://doi.org/https://doi.org/10.1016/0079-6786\(88\)90005-2](https://doi.org/https://doi.org/10.1016/0079-6786(88)90005-2).
- [126] H. Qin, Synthesis of VO₂ Nanomaterials Using Green Solvents for Thermo-chromic Window Coatings, Western University, 2017.
- [127] B.-H. Lim, W.-H. Choe, J.-J. Shim, C.S. Ra, D. Tuma, H. Lee, C.S. Lee, High-

pressure solubility of carbon dioxide in imidazolium-based ionic liquids with anions [PF₆] and [BF₄], *Korean J. Chem. Eng.* 26 (2009) 1130–1136.

<https://doi.org/10.1007/s11814-009-0188-5>.

- [128] A. Karout, A.C. Pierre, Silica gelation catalysis by ionic liquids, *Catal. Commun.* 10 (2009) 359–361. <https://doi.org/https://doi.org/10.1016/j.catcom.2008.07.046>.
- [129] L. Viau, M.-A. Néouze, C. Biolley, S. Volland, D. Brevet, P. Gaveau, P. Dieudonné, A. Galarneau, A. Vioux, Ionic Liquid Mediated Sol-Gel Synthesis in the Presence of Water or Formic Acid: Which Synthesis for Which Material?, *Chem. Mater.* 24 (2012) 3128–3134. <https://doi.org/10.1021/cm301083r>.
- [130] M. Klähn, A. Seduraman, What Determines CO₂ Solubility in Ionic Liquids? A Molecular Simulation Study, *J. Phys. Chem. B.* 119 (2015) 10066–10078. <https://doi.org/10.1021/acs.jpcc.5b03674>.
- [131] M.B. Shiflett, A. Yokozeki, Phase Behavior of Carbon Dioxide in Ionic Liquids: [emim][Acetate], [emim][Trifluoroacetate], and [emim][Acetate] + [emim][Trifluoroacetate] Mixtures, *J. Chem. Eng. Data.* 54 (2009) 108–114. <https://doi.org/10.1021/je800701j>.
- [132] I. Mejía, K. Stanley, R. Canales, J.F. Brennecke, On the High-Pressure Solubilities of Carbon Dioxide in Several Ionic Liquids, *J. Chem. Eng. Data.* 58 (2013) 2642–2653. <https://doi.org/10.1021/je400542b>.
- [133] A.M. Schilderman, S. Raeissi, C.J. Peters, Solubility of carbon dioxide in the ionic liquid 1-ethyl-3-methylimidazolium bis(trifluoromethylsulfonyl)imide, *Fluid Phase Equilib.* 260 (2007) 19–22. <https://doi.org/https://doi.org/10.1016/j.fluid.2007.06.003>.
- [134] Y. Cao, T. Mu, Comprehensive Investigation on the Thermal Stability of 66 Ionic Liquids by Thermogravimetric Analysis, *Ind. Eng. Chem. Res.* 53 (2014) 8651–8664. <https://doi.org/10.1021/ie5009597>.
- [135] C. Maton, N. De Vos, C. V Stevens, Ionic liquid thermal stabilities: decomposition mechanisms and analysis tools, *Chem. Soc. Rev.* 42 (2013) 5963–5977. <https://doi.org/10.1039/C3CS60071H>.

- [136] N. Zhao, Y. Liu, X. Zhao, H. Song, Liquid crystal self-assembly of halloysite nanotubes in ionic liquids: a novel soft nanocomposite ionogel electrolyte with high anisotropic ionic conductivity and thermal stability, *Nanoscale*. 8 (2016) 1545–1554. <https://doi.org/10.1039/C5NR06888F>.
- [137] C. Weeks, Y. Song, M. Suzuki, N.A. Chernova, P.Y. Zavalij, M.S. Whittingham, The one dimensional chain structures of vanadyl glycolate and vanadyl acetate, *J. Mater. Chem.* 13 (2003) 1420–1423. <https://doi.org/10.1039/B208100H>.
- [138] R. Neumann, Polyoxometalate Complexes in Organic Oxidation Chemistry, *Prog. Inorg. Chem.* (1997) 317–370. <https://doi.org/doi:10.1002/9780470166482.ch3>.
- [139] R.K. Donato, M. V Migliorini, M.A. Benvegnú, M.P. Stracke, M.A. Gelesky, F.A. Pavan, C.M.L. Schrekker, E. V Benvenutti, J. Dupont, H.S. Schrekker, Synthesis of silica xerogels with highly distinct morphologies in the presence of imidazolium ionic liquids, *J. Sol-Gel Sci. Technol.* 49 (2009) 71–77. <https://doi.org/10.1007/s10971-008-1829-6>.
- [140] D. Malarde, M.J. Powell, R. Quesada-Cabrera, R.L. Wilson, C.J. Carmalt, G. Sankar, I.P. Parkin, R.G. Palgrave, Optimized Atmospheric-Pressure Chemical Vapor Deposition Thermochromic VO₂ Thin Films for Intelligent Window Applications, *ACS Omega*. 2 (2017) 1040–1046. <https://doi.org/10.1021/acsomega.7b00042>.
- [141] C. Ji, Z. Wu, L. Lu, X. Wu, J. Wang, X. Liu, H. Zhou, Z. Huang, J. Gou, Y. Jiang, High thermochromic performance of Fe/Mg co-doped VO₂ thin films for smart window applications, *J. Mater. Chem. C*. 6 (2018) 6502–6509. <https://doi.org/10.1039/C8TC01111G>.
- [142] D. Zhang, M. Zhu, Y. Liu, K. Yang, G. Liang, Z. Zheng, X. Cai, P. Fan, High performance VO₂ thin films growth by DC magnetron sputtering at low temperature for smart energy efficient window application, *J. Alloys Compd.* 659 (2016) 198–202. <https://doi.org/https://doi.org/10.1016/j.jallcom.2015.11.047>.
- [143] Z.A. Umar, N. Ahmed, R. Ahmed, M. Arshad, M. Anwar-Ul-Haq, T. Hussain, M.A. Baig, Substrate temperature effects on the structural, compositional, and

- electrical properties of VO₂ thin films deposited by pulsed laser deposition, *Surf. Interface Anal.* 50 (2017) 297–303. <https://doi.org/10.1002/sia.6368>.
- [144] D. Graf, J. Schläfer, S. Garbe, A. Klein, S. Mathur, Interdependence of Structure, Morphology, and Phase Transitions in CVD Grown VO₂ and V₂O₃ Nanostructures, *Chem. Mater.* 29 (2017) 5877–5885. <https://doi.org/10.1021/acs.chemmater.7b01018>.
- [145] O. Berezina, D. Kirienko, A. Pergament, G. Stefanovich, A. Velichko, V. Zlomanov, Vanadium oxide thin films and fibers obtained by acetylacetonate sol-gel method, *Thin Solid Films.* 574 (2015) 15–19. <https://doi.org/https://doi.org/10.1016/j.tsf.2014.11.058>.
- [146] R.G.S.P. Bogolitsyn, Kinetics of oxidation of vanadyl acetylacetonate by oxygen in methanolic solution, *Transit. Met. Chem.* 22 (1997) 61–64. <https://doi.org/https://doi.org/10.1023/A:1018426004961>.
- [147] J.-H. Yu, S.-H. Nam, D. Kim, M. Kim, H.J. Seo, Y.H. Ro, Y.T. Joo, J. Lee, J.-H. Boo, Thermal aging effect of vanadyl acetylacetonate precursor for deposition of VO₂ thin films with thermochromic properties, *Mater. Res. Bull.* 82 (2016) 11–15. <https://doi.org/https://doi.org/10.1016/j.materresbull.2016.01.051>.
- [148] R. Lipson, L. Cheng, Methods for inhibition of the oxidation of VO(acac)₂ in the solution, US patent: US9376363B2, 2016.
- [149] C. Wu, J. Dai, X. Zhang, J. Yang, F. Qi, C. Gao, Y. Xie, Direct Confined-Space Combustion Forming Monoclinic Vanadium Dioxides, *Angew. Chemie Int. Ed.* 49 (2009) 134–137. <https://doi.org/10.1002/anie.200905227>.
- [150] Z. Cao, X. Xiao, X. Lu, Y. Zhan, H. Cheng, G. Xu, A simple and low-cost combustion method to prepare monoclinic VO₂ with superior thermochromic properties, *Sci. Rep.* 6 (2016) 39154. <https://doi.org/10.1038/srep39154>.
- [151] D. Kasprzak, I. Stępnik, M. Galiński, Acetate- and lactate-based ionic liquids: Synthesis, characterisation and electrochemical properties, *J. Mol. Liq.* 264 (2018) 233–241. <https://doi.org/https://doi.org/10.1016/j.molliq.2018.05.059>.
- [152] M. Watanabe, M.L. Thomas, S. Zhang, K. Ueno, T. Yasuda, K. Dokko,

Application of Ionic Liquids to Energy Storage and Conversion Materials and Devices, *Chem. Rev.* 117 (2017) 7190–7239.

<https://doi.org/10.1021/acs.chemrev.6b00504>.

- [153] A. Mota, J.P. Hallett, M.L. Kuznetsov, I. Correia, Structural characterization and DFT study of VIVO(acac)₂ in imidazolium ionic liquids, *Phys. Chem. Chem. Phys.* 13 (2011) 15094–15102. <https://doi.org/10.1039/C1CP20800D>.
- [154] D.B. Williams, M.E. Stoll, B.L. Scott, D.A. Costa, W.J. Oldham, Jr., Coordination chemistry of the bis(trifluoromethylsulfonyl)imide anion: molecular interactions in room temperature ionic liquids, *Chem. Commun.* (2005) 1438–1440. <https://doi.org/10.1039/B416830E>.
- [155] Y. Chauvin, L. Mussmann, H. Olivier, A Novel Class of Versatile Solvents for Two-Phase Catalysis: Hydrogenation, Isomerization, and Hydroformylation of Alkenes Catalyzed by Rhodium Complexes in Liquid 1,3-Dialkylimidazolium Salts, *Angew. Chemie Int. Ed. English.* 34 (1996) 2698–2700. <https://doi.org/10.1002/anie.199526981>.
- [156] K. Nakamura, T. Saiwaki, K. Fukao, T. Inoue, Viscoelastic Behavior of the Polymerized Ionic Liquid Poly(1-ethyl-3-vinylimidazolium bis(trifluoromethanesulfonylimide)), *Macromolecules.* 44 (2011) 7719–7726. <https://doi.org/10.1021/ma201611q>.
- [157] C.J. Ballhausen, H.B. Gray, The Electronic Structure of the Vanadyl Ion, *Inorg. Chem.* 1 (1962) 111–122. <https://doi.org/10.1021/ic50001a022>.
- [158] I. Bernal, P.H. Rieger, Solvent Effects on the Optical and Electron Spin Resonance Spectra of Vanadyl Acetylacetonate, *Inorg. Chem.* 2 (1963) 256–260. <https://doi.org/10.1021/ic50006a004>.
- [159] D.T. Bowron, C. D'Agostino, L.F. Gladden, C. Hardacre, J.D. Holbrey, M.C. Lagunas, J. McGregor, M.D. Mantle, C.L. Mullan, T.G.A. Youngs, Structure and Dynamics of 1-Ethyl-3-methylimidazolium Acetate via Molecular Dynamics and Neutron Diffraction, *J. Phys. Chem. B.* 114 (2010) 7760–7768. <https://doi.org/10.1021/jp102180q>.

- [160] Y. Yang, H. Fan, Q. Meng, Z. Zhang, G. Yang, B. Han, Ionic liquid [OMIm][OAc] directly inducing oxidation cleavage of the β -O-4 bond of lignin model compounds, *Chem. Commun.* 53 (2017) 8850–8853.
<https://doi.org/10.1039/C7CC04209D>.
- [161] K.C.V. E.F. Vansant, P. Van Der Voort, *Characterization and Chemical Modification of the Silica Surface*, 1965.
- [162] M.E.A. Warwick, I. Ridley, R. Binions, The effect of variation in the transition hysteresis width and gradient in thermochromic glazing systems, *Sol. Energy Mater. Sol. Cells.* 140 (2015) 253–265.
<https://doi.org/http://dx.doi.org/10.1016/j.solmat.2015.04.022>.
- [163] Z. Chen, Y. Gao, L. Kang, C. Cao, S. Chen, H. Luo, Fine crystalline VO₂ nanoparticles: synthesis, abnormal phase transition temperatures and excellent optical properties of a derived VO₂ nanocomposite foil, *J. Mater. Chem. A.* 2 (2014) 2718–2727. <https://doi.org/10.1039/C3TA14612J>.
- [164] M. Xygkis, E. Gagaoudakis, L. Zouridi, O. Markaki, E. Aperathitis, K. Chrissopoulou, G. Kiriakidis, V. Binas, Thermochromic Behavior of VO₂/Polymer Nanocomposites for Energy Saving Coatings, *Coatings* . 9 (2019).
<https://doi.org/10.3390/coatings9030163>.
- [165] J.-H. Yu, S.-H. Nam, J.W. Lee, D.I. Kim, J.-H. Boo, Selective near infrared transmittance control of thermochromic VO₂ thin films through colloidal lithography, *Appl. Surf. Sci.* (2018).
<https://doi.org/https://doi.org/10.1016/j.apsusc.2018.02.243>.
- [166] M. Lübke, N. Ding, M.J. Powell, D.J.L. Brett, P.R. Shearing, Z. Liu, J.A. Darr, VO₂ nano-sheet negative electrodes for lithium-ion batteries, *Electrochem. Commun.* 64 (2016) 56–60.
<https://doi.org/https://doi.org/10.1016/j.elecom.2016.01.013>.
- [167] X. Li, S. Zhang, L. Yang, X. Li, J. Chen, C. Huang, A convenient way to reduce the hysteresis width of VO₂(M) nanomaterials, *New J. Chem.* 41 (2017) 15260–15267. <https://doi.org/10.1039/C7NJ02632C>.

- [168] S. Chen, J. Liu, L. Wang, H. Luo, Y. Gao, Unraveling Mechanism on Reducing Thermal Hysteresis Width of VO₂ by Ti Doping: A Joint Experimental and Theoretical Study, *J. Phys. Chem. C*. 118 (2014) 18938–18944. <https://doi.org/10.1021/jp5056842>.
- [169] A.R. and Y.A. and W.C. and Y.N. and S. Yin, Supercritical temperature synthesis of fluorine-doped VO₂ (M) nanoparticle with improved thermochromic property, *Nanotechnology*. 29 (2018) 244005. <http://stacks.iop.org/0957-4484/29/i=24/a=244005>.
- [170] M.J. Powell, R. Quesada-Cabrera, A. Taylor, D. Teixeira, I. Papakonstantinou, R.G. Palgrave, G. Sankar, I.P. Parkin, Intelligent Multifunctional VO₂/SiO₂/TiO₂ Coatings for Self-Cleaning, Energy-Saving Window Panels, *Chem. Mater.* 28 (2016) 1369–1376. <https://doi.org/10.1021/acs.chemmater.5b04419>.
- [171] G. Sun, H. Zhou, X. Cao, R. Li, M. Tazawa, M. Okada, P. Jin, Self-Assembled Multilayer Structure and Enhanced Thermochromic Performance of Spinodally Decomposed TiO₂–VO₂ Thin Film, *ACS Appl. Mater. Interfaces*. 8 (2016) 7054–7059. <https://doi.org/10.1021/acsami.5b12476>.
- [172] Y. Zhou, Y. Cai, X. Hu, Y. Long, VO₂/hydrogel hybrid nanothermochromic material with ultra-high solar modulation and luminous transmission, *J. Mater. Chem. A*. 3 (2015) 1121–1126. <https://doi.org/10.1039/C4TA05035E>.
- [173] K. Laaksonen, S.-Y. Li, S.R. Puisto, N.K.J. Rostedt, T. Ala-Nissila, C.G. Granqvist, R.M. Nieminen, G.A. Niklasson, Nanoparticles of TiO₂ and VO₂ in dielectric media: Conditions for low optical scattering, and comparison between effective medium and four-flux theories, *Sol. Energy Mater. Sol. Cells*. 130 (2014) 132–137. <https://doi.org/https://doi.org/10.1016/j.solmat.2014.06.036>.
- [174] N. Shen, B. Dong, C. Cao, Z. Chen, H. Luo, Y. Gao, Solid-state-reaction synthesis of VO₂ nanoparticles with low phase transition temperature, enhanced chemical stability and excellent thermochromic properties, *RSC Adv.* 5 (2015) 108015–108022. <https://doi.org/10.1039/C5RA20732K>.
- [175] X. Li, L. Yang, S. Zhang, X. Li, J. Chen, C. Huang, VO₂(M) with narrow

hysteresis width from a new metastable phase of crystallized $\text{VO}_2(\text{M}) \cdot 0.25\text{H}_2\text{O}$, *Mater. Lett.* 211 (2018) 308–311.

<https://doi.org/https://doi.org/10.1016/j.matlet.2017.09.105>.

- [176] S. Ding, Z. Liu, D. Li, W. Zhao, Y. Wang, D. Wan, F. Huang, Tunable Assembly of Vanadium Dioxide Nanoparticles to Create Porous Film for Energy-Saving Applications, *ACS Appl. Mater. Interfaces.* 5 (2013) 1630–1635.

<https://doi.org/10.1021/am3023724>.

- [177] C. Cao, Y. Gao, H. Luo, Pure Single-Crystal Rutile Vanadium Dioxide Powders: Synthesis, Mechanism and Phase-Transformation Property, *J. Phys. Chem. C.* 112 (2008) 18810–18814. <https://doi.org/10.1021/jp8073688>.

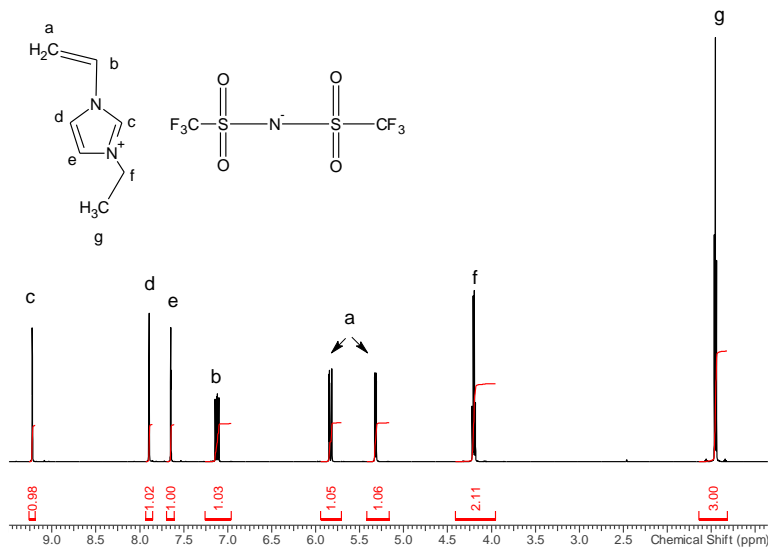
- [178] S.S. Moganty, S. Srivastava, Y. Lu, J.L. Schaefer, S.A. Rizvi, L.A. Archer, Ionic Liquid-Tethered Nanoparticle Suspensions: A Novel Class of Ionogels, *Chem. Mater.* 24 (2012) 1386–1392. <https://doi.org/10.1021/cm300424v>.

- [179] X. Chen, Q. Li, J. Zhao, L. Qiu, Y. Zhang, B. Sun, F. Yan, Ionic liquid-tethered nanoparticle/poly(ionic liquid) electrolytes for quasi-solid-state dye-sensitized solar cells, *J. Power Sources.* 207 (2012) 216–221.

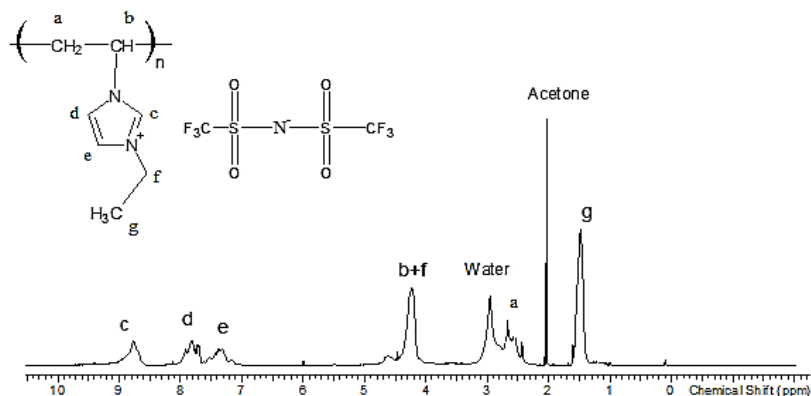
<https://doi.org/https://doi.org/10.1016/j.jpowsour.2012.01.143>.

Appendices

Characterization of synthesized IL and PIL by ¹H NMR:

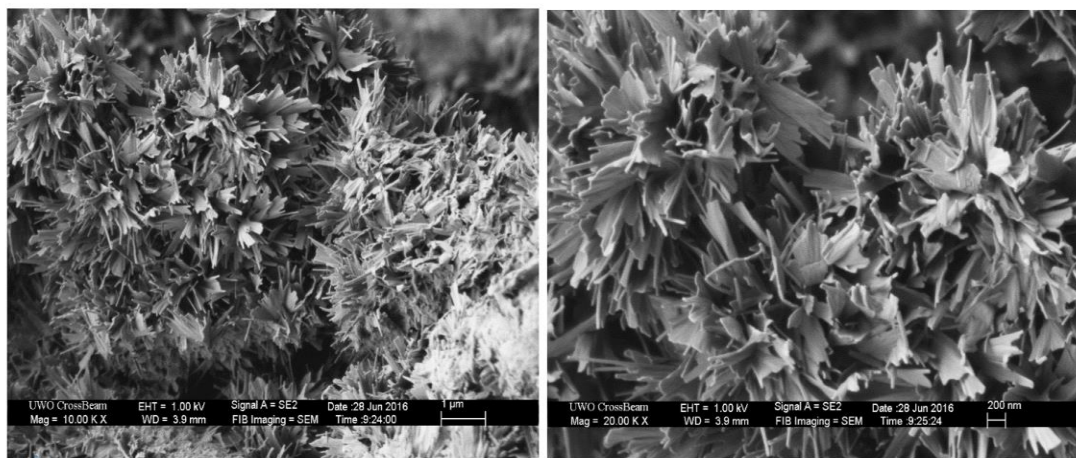


Appendix A: ¹H NMR spectrum of 1-ethyl-3-vinylimidazolium bis(trifluoromethanesulfonylimide) in DMSO-d₆



Appendix B: ¹H NMR spectrum of poly(1-ethyl-3-vinylimidazolium bis(trifluoromethanesulfonylimide)) in acetone-d₆

SEM of VO₂ (M) film prepared from VO(acac)₂ precursor



Appendix C. The flower-like morphology consists of a large number of uniform sheets with nano-size width and thickness and micro size length

Copyright Permissions



RightsLink®

Home

Create Account

Help



ACS Publications
Most Trusted. Most Cited. Most Read.

Title: Nanoporous Thermochromic VO₂ Films with Low Optical Constants, Enhanced Luminous Transmittance and Thermochromic Properties
Author: Litao Kang, Yanfeng Gao, Hongjie Luo, et al
Publication: Applied Materials
Publisher: American Chemical Society
Date: Feb 1, 2011
Copyright © 2011, American Chemical Society

PERMISSION/LICENSE IS GRANTED FOR YOUR ORDER AT NO CHARGE

This type of permission/license, instead of the standard Terms & Conditions, is sent to you because no fee is being charged for your order. Please note the following:

- Permission is granted for your request in both print and electronic formats, and translations.
- If figures and/or tables were requested, they may be adapted or used in part.
- Please print this page for your records and send a copy of it to your publisher/graduate school.
- Appropriate credit for the requested material should be given as follows: "Reprinted (adapted) with permission from (COMPLETE REFERENCE CITATION). Copyright (YEAR) American Chemical Society." Insert appropriate information in place of the capitalized words.
- One-time permission is granted only for the use specified in your request. No additional uses are granted (such as derivative works or other editions). For any other uses, please submit a new request.

If credit is given to another source for the material you requested, permission must be obtained from that source.

BACK

CLOSE WINDOW



RightsLink®

[Home](#)[Account Info](#)[Help](#)**SPRINGER NATURE**

Title: How to be smart and energy efficient: A general discussion on thermochromic windows
Author: Linshuang Long, Hong Ye
Publication: Scientific Reports
Publisher: Springer Nature
Date: Sep 19, 2014
Copyright © 2014, Springer Nature

Creative Commons

The request you have made is considered to be non-commercial/educational. As the article you have requested has been distributed under a Creative Commons license (Attribution-Noncommercial), you may reuse this material for non-commercial/educational purposes without obtaining additional permission from Springer Nature, providing that the author and the original source of publication are fully acknowledged (please see the article itself for the license version number). You may reuse this material without obtaining permission from Springer Nature, providing that the author and the original source of publication are fully acknowledged, as per the terms of the license. For license terms, please see <http://creativecommons.org/>

[BACK](#)[CLOSE WINDOW](#)

Copyright © 2019 [Copyright Clearance Center, Inc.](#) All Rights Reserved. [Privacy statement](#); [Terms and Conditions](#).
Comments? We would like to hear from you. E-mail us at customerscare@copyright.com



Note: Copyright.com supplies permissions but not the copyrighted content itself.

1
PAYMENT

2
REVIEW

3
CONFIRMATION

Step 3: Order Confirmation

Thank you for your order! A confirmation for your order will be sent to your account email address. If you have questions about your order, you can call us 24 hrs/day, M-F at +1.855.239.3415 Toll Free, or write to us at info@copyright.com. This is not an invoice.

Confirmation Number: 11782389
Order Date: 01/14/2019

If you paid by credit card, your order will be finalized and your card will be charged within 24 hours. If you choose to be invoiced, you can change or cancel your order until the invoice is generated.

Order Details

Journal of materials chemistry. A, Materials for energy and sustainability

Order detail ID:	71766276	Permission Status:	✔ Granted
Order License Id:	4507891167710	Permission type:	Republish or display content
ISSN:	2050-7496	Type of use:	Thesis/Dissertation
Publication Type:	e-Journal	Requestor type	Academic Institution
Volume:		Format	Print, Electronic
Issue:		Portion	image/photo
Start page:		Number of images/photos requested	2
Publisher:	Royal Society of Chemistry	The requesting person/organization	Western University
Author/Editor:	Royal Society of Chemistry (Great Britain)	Title or numeric reference of the portion(s)	Figure 1-4, Figure 1-5
		Title of the article or chapter the portion is from	N/A

Copyright

Describes the rights related to the publication and distribution of research. It governs how authors (as well as their employers or funders), publishers and the wider general public can use, publish and distribute articles or books.

[Journal author rights](#) [Government employees](#) [Elsevier's rights](#) [Protecting author rights](#) [Open access](#)

Journal author rights

In order for Elsevier to publish and disseminate research articles, we need publishing rights. This is determined by a publishing agreement between the author and Elsevier. This agreement deals with the transfer or license of the copyright to Elsevier and authors retain significant rights to use and share their own published articles. Elsevier supports the need for authors to share, disseminate and maximize the impact of their research and these rights, in Elsevier proprietary journals* are defined below:

For subscription articles	For open access articles
<p>Authors transfer copyright to the publisher as part of a journal publishing agreement, but have the right to:</p> <ul style="list-style-type: none"> Share their article for Personal Use (https://www.elsevier.com/about/policies/copyright/personal-use), Internal Institutional Use (https://www.elsevier.com/about/policies/copyright/internal-use) and Scholarly Sharing (https://www.elsevier.com/about/policies/sharing) purposes, with a DOI link to the version of record on ScienceDirect (and with the Creative Commons CC-BY-NC-ND license (https://www.elsevier.com/about/policies/sharing/how-to-attach-a-user-license) for author manuscript versions) Retain patent, trademark and other intellectual property rights (including research data). Proper attribution and credit for the published work. 	<p>Authors sign an exclusive license agreement, where authors have copyright but license exclusive rights in their article to the publisher**. In this case authors have the right to:</p> <ul style="list-style-type: none"> Share their article in the same ways permitted to third parties under the relevant user license (together with Personal Use (https://www.elsevier.com/about/policies/copyright/personal-use) rights) so long as it contains a CrossMark logo (https://www.elsevier.com/about/policies/crossmark), the end user license (https://www.elsevier.com/about/policies/open-access-licenses), and a DOI link to the version of record on ScienceDirect. Retain patent, trademark and other intellectual property rights (including research data). Proper attribution and credit for the published work.

*Please note that society or third party owned journals may have different publishing agreements. Please see the journal's guide for authors for journal specific copyright information.

**This includes the right for the publisher to make and authorize commercial use, please see "Rights granted to Elsevier (<https://www.elsevier.com/about/policies/copyright#Elsevier%20rights>)" for more details.

Help and Support

- Download a sample publishing agreement for subscription articles in [English](#) (https://www.elsevier.com/_data/assets/pdf_file/0004/727600/JPA_V22_2017_Clean-copy.pdf) and [French](#)



RightsLink®

Home

Create Account

Help



ACS Publications
Most Trusted. Most Cited. Most Read.

Title: Structure and Dynamics of 1-Ethyl-3-methylimidazolium Acetate via Molecular Dynamics and Neutron Diffraction
Author: D. T. Bowron, C. D'Agostino, L. F. Gladden, et al
Publication: The Journal of Physical Chemistry B
Publisher: American Chemical Society
Date: Jun 1, 2010

Copyright © 2010, American Chemical Society

LOGIN
If you're a [copyright.com](#) user, you can login to RightsLink using your [copyright.com](#) credentials. Already a [RightsLink](#) user or want to [learn more?](#)

PERMISSION/LICENSE IS GRANTED FOR YOUR ORDER AT NO CHARGE

This type of permission/license, instead of the standard Terms & Conditions, is sent to you because no fee is being charged for your order. Please note the following:

- Permission is granted for your request in both print and electronic formats, and translations.
- If figures and/or tables were requested, they may be adapted or used in part.
- Please print this page for your records and send a copy of it to your publisher/graduate school.
- Appropriate credit for the requested material should be given as follows: "Reprinted (adapted) with permission from (COMPLETE REFERENCE CITATION). Copyright (YEAR) American Chemical Society." Insert appropriate information in place of the capitalized words.
- One-time permission is granted only for the use specified in your request. No additional uses are granted (such as derivative works or other editions). For any other uses, please submit a new request.

If credit is given to another source for the material you requested, permission must be obtained from that source.

BACK

CLOSE WINDOW

Curriculum Vitae

Name: Shidokht Nazari

Post-secondary Education and Degrees: Shahid Beheshti University
Tehran, Iran
Sep 2004- Jun 2008, B.Sc. in Chemistry

Sharif University of Tech.
Tehran, Iran
Sep 2009-Aug 2010 M.Sc. in Chemistry

Mount Allison University
Sackville, NB, Canada
Sep 2010-May 2013 M.Sc. in Chemistry

Honors and Awards: Robert Rice Memorial Graduate Fellowship, 2010

Related Work Experience

Process Chemist
Ionomr Innovations Inc., Vancouver Canada
Aug 2018- now

Teaching Assistant
Western University, London, Canada
Jan 2015- Jan 2018

R&D Chemist
Varian Pharmed, Tehran, Iran
Sep 2014- Jan 2015

R&D Chemist
Cosar Pharmaceutical Co., Tehran, Iran
Sep 2013- Aug 2014

Publications:

1. **Shidokht Nazari**, Paul Charpentier, “Stabilizing vanadyl acetylacetonate using imidazolium ionic liquids for VO₂ thermochromic thin films”, **Journal of Thin Solid Films** (2021), 725: 138640
2. **Shidokht Nazari**, Paul Charpentier, “Sol-gel processing of VO₂ (M) in supercritical CO₂ (scCO₂) and supercritical CO₂ (scCO₂)/ ionic liquid biphasic system”, **Journal of Supercritical Fluids** (2020), 165: 104989

3. **Shidokht Nazari**, Khashayar Ghandi, “Solvent and microwave effects on oxidation of aromatic α - Diketones”, **Journal of Industrial and Engineering Chemistry** (2015), 21: 198–205
4. **Shidokht Nazari**, Khashayar Ghandi, “Green methods for oxidation of an aromatic diketone to an aromatic anhydride: oxidation of aceanthraquinone”, **Fresenius Environmental Bulletin** (2015), 24:1350-1355
5. **Shidokht Nazari**, Khashayar Ghandi, “Physicochemical properties of imidazopyridine protic ionic liquids”, **Journal of Materials Chemistry A** (2013) 1: a 11570-11579 (**cover article**)
6. Mohammad Reza Nabid, Zahra Zamiraei, Roya Sedghi, **Shidokht Nazari**, “Synthesis and characterization of poly (catechol) catalyzed by porphyrin and enzyme”, **Polymer Bulletin** (2010) 64: 855–865

Patent:

Khashayar Ghandi, **Shidokht Nazari**, Marco Farren Dai **WO2014153642A1** (2014),
Synthesis of Protic Ionic Liquids